Deliverable D13.2
Monitoring of tunnel, sub-ballast layers, subsoil and predictive maintenance for tunnels implementation & data analysis for condition monitoring system implementation report

Project acronym:	FP3 - IAM4RAIL
Starting date:	01/12/2022
Duration (in months):	48
Call (part) identifier:	HORIZON-ER-JU-2022-01
Grant agreement no:	101101966
Due date of deliverable:	Month 32
Actual submission date:	16/09/2025
Responsible/Author:	Amine Dhemaied (SNCF)
Dissemination level:	PU
Status:	Issued

This project has received funding from the European Union's Horizon Europe research and innovation programme under Grant Agreement No 101101966.

Document history		
Revision	*Date*	*Description*
0.1	20.01.2025	Table of contents
0.2	05.05.2025	First version full UCs (paragraphs and chapters)
0.3	30.05.2025	Final draft version
0.4	25.06.2025	Final version
1.0	16.09.2025	Final approved version submitted to ERJU

Report contributors		
Name	**Beneficiary Short Name**	**Details of the contribution**
Jose Solís Hernández	CEMOSA	Table of contents
Andrea Palomar	ADIF	Description of the developments carried out on the magnetic microwire
Amine Dhemaied	SNCF Réseau	Coordination of contributions to the document, main contributor chapter 7 (UC13.3, France), contributor chapters 1-6, 10
Rune Schlanbusch	NRD/NORCE	Contributor chapter 8.2 (UC13.4, Norway), 8.4, 6, 9
Christos Sakaris	NRD/SINTEF	Contributor chapter 8.2 (UC13.4, Norway)
Afaf Saai	NRD/SINTEF	Main contributor chapter 8.2 (UC13.4, Norway)
Stefano Derosa	NRD	Contributor chapter 3, 6, 8.4, 9
Alfredo Nunez Vicencio	ProRail/TUDelft	Contributor chapter 8.3 (UC13.4, Netherlands), 8.4, 6, 9
Rolf Dollevoet	ProRail/TUDelft	Contributor chapter 8.3 (UC13.4, Netherlands)
Zili Li	ProRail/TUDelft	Contributor chapter 8.3 (UC13.4, Netherlands)
Wassamon Phusakulkajorn	ProRail/TUDelft	Contributor chapter 8.3 (UC13.4, Netherlands) – Enhanced KPI
Chen Shen	ProRail/TUDelft	Contributor chapter 8.3 (UC13.4, Netherlands) – Vertical dynamics, enhanced KPI
Siwarak Unsiwilai	ProRail/TUDelft	Contributor chapter 8.3 (UC13.4, Netherlands)
Li Wang	ProRail/TUDelft	Contributor chapter 8.3 (UC13.4, Netherlands) – Vertical dynamics, Multi-ABA at transition zones
Yuanchen Zeng	ProRail/TUDelft	Contributor chapter 8.3 (UC13.4, Netherlands) – Vertical dynamics
Arjen Zoeteman	ProRail	Contributor chapter 8.3 (UC13.4, Netherlands)
Vincenzo Scarnera	MERMEC	Work Package Leader, final review

Table of Contents

List of Figures

List of Tables

1. Executive Summary

This deliverable, part of WP13, presents the implementation and demonstration of monitoring technologies for tunnels, sub-ballast layers, and subsoil (task T13.3), as well as bridges and embankments (task T13.4). Building on the technical specifications developed in WP12, the main goal is to support intelligent maintenance strategies based on real-time condition monitoring.

The approach includes defining user needs, deploying in-situ monitoring acquisition, collecting and processing data, and applying analysis tools designed for predictive maintenance. This deliverable demonstrates the feasibility and assesses the relevance of the developed systems and technologies. Field tests and a benchmark have been conducted along a railway track and in tunnels. Initial field demonstrations have validated the operational effectiveness of the systems, their capability to detect early structural or geotechnical issues, and their potential to improve maintenance planning and asset management. This deliverable presents the design of a monitoring system for bridges, along with the development and analysis of a new track quality index for on-board monitoring of support conditions by combining track geometry (from standard measurement vehicles) and axle box acceleration measurements (from potentially passenger trains).

The present document is divided into the following chapters:

Chapter 3: recapitulates the background related to the development and implementation of high-performance systems dedicated to monitoring tunnels, sub-ballast layers, subsoil, and bridges. The two use cases (France and Spain, the Netherlands and Norway) have been developed by industrial partners and infrastructure managers, accordingly to the specifications described in WP12.

Chapter 4: briefly describes the aims of the two use cases. The France and Spain use case involves tunnels, sub-ballast layers, and subsoil inspection and monitoring. The Netherlands and Norway use case focuses on practical methods for condition monitoring of railway infrastructure, with a focus on embankments and bridges.

Chapter 5: The objective of this chapter is the development and implementation of systems to evaluate the mechanical properties of sub-ballast layers and subsoil. This approach will help us understand and comprehend the emergence of anomalies in the subsurface by using the MASW method. For the tunnel asset, two objectives will be addressed to develop (1) high-efficiency tunnel inspection systems to detect visual damage evolution and Predictive maintenance for tunnels automatically, and (2) analysis of the use of passive contactless magnetic microwire sensor arrays for high-definition tunnel convergence monitoring systems.

Chapter 6: The objective of this chapter is to explain the activities related to Use Case 12.4, which investigates practical methods for condition monitoring of railway infrastructure, focusing on embankments and bridges both in Norway and the Netherlands. The Dutch contribution focuses on monitoring the condition of railway support at embankments by identifying locations where

excessive track geometry deformation occurs, using track geometry data as the current standard, in combination with dynamic onboard measurements using ABA measurements. The Norwegian contribution addresses the challenge of upgrading and extending the life of existing bridges to meet future demand for freight transport. The current methodology relies on manual inspection and conservative assumptions and will be updated with advanced structural models supported by data from a multi-sensor monitoring system.

Chapter 7: This section describes the assets on which the Key Performance Indicators (KPIs) will be calculated in the upcoming deliverable D13.3: Civil Engineering Asset Management Demonstration and Validation Report. The MAWP KPIs will be linked to the performance indicators of Use Case 12.3 (Franch and Spain) and Use Case 12.4 (the Netherlands/Norway).

2. Abbreviations and acronyms

Abbreviation / Acronym	Description
ABA	Axle Box Acceleration
ACF	AutoCorrelation Function
ADIF	Administrador de Infraestructuras Ferroviarias
ADN OST	Analysis of Digital Data for Underground Structures
AI	Artificial Intelligence
AL	Alert Limit
AUC	Area Under the Curve
BBMS	Branche Breed Monitoring Systeem
BIC	Bayesian Information Criterion
CAD	Computer-Aided Design
CL	Conventional Lines
CNN	Convolutional Neural Network
CWT	Continuous Wavelet Transform
DCP	Dynamic Cone Penetrometer
DEM	Digital Elevation Model
ELISE	Exploitation et Maintenance des Installations de Suivi des Essais
EnVTQI	Enhanced Vertical Track Quality Index
FD	Finite Difference
FEA	Finite Element Analysis
FRF	Frequency Response Function
FT	Full Track
FWD	Falling Weight Device
InSAR	Interferometric Synthetic Aperture Radar
LL	Longitudinal Level
MAC	Modal Assurance Criterion
MASW	Multichannel Analysis of Surface Waves
MAWP	Multi-Annual Work Program
ML	Machine Learning
MM-AR	Multiple Model AutoRegressive
ODS	Operational Deflection Shape
OLS	Ordinary Least Squares
OST	Underground Structures
PDF	Probability Density Functions
PLA	Polylactic Acid
PM	Prediction Model
PSD	Power Spectral Density
RADIS	Computerized Detailed Damage Survey of Underground Structures

Abbreviation / Acronym	Description
RE	Railway Earthwork
SAWP	Scale Averaged Wavelet Power
SCANTUBES®	Name of a system for scanning tubular structures, such as tunnels
SD	Standard Deviation
SITES	Name of the company that performed photogrammetric surveys
SNCF	Société Nationale des Chemins de fer Français
TG	Track Geometry
TPU	Thermoplastic Polyurethane
TRL	Technology Readiness Level
UC	Use Case
VAR	Vector AutoRegressive
VS	Shear-Wave Velocity

3. Background

The present document constitutes Deliverable D13.2, “Monitoring of tunnel, sub-ballast layers, subsoil and predictive maintenance for tunnels implementation & data analysis for condition monitoring system implementation report,” in the framework of the Flagship Project 3 – IAM4RAIL (GA 101101966), as described in the EU-RAIL MAWP.

This work focuses on the development and implementation of high-performance systems designed for monitoring tunnels, sub-ballast layers, subsoil, track support condition (embankments), and bridges. These systems are designed to provide inputs for condition monitoring strategies by enabling the early detection of structural and geotechnical issues.

By continuously assessing the condition of these infrastructure components, the systems contribute to ensuring operational safety and infrastructure reliability. In the long term, their deployment will enhance predictive maintenance capabilities and significantly improve the life-cycle management of railway tunnels and related subsurface assets.

The background of use case 12.4, Dutch analysis, utilizes the ABA technology developed and patented by TUDelft. This technology has been utilized in the In2Track3 project to achieve Technology Readiness Level 7 in the detection of rolling contact fatigue (RCF). In the FP3-IAM4RAIL project, this technology was further developed by integrating it with conventional/standard track geometry data. This combination enabled the monitoring of track support conditions, specifically the condition of ballast and under ballast layers, with the aim of assessing embankment stability.

4. Objective/Aim

The present Deliverable D13.2 is linked to task T13.3 (French Use Case) and task T13.4 (Norwegian and Dutch Use Case, respectively), both described in the Grant Agreement.

In relation to task T13.3, this document outlines the methodologies adopted for monitoring tunnels, sub-ballast layers, and subsoil. It details the strategies for in-situ data acquisition and the data analysis approaches developed to support predictive maintenance.

For tunnel monitoring, this strategy is implemented through three approaches:

- The development and deployment of degradation prediction algorithms. These algorithms leverage all available data related to the structural and environmental characteristics of the tunnels, as well as condition data collected during monitoring operations.
- The deployment of new inspection technologies aimed at facilitating the detection and quantification of defect evolution.
- The evaluation of magnetic microwires as passive, non-invasive sensors capable of detecting structural deformations, offering a promising solution for continuous tunnel condition monitoring.

For the monitoring of sub-ballast layers and subsoil, one of the key objectives of this task is to develop an optimized workflow for data acquisition, processing, inversion, and interpretation of seismic data. These data are then combined with geotechnical and hydrogeological data.

In relation to task T13.4, this document outlines the methodologies adopted for condition monitoring of civil structures and works (Norway) and embankment stability assessments (the Netherlands). Additionally, new requirements for the type of data and sensors are being evaluated to provide pieces of experimental evidence that can be used in the definition of future European standards. For structural condition monitoring of civil structures and work the approach sees the installation of a new measuring system on two adjacent concrete bridges and relative transition zones, which will provide data to validate a numerical model of both and will allow the creation of new method for data analysis for structural health assessment of the bridge in various operating conditions. For the embankment stability assessment, the approach is to utilize train-borne measurements (ABA) to enhance the current methodology, which is based solely on track geometry measurements. We considered locations with significant variations in track geometry, exhibiting excessive deformation compared to other locations. In FP3-IAM4RAIL, we first evaluated the capabilities of ABA to detect variations in the support condition. For this reason, we initially focused on the analysis of transition zones, where a sharp transition in the embankment occurs. Once we identified and quantified the physical aspects of the signals at transition zones, the next step was to propose a new track quality index that combines track geometry and ABA, capturing more subtle changes than those at transition zones. Field test validation, including data from the Netherlands, Sweden, and Norway, is reported in this deliverable, along with measurements taken using the CTO train of TUDelft in the Netherlands for the definition of the new track quality index.

5. Monitoring of tunnel, sub-ballast layers, subsoil, and predictive maintenance for tunnels (Use Case 13.3, France and Spain)

5.1. Introduction

This section describes the activities of Use Case 13.3. Regarding tunnels, degradation prediction models for the structures were developed as part of this project. These models utilize data collected during inspections conducted every six years. A tool has been deployed to run simulations and assist engineers in optimizing their diagnostics and maintenance recommendations.

New inspection technologies have also been tested to improve the traditional inspection methods. Algorithms have been tested to automatically detect visual or geometric changes.

During this project, the use of the seismic method (active and passive approach) to assess the quality of the sub-ballast layer and to monitor the subsoil (sinkhole hazard and hydrogeological context) has been widely developed and adapted to the railway environment. The improved approaches have been tested in real conditions: the field with mechanical evolution of the sub-ballast layers and sites with sinkhole phenomena. The development of new processing methods will be presented in this report.

The use of magnetic microwires has been investigated as non-invasive sensors for monitoring deformations in railway tunnels, offering an alternative to traditional methods that require on-track personnel and traffic interruptions. These microwires, due to their magnetostrictive properties, alter their electromagnetic response when subjected to mechanical stress.

5.2. Tunnel monitoring and predictive maintenance

5.2.1. Tunnel predictive maintenance

5.2.1.1. Introduction

Tunnel monitoring is based on conducting periodic and detailed inspections. The findings from these detailed inspections are recorded in a damage report. To best assess the progression of structural degradation, these reports need to be precise and exhaustive. To enable optimized asset management (particularly in terms of prioritizing regeneration operations), these reports must also be homogeneous for all structures.

Figure 1: Traditional periodic detailed inspections

To better meet these needs, SNCF Réseau developed the "Detailed Computerized Damage Survey of Underground Structures" application (known as RADIS) in 1997, allowing for computerized entry of observations from detailed inspections to standardize practices and limit the risks of heterogeneity, especially in terms of representing disorders symbolically. This application is associated with Computer-Aided Design (CAD) software such as Autocad® or Bricscad®.

Since 2006, the evaluation of the condition of structures has been integrated into the software. This is an automated application, called "tunnel rating or tunnel quotation," which is based on information from the facade survey produced during regulatory detailed inspections. The obtained score is a numerical representation of the density of listed disorders over a given area, specifically a 10-meter window. A calculation is performed every 5 meters to obtain a continuous curve of condition scores based on metric points.

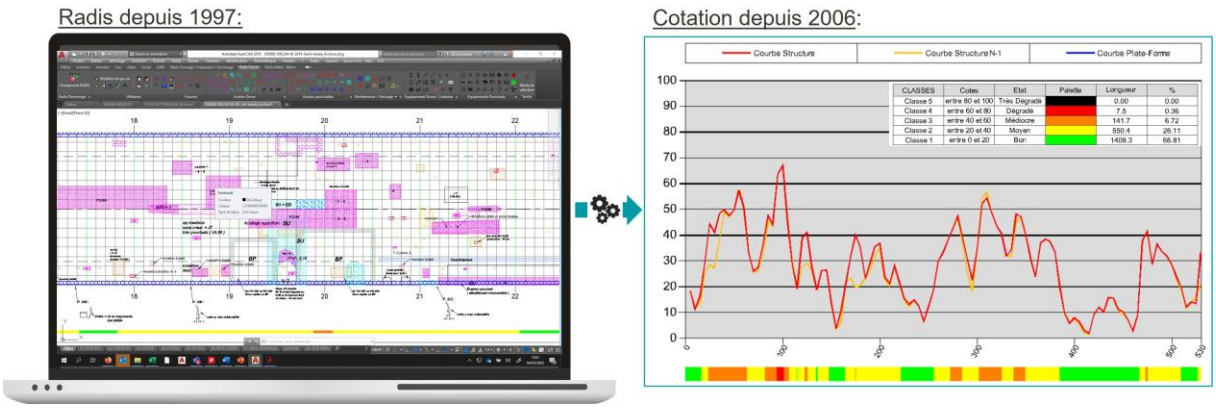

Figure 2: Illustration of RADIS and tunnel rating

The tunnel score ranges between 0 and a maximum of 100 points, and condition classes have been defined (Good condition, Average, Poor, Degraded, Very Degraded). A structure in good condition has a low score, whereas a degraded area has a high score.

The analysis of the automatic grading allows for quick identification of tunnel sections that are in poor condition and/or exhibit significant changes in their condition.

The objective of the work carried out within the framework of this project was to utilize all the data collected in the RADIS application to attempt to predict the degradation of underground structures and thereby optimize the planning and funding of regeneration operations.

5.2.1.2. Methodology

The methodology is organized into several steps:

- Analysis, structuring, and data quality improvement of the database;
- Selection and configuration of prediction models;
- Evaluation of the performance and limitations of the prediction models;
- Development of a simulation tool for the degradation of structures.

5.2.1.3. Database structuring

In 2022, a company specialized in data science and predictive maintenance analysed the SNCF data sources to assess data quality and determine the feasibility of a predictive maintenance project.

Several factors (length of the structure, age of the structure, type of predominant coating, etc.) are available in the data.

The analysis allowed us to assess the impact and significance of certain factors on the evolution of the rating.

For example, we observed that the entries and exits of the structures age faster than the center of the structures.

Table 1: Influence of factors on speed (examples)

Factor	Influence on the speed of degradation
Rating	A higher minimum rating leads to higher speeds
The year of inspection	The most recent inspection records lower speeds
The position or metric point	Speeds are higher at the ends of the structures
The size of the structure	Smaller structures age more quickly than medium-sized ones

The analysis also made it possible to highlight, complete, or refine certain data, such as geology or ground thickness above the tunnel. The database was therefore updated accordingly.

The same type of analysis was conducted on the disorders to evaluate those that have a significant influence on the degradation of the structure.

5.2.1.4. Selection and configuration of prediction models

Two prediction models were studied.

- ***Decision tree model :***

A decision tree is a decision-support tool that represents a set of choices in the graphical form of a tree. The different possible decisions are located at the ends of the branches (the 'leaves' of the tree) and are reached based on decisions made at each step. A variant is known as a 'Random Forest.' This algorithm combines the concepts of random subspaces and 'bagging' by learning multiple decision trees and then applying a rule to make a single decision (typically majority voting).

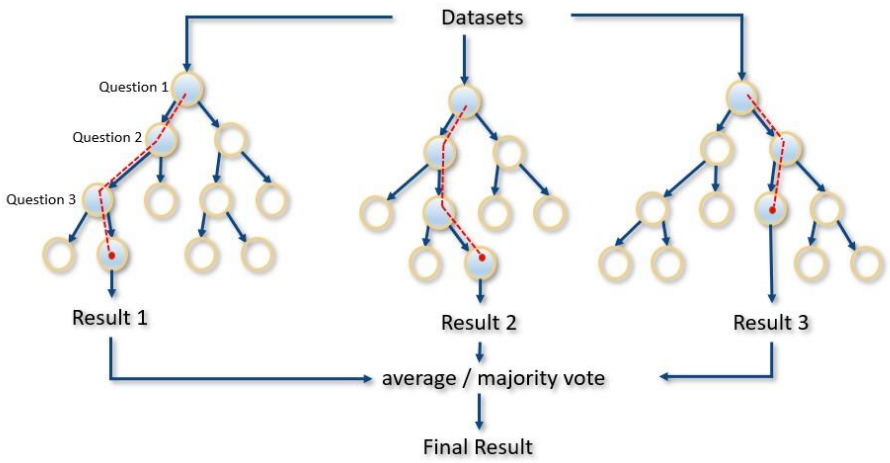

Figure 3: Synthetic example of how a decision tree model works

- ***Neural network model :***

The proposed architecture is a neural network designed to handle spatial correlations of ratings and archival data; it is divided into two sub-models. Initially, the time series of neighboring ratings and the rating to be predicted are encoded using convolutional layers. This first sub-model addresses the spatial aspect of the data. The encoded time series is then fed into a second model, along with the influencing factors. This second sub-model is a neural network that handles temporal dependencies.

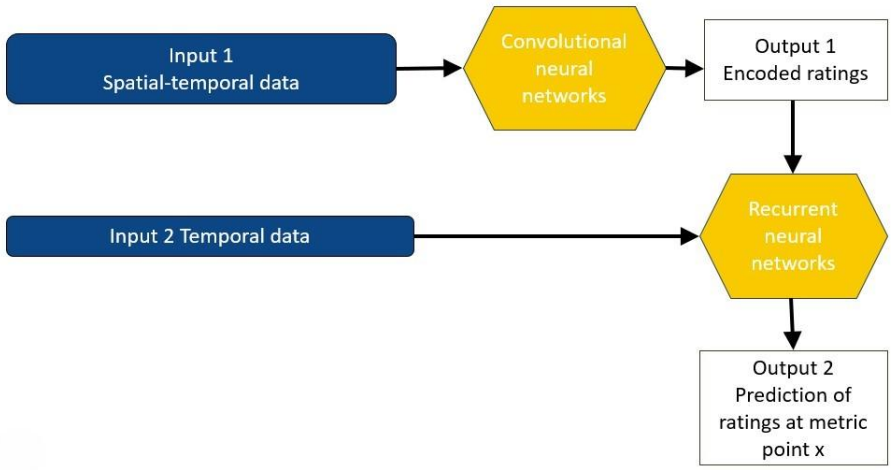

Figure 4: Synthetic example of how a neural network model works

Performance of the neural network model:

The neural network predicts a rating per PM. The distribution of the prediction error (or residual) is centered around 0 and is concentrated within the [-5; 5] rating interval. However, it is slightly skewed towards negative values, indicating a tendency to underestimate observations. It should be noted, however, that the model performs well regardless of the observation value, with high ratings being predicted accurately.

Due to the difficulty in explaining the prediction process despite highly satisfactory results, SNCF decided not to continue with this model, as it is too opaque (black box)

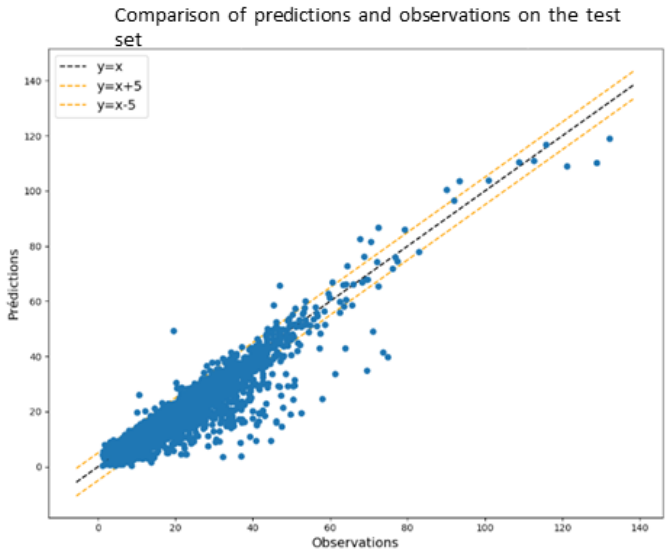

Figure 5: Performance results for the neural network model. 75% of the predictions fall within the [rating-5; rating+5] interval

Performance of the decision tree model: Gradient Boosting:

The gradient boosting model predicts a speed per metric point. The rating per metric point is reconstructed from this predicted speed. The performance shown by this model (76.6% within [-5; 5]) is better than the results provided by the neural network (75% within [-5; 5]). At the end of 2023, SNCF decided to retain this model to integrate it into the digital decision-making tool, with the aim of improving transparency and the understanding of its outcomes.

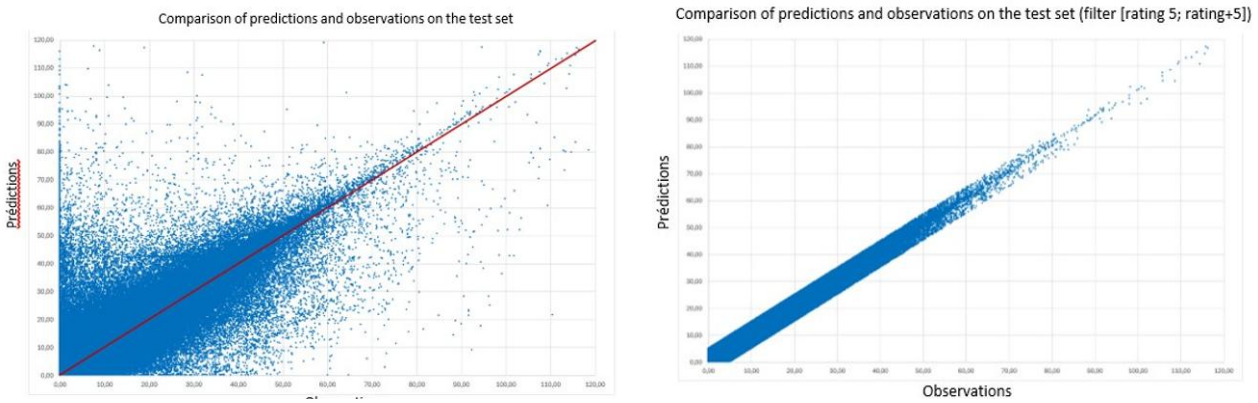

Figure 6: Performance results for the Gradient Boosting model. 76,6% of the predictions fall within the [rating-5; rating+5] interval

The limitations of forecasting models are primarily evident through several critical aspects, including:

- The inability to predict significant price increases without prior indicators or linked to an unforeseen event:

Forecasting models generally relies on past trends, historical correlations, and rational assumptions. However, they show their limitations when it comes to anticipating sudden or unpredictable events, such as natural disasters, extreme climate events, unexpected structural disruptions, or repair operations. These events, which can cause sharp price increases or decreases, often do not fit into any of the modeled trends, making them difficult to account for. Traditional models fail to predict these movements as they lack clear early warning indicators and are often incapable of reacting to unmodeled external factors.

- The quality of input data:

The reliability and accuracy of models directly depend on the quality of the data provided to them. If the input data is incomplete, inaccurate, or biased, the model will produce forecasts that deviate from reality. Data management is, therefore, crucial: its collection, cleaning, and updating must be done with care. Models are thus exposed to misinterpretation or suboptimal decisions when the data is insufficient or skewed.

In conclusion, while forecasting models are powerful tools, they remain limited, particularly when faced with the unpredictability of sudden events and the variability of input data quality. These factors must be considered to avoid placing excessive trust in the results provided by these models.

5.2.1.5. Development of a simulation tool for the degradation of structures.

A decision support tool (ADN OST – Analysis of Digital Data for Underground Structures), assisted by AI, is developed since 2024. It builds on research conducted in 2022 and 2023.

The tool incorporates a Machine Learning model (Gradient Boosting) and a prediction module that allows visualization of the projected aging of underground structures using two indicators:

- The potential rate of deterioration of tunnels.
- A forecast of the condition rating of the structures at future timeframes.

It is an operational tool that allows engineers specializing in tunnel inspection to easily use the prediction model. Without this tool, the use of the models would remain a field reserved for data science specialists.

Figure 7: Application Interface of ADN OST

5.2.2. High-efficiency tunnel inspection systems

5.2.2.1. Introduction

The project aims to evaluate and deploy new technologies to assist with tunnel inspections.

These constantly evolving systems rely primarily on technologies from the fields of photography, lidar, and infrared thermography. They offer the ability to obtain realistic, ultra-high-definition representations of structures, in both 2D and 3D. Mounted on mobile platforms, they also enable high-efficiency data acquisition.

SNCF Réseau has conducted several tests in railway tunnels to assess the potential of these new tools in supporting inspection tasks.

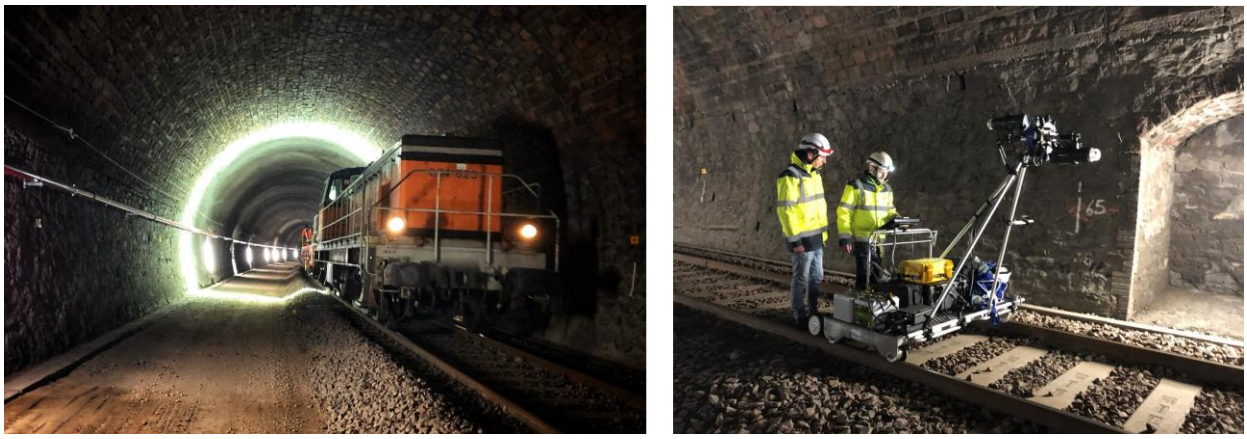

Figure 8: Examples of measurement systems (TS4® system by the company SPACETEC installed on an SNCF Réseau train on the left, and SCANTUBES® system by the company SITES on the right)

5.2.2.2. Description of new inspection technologies

- ***Photography and photogrammetry:***

Photographic capture allows for the reconstruction of two types of inspection-relevant renderings using stitching, photogrammetry, and projection techniques:

  - *A high-resolution, colour orthophotograph of the tunnel intrados:*

The resolution achieved (around 1 mm/pixel) makes it possible to detect cracks approximately 0.3 mm wide.

This orthophotograph can be directly used to map defects, facilitating the documentation of damage and the detection of changes over time. It also serves as an excellent tool for visit preparation and post-inspection self-checks.

However, it does not provide any depth information.

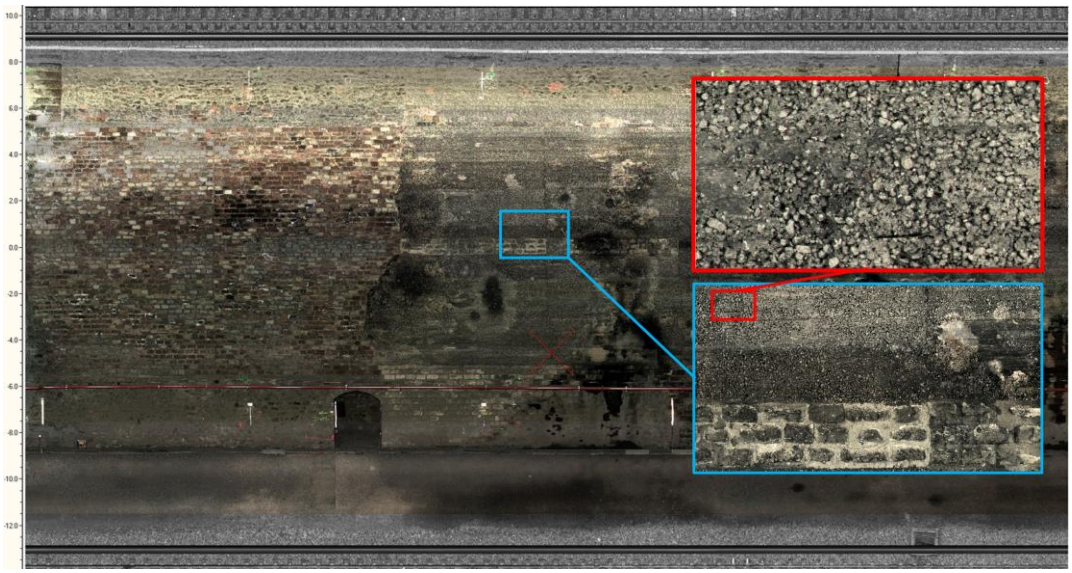

Figure 9: Illustration of a tunnel intrados orthophotograph and the achievable resolution level

- *A photorealistic 3D model:*

Although the point cloud accuracy—ranging from several millimeters to centimeters at the section scale—does not allow for fine geometric analysis, it is sufficient to visualize large-scale geometric irregularities (on the order of several tens of centimeters).

This type of rendering is particularly useful for visit preparation, as it provides an additional perspective on the structure, complementing the orthophotograph.

Figure 10: Example of a photorealistic 3D model

High-efficiency acquisition requires the use of cameras capable of 360° imaging. Given the low lighting conditions, powerful illumination must be combined with photography using LED light rings or flashes synchronized with the shutter release.

The acquisition speed inside the structures ranges from 2 to 60 km/h or even higher, depending on the type of cameras (area sensors/line sensors) and lighting used.

- ***Lasergrammetry or lidar:***

Lasergrammetry uses motorized digital sensors, or scanners, that capture points with X, Y, Z coordinates with a relative accuracy of around 0.5 mm.

The resolution of the point cloud depends on the scanner's characteristics (rotation speed and number of points measured per revolution), the speed of the moving platform, and the distance between the scanned object and the scanner. The optimal speed should be between 2 and 5 km/h to achieve sufficient transverse resolution to identify masonry joints.

Lasergrammetry systems provide two types of renderings useful for tunnel inspection:

  - *A pseudo-orthophotograph of the intrados in black and white:*

It is obtained by representing the shades of gray corresponding to the reflectivity values of the measured points and by a "flat" projection according to the tunnel's development.

The resolution is significantly lower than that of orthophotographs obtained with photography (2.5 to 5 mm/pixel), but it still facilitates the identification and positioning of observed defects on site.

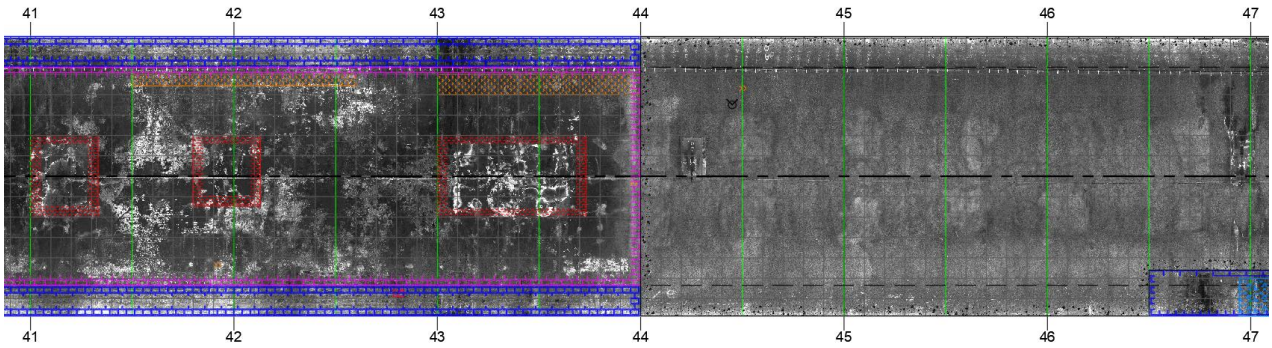

Figure 11: Overlay of a defect survey with a pseudo-orthophotograph obtained from a scanner

  - *A 3D point cloud:*

The higher accuracy compared to point clouds derived from photogrammetry allows for geometric analyses to characterize geometric irregularities or material losses (joint openings and surface defects). Identification can be performed automatically by comparing the measured profiles with one or more theoretical profiles.

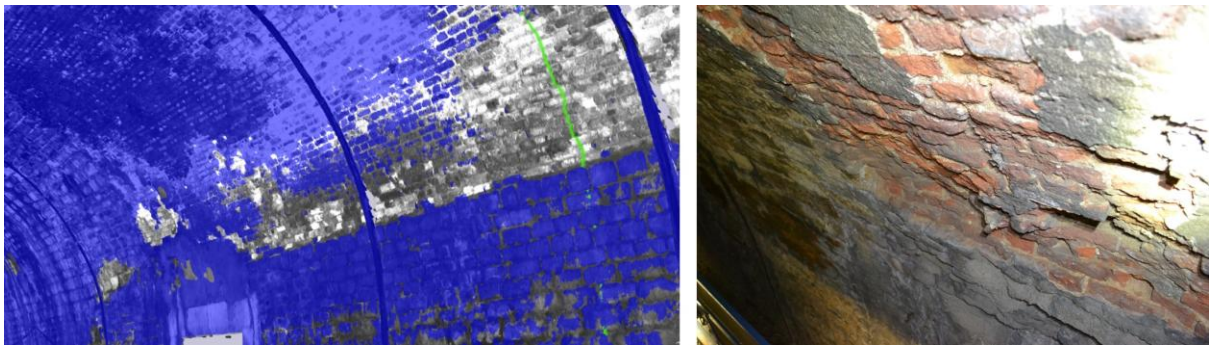

Figure 12: Automatic detection of a brick spalling area by comparing profiles measured by a scanner with a theoretical profile, alongside an in-situ photograph of the area taken during an inspection.

- ***Infrared Thermography:***

This involves measuring the tunnel's radiation, which is proportional to the surface temperature, to produce a map of the apparent temperature of the lining.

This technique notably allows indirect assessment of moisture intensity in the lining and makes it easier to distinguish active zones.

Producing a temperature map at the scale of the intrados enables its use in a defect survey. It is also possible to overlay this map with an orthophotograph to correlate the presence of defects with moisture areas.

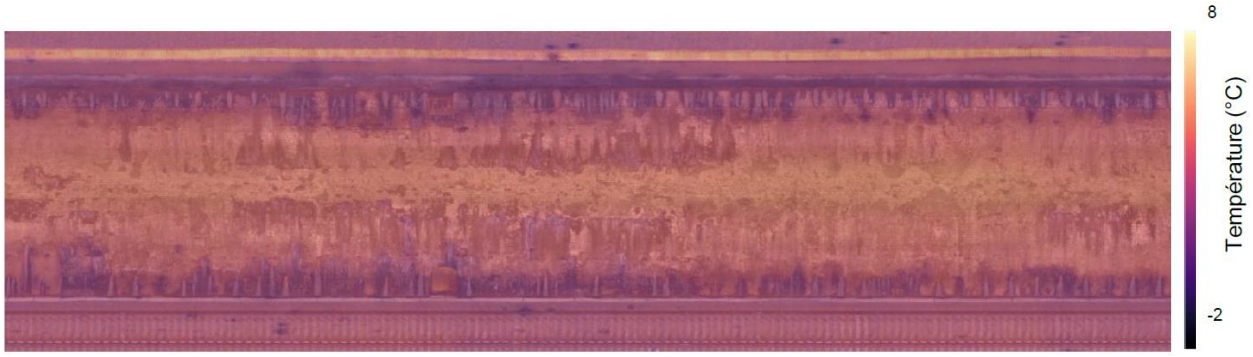

Figure 13: Overlay of an orthophotograph with the temperature survey

5.2.2.3. Evaluation of the performance and limitations of new inspection technologies

The main defects identified during traditional inspections are listed in the table below.

Table 2: Main defects investigated during detailed inspections (non-exhaustive list)

Types of Damage	Characterization
Cracking	Elongation – opening – spalling – misalignment
Surface damage (scaling, exfoliation, etc.)	Surface – maximum depth
Geometric irregularity	Surface – maximum amplitude
Joint separation	Surface – maximum depth
Moisture	Surface – Type (runoff, concretions, etc.)
Abnormal sounds during hammer tapping	Surface – Type (hollow, dull, clear)
Dislocation	Surface
Localized damage (broken/fallen rubble stones)	Units

New technologies supporting tunnel inspections can be an asset for identifying and characterizing defects. They improve the accuracy of surveys and, consequently, the assessment of structural deterioration. These technologies also assist in inspection preparation and self-checking at the end of the process.

For the most comprehensive identification and characterization of defects, the three technologies should be combined:

- **Photography** mainly provides a realistic, high-resolution view of the tunnel intrados, but offers little depth information (e.g., it cannot characterize crack spalling or joint separation depth).
- **Laser scanning (lasergrammetry)** enables the acquisition of precise three-dimensional geometric data. Orthophotos can also be generated to assist in defect mapping.
- **Infrared thermography** helps to pinpoint the location and intensity of moisture areas.
- For effective use of these surveys, it is essential that the acquisition and processing protocols are standardized across all three technologies. This is particularly important to enable comparison of data collected at different times.
- However, these technologies cannot fully replace traditional inspections, as not all defects can be identified and characterized using them. For example, hammer sounding has no real alternative, yet it is essential for detecting early signs of visual defects, identifying stressed or deteriorated surface zones, and performing safety purging.
- Some cracks may also be difficult to detect and characterize without close visual inspection of the lining, due to the roughness of masonry surfaces. Furthermore, despite the high resolution and precision of these new tools, the characterization of crack spalling and misalignment remains challenging and can even be inaccurate depending on the acquisition protocol and the location of the crack.
- Adjacent structures (e.g., recesses, tunnel portals, etc.) are also typically not covered during high-efficiency data collection.

- Finally, these technologies cannot currently replace the main types of instrumentation used in tunnels (such as convergence measurements or crackmeters), which require highly accurate and high-resolution measurements.
- Considering both the advantages and limitations of these new tools, their use is currently seen as a complement to existing methods. The goal is to further improve the accuracy and objectivity of deterioration assessments and thereby optimize the prioritization of rehabilitation operations.

5.2.2.4. Disorder or change detection algorithms

Tests have also been conducted to automatically detect failures using image processing algorithms.

At this stage, and for tunnels representative of SNCF Réseau's assets, which have masonry coverings, the results have not been satisfactory due to an excessively high number of false detections. This is mainly due to the high heterogeneity of the materials used, construction defects, the presence of soot, inscriptions on the facings, moisture, etc. For concrete facings, uniform and homogeneous in terms of colorimetry/contrast, the results should be more positive.

A reorientation of the tests has therefore been made to this time attempt to automatically detect visual or geometric changes between two measurements.

For this purpose, failures were artificially created in an abandoned railway tunnel. Four photogrammetric surveys were conducted with SITES company and the SCANTUBES system after simulating disorders of different intensities. Orthophotographs and overlays between the digital elevation model (DEM) and the slope map were generated during each pass.

Figure 14: Disorder simulation

Figure 15: Photogrammetric survey with the SCANTUBES system from the company SITES

Orthophotographs and overlays between the digital elevation model and the slope map were generated during each pass:

Figure 16: Extract from the orthophotography

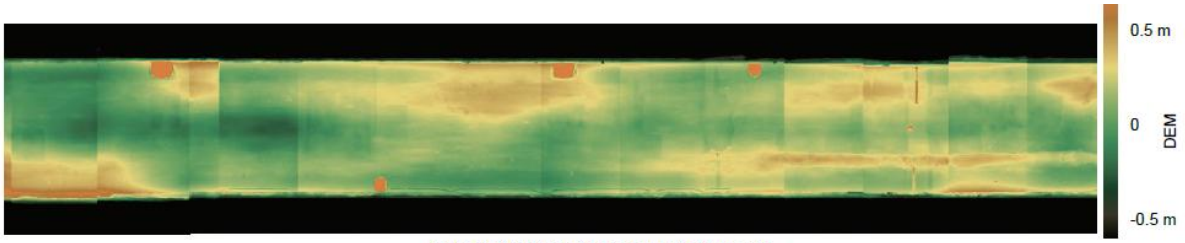

Extrait DEM du tunnel de Pommeraie

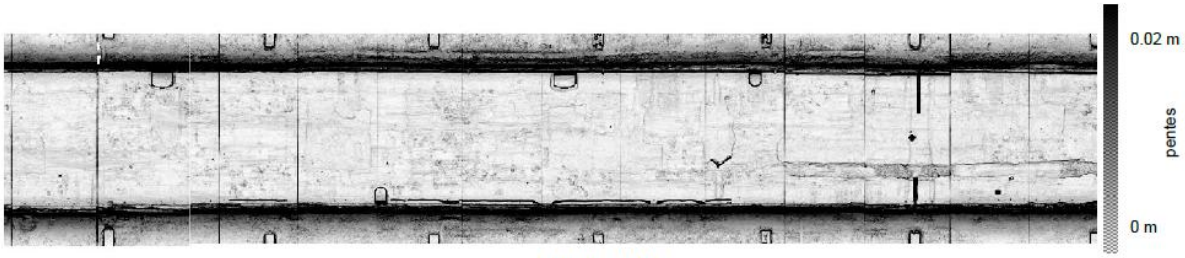

Extrait pentes

Extrait superposition carte des pentes / DEM

Figure 17: Extract from the orthophotography

These different renderings are overlaid pixel by pixel during each pass.

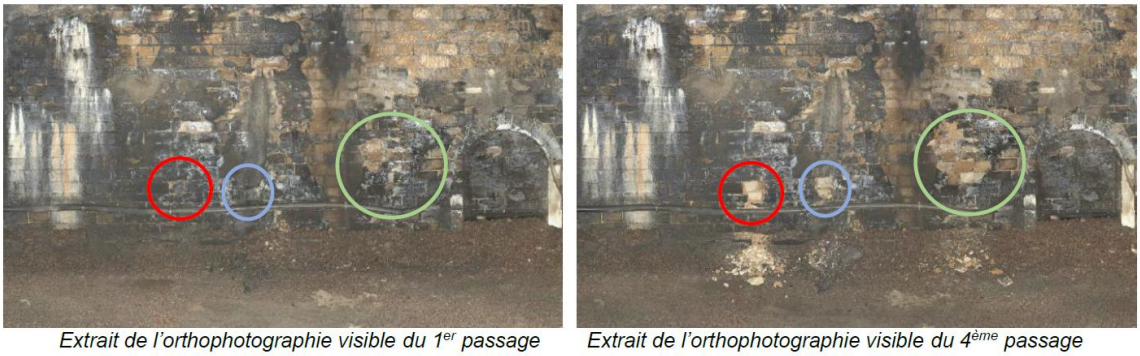

Extrait de l'orthophotographie visible du 1er passage

Extrait de l'orthophotographie visible du 4ème passage

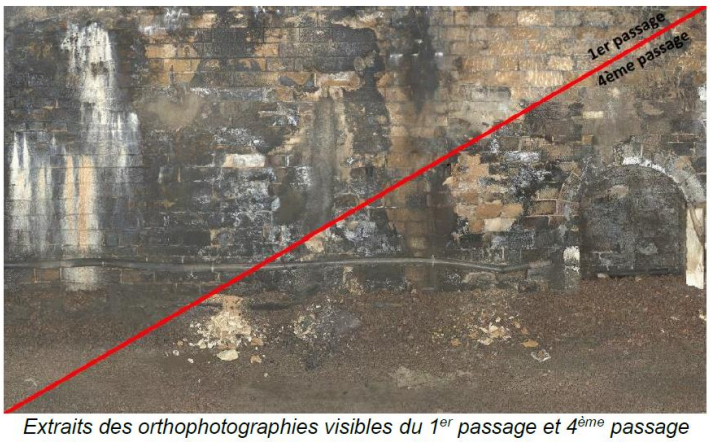

Extraits des orthophotographies visibles du 1er passage et 4ème passage

Figure 18: Extracts of orthophotographs at different pass

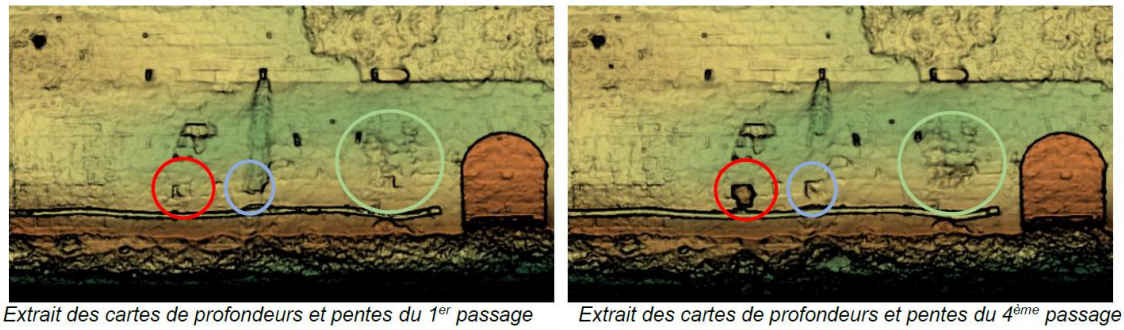

Extrait des cartes de profondeurs et pentes du 1er passage

Extrait des cartes de profondeurs et pentes du 4ème passage

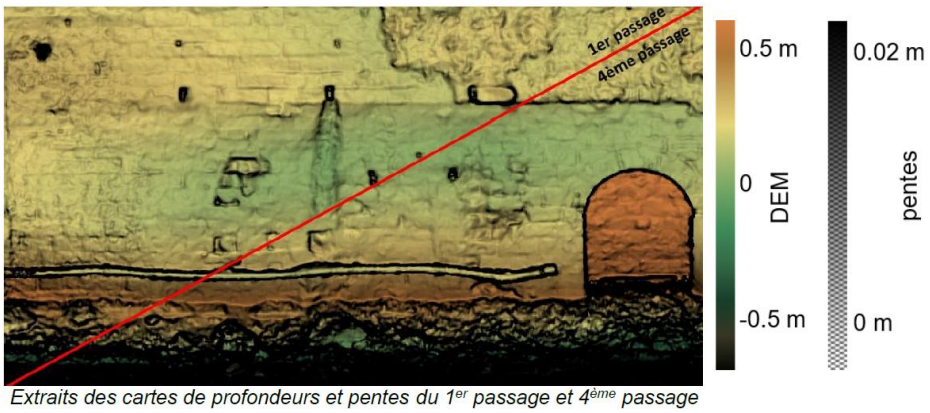

Extraits des cartes de profondeurs et pentes du 1er passage et 4ème passage

Figure 19: Extracts of DEM at different pass

To detect changes between the different renderings, we focus on the difference between them as they are overlaid pixel by pixel.

- ***Differences in depth maps between the 4th and the 1st pass:***

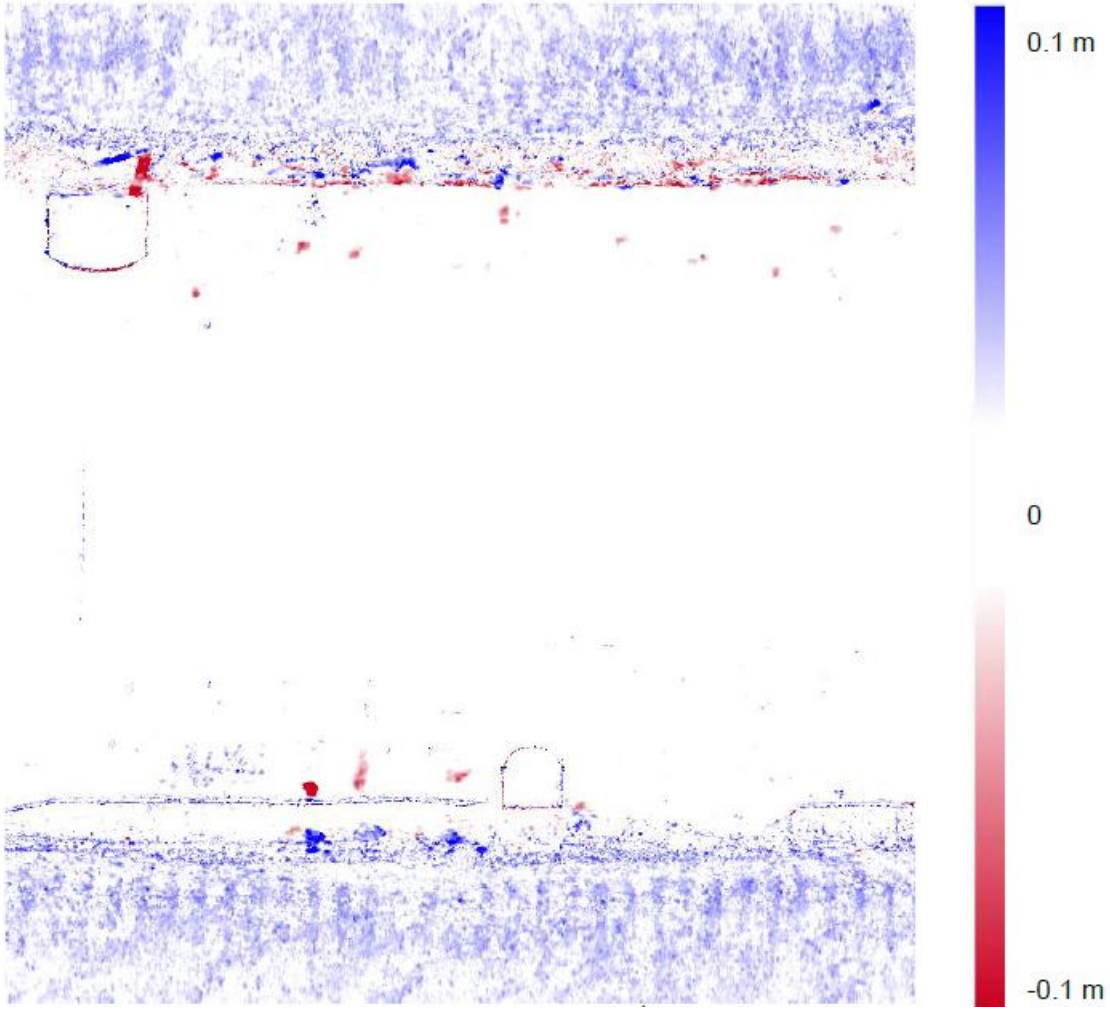

Figure 20: Identification of differences in depth maps between the 4th and the 1st pass

The material losses on the pier and the material gains on the ground are visually easy to spot. The 3D reconstruction of the ground being complicated on gravel, the mesh and the DEM smooth the ground and cause false positives.

- ***Differences in orthophotographs visible between the 4th and 1st pass***

Subtracting the 1st pass from the 4th pass gives us dark pixels in areas that have not undergone visual changes. In white, the differences are striking. However, be cautious, as this method is sensitive to slight differences in lighting.

Figure 21: Identification of differences in orthophotographs visible between the 4th and 1st pass

5.2.3. Passive contactless magnetic microwire

Throughout the project and up to deliverable 12.1, key parameters were optimized, such as the microwire length (8 cm), the number of wires (8), and the operating frequency (1.71 GHz). These parameters enabled the design of an optimal sensing patch capable of detecting the highest possible deformation.

Figure 22: First patch and prototype used

The system was tested on a tunnel prototype made of PVC material, under both confined and unconfined conditions, demonstrating that the microwire is capable of detecting even millimeter-scale deformations.

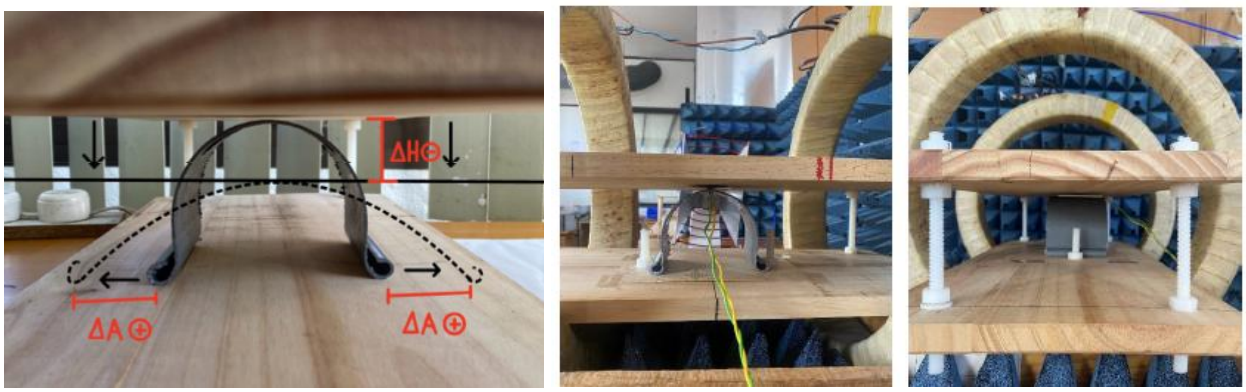

Figure 23: Load application on the old prototype

The results confirmed its effectiveness as a reliable sensing element for continuous structural health monitoring in railway infrastructure. This delivery presents the new tests and experiments carried out to further validate this capability.

Building on the experimental foundation and previous results, new developments have been conducted to enhance the system's sensitivity, structural integration, and real-world applicability. The steps taken are described below:

The first step was the construction of a larger-scale setup to closely simulate real-world conditions and progressively increase the size of the experimental tests. Additionally, tests were performed by increasing the distance between antennas to evaluate potential limitations in realistic deployment scenarios.

The first trial in this new phase used a concrete tunnel prototype, chosen because concrete is the most common material used in railway tunnels. For the first time, the press was used to apply a greater load than in previous tests. However, it was concluded that this prototype was unsuitable: the concrete broke almost immediately upon load application, without undergoing measurable deformation. This renders it ineffective for the objective of this study, which is to assess the microwire's ability to detect structural deformations.

Figure 24: New load-applying press and concrete prototype

In parallel, a new patch was developed using 3D printing, in which the microwires were embedded into TPU material, known for its flexibility and deformability. This new design proved to be significantly more promising than the previous version, where microwires were simply attached to paper.

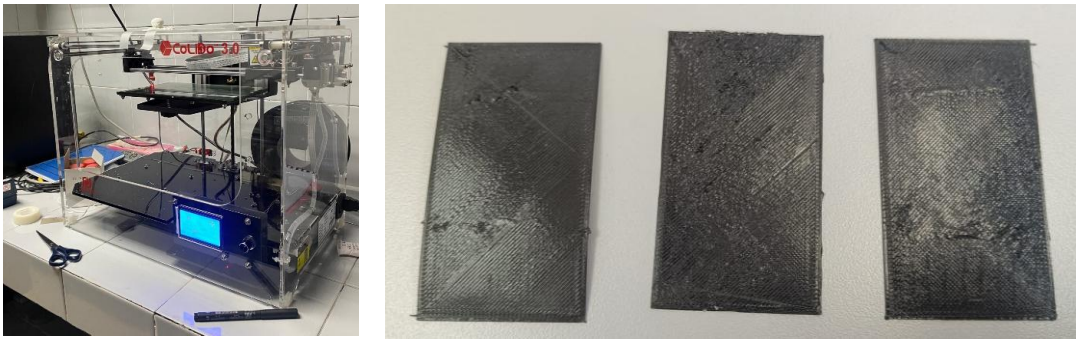

Figure 25: New patch made with TPU in 3D printer

Subsequently, another prototype was tested using 3D-printed PLA material, which is much more rigid. Like concrete, this material did not allow for meaningful deformation and fractured quickly under load, resulting in similar and equally unhelpful outcomes.

Figure 26: New prototype made with PLA in 3D printer

Finally, a tunnel prototype was fabricated using 3D-printed TPU, which demonstrated much greater deformability and the capacity to absorb progressive stress. This model provided a more suitable basis for continuing the evaluation of the microwire's sensing capabilities.

Figure 27: New prototype made with TPU in a 3D printer

The results obtained from this device were as expected and followed the same trend observed in initial trials: as the applied load increases, so does the variation in the S21 parameter, thereby reinforcing the viability of microwires as structural sensors.

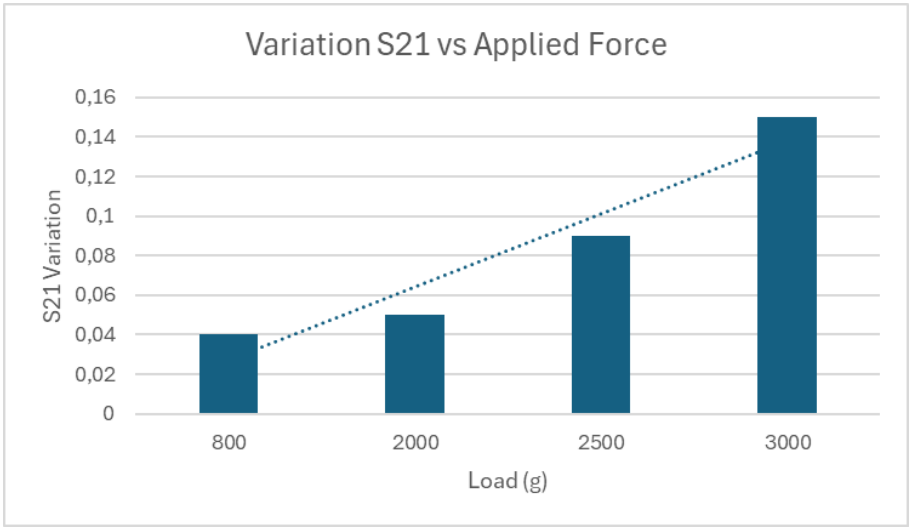

Figure 28: Variation S21- Applied Force Graph

5.3. Sub-ballast layers and subsoil monitoring

After validating the seismic approach using an adapted acquisition and processing workflow, the robustness and reliability of the method have been clearly demonstrated in previous studies. The results confirm that the seismic technique is well-suited for detecting variations in VS within the sub-ballast layers and underlying subsoil. This validation phase was essential to establish a solid reference framework before implementing more advanced techniques of acquisition, processing, inversion, and interpretation.

5.3.1. Acquisition and processing

The objective of this section is to enhance the overall efficiency of seismic data acquisition and to move towards greater automation in data processing. Traditional seismic methods, while accurate and widely validated, often involve labor-intensive and time-consuming procedures that limit their applicability in operational contexts such as RE characterisation and monitoring.

By significantly increasing the acquisition speed and by integrating automated or semi-automated tools for data processing, the proposed approach aims to make both active seismic surveys and passive seismic monitoring more practical, repeatable, and scalable.

This evolution is particularly important in the context of railway environments, where accessibility is often constrained, time windows for field operations are limited, and safety requirements are strict. The ability to rapidly acquire high-quality data with minimal manual intervention and to process it efficiently and consistently opens the door to more routine deployment of seismic methods for infrastructure assessment.

Ultimately, the integration of high-efficiency acquisition and automated processing contributes to making seismic techniques more compatible with the operational constraints and inspection

cycles of modern railway networks. This paves the way for their use not only in one-off diagnostic campaigns but also in long-term monitoring strategies aimed at ensuring the structural integrity and performance of railway earthworks over time.

5.3.1.1. Active seismic data acquisition with higher efficiency

For seismic data acquisition, we implemented and tested a seismic landstreamer system, which consists of a linear array of geophones integrated into a robust, towable cable (Figure 29). This setup allows the sensors to maintain good ground coupling while being easily moved along the railway track, enabling rapid and repeatable acquisition across extended profiles. In contrast to conventional acquisition methods, where geophones must be manually planted and repositioned at each measurement point, the landstreamer offers a highly mobile and time-efficient solution, particularly advantageous in environments with limited access or operational constraints, such as RE. The main benefit of this system lies in its ability to perform high-resolution surveys quickly and with minimal disruption to the site. The landstreamer reduces the logistical burden, shortens acquisition time, and minimizes human intervention, all while maintaining data quality.

To evaluate the performance and data reliability of the landstreamer setup, a dedicated comparative measurement campaign was conducted. This campaign aimed to benchmark the landstreamer against a conventional fixed geophone array, which serves as the standard reference in seismic surface-wave studies. The comparison focused on key aspects such as quality of the data, signal-to-noise ratio, and the resulting dispersion curves. This validation step was essential to confirm that the increased operational efficiency provided by the landstreamer does not come at the expense of data quality or interpretability.

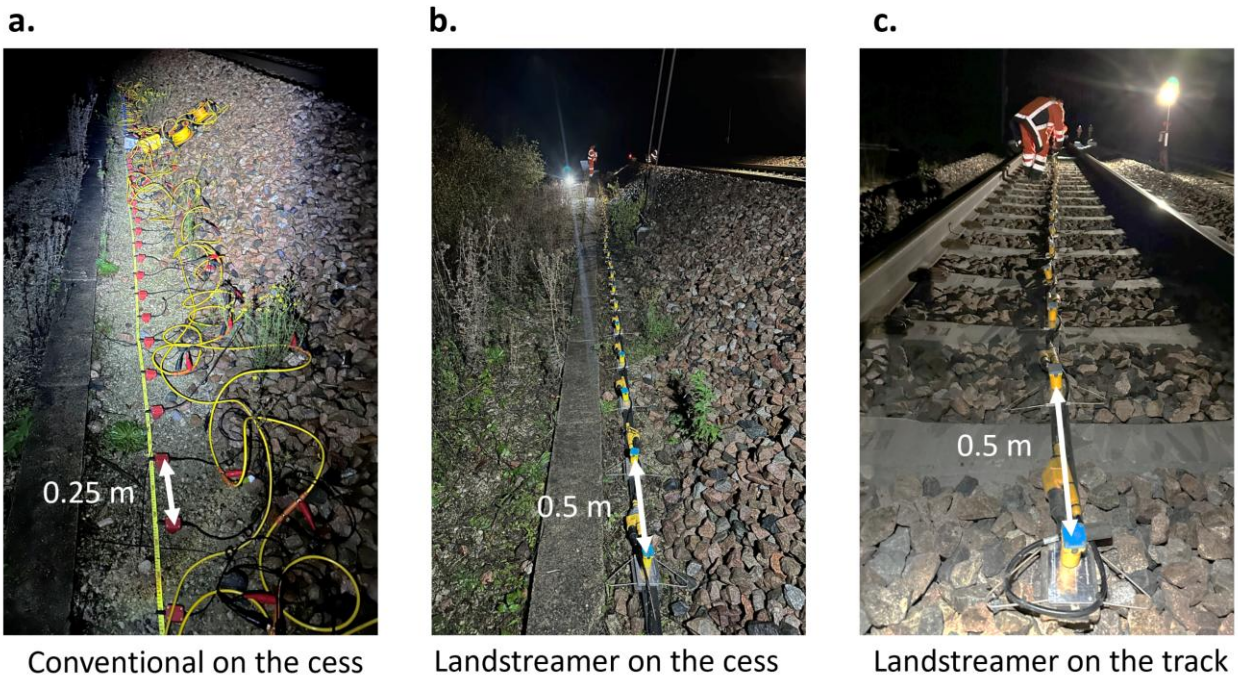

Figure 29: Photography of the conventional seismic setup placed on the cess. b. Photography of the landstreamer placed on the cess. c. Photography of the landstreamer placed on the track

Equivalent acquisition parameters were used in both configurations on identical test sections along a track maintenance anomaly zone, with fault geometry and mud pumping into the ballast layer on the South-East European HSL. Raw and processed seismic data from both the conventional and landstreamer acquisition setups were meticulously compared to assess their respective performance and reliability (Figure 30). The comparison included an evaluation of the seismogram, frequency content, signal-to-noise ratio, and dispersion curves. Despite differences in acquisition parameters—such as source type, geophone coupling, and sampling configurations—the landstreamer data exhibited comparable quality to that of the conventional setup. In particular, the surface-wave energy was clearly identifiable, and the resulting dispersion curves were consistent across both systems. These results confirm that the landstreamer setup, although more mobile and operationally efficient, provides data of sufficient quality for reliable surface-wave analysis in railway environments.

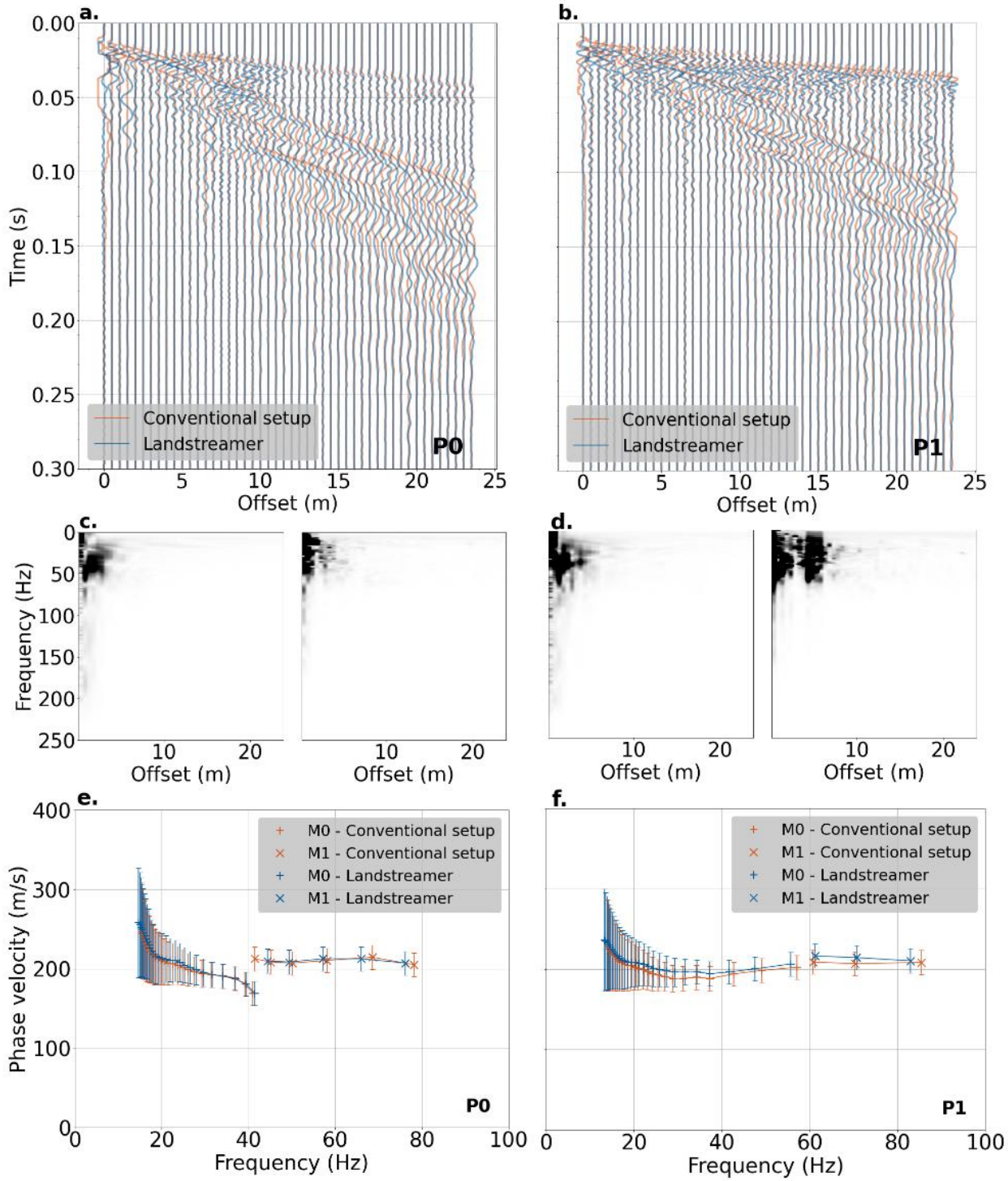

Figure 30: Comparison of seismic data from a conventional setup (orange) and landstreamer (blue lines) of the direct shot for two distinct positions (P0 and P1) along the line.

5.3.1.2. Tools for automatic processing

To automate the processing of surface-wave data, we developed an automatic processing tool specifically designed for the extraction of surface-wave dispersion curves. This step, traditionally performed manually, is not only time-consuming but also subject to operator bias. Our objective was to automate this critical phase to enable efficient and consistent processing across large monitoring datasets.

The core of our tool is a deep learning algorithm based on the U-Net architecture (*Figure **31**a*), originally developed for biomedical image segmentation. We adapted this architecture to create a custom model, named U2-pick. U2-pick is designed to perform two primary tasks:

- identify energy maxima within dispersion images, corresponding to propagating surface-wave modes;
- and associate the range of the previously identified modes.

To train U2-pick, we constructed a large synthetic training dataset using a Finite Difference (FD) modelling tool. This dataset includes a wide range of RE scenarios, incorporating variations in layer properties, velocity inversions, and noise levels (Figure 31).

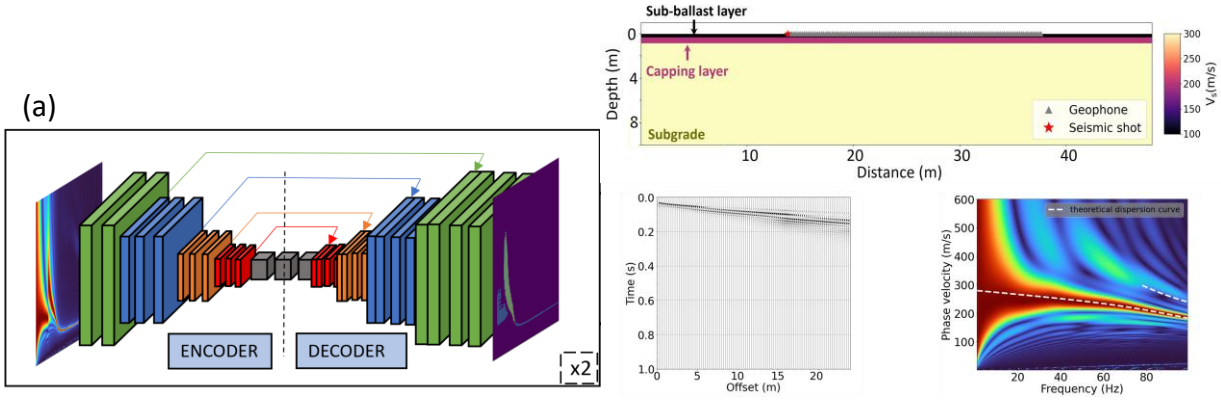

Figure 31: Database generation & conventional neural network (CNN) and U-Net architecture

The initial tests on synthetic data showed that U2-pick is capable of accurately detecting and classifying dispersion (Figure 32a).

Subsequently, the model was applied to real seismic datasets acquired in the field, particularly within the HSL context. While U2-pick performed well in recognising fundamental modes and capturing their behaviours, the transition to real-world data also revealed several limitations (*Figure 32: (a) U2-pick results on synthetic data. (b) U2-pick results on real data acquired along the French North HSL.).* In particular, the model's performance degraded in cases involving high levels of ambient noise, weak dispersion signals, or overlapping modes—scenarios.

These findings underscore the importance of further enriching the training dataset with field-

acquired examples that encompass the full range of complexities encountered in practice. Increasing the diversity and realism of training inputs is a necessary step to enhance the model's generalisation ability and ensure its robustness across different site conditions and acquisition setups. Future work will focus on integrating such real-case data and more complex synthetic data.

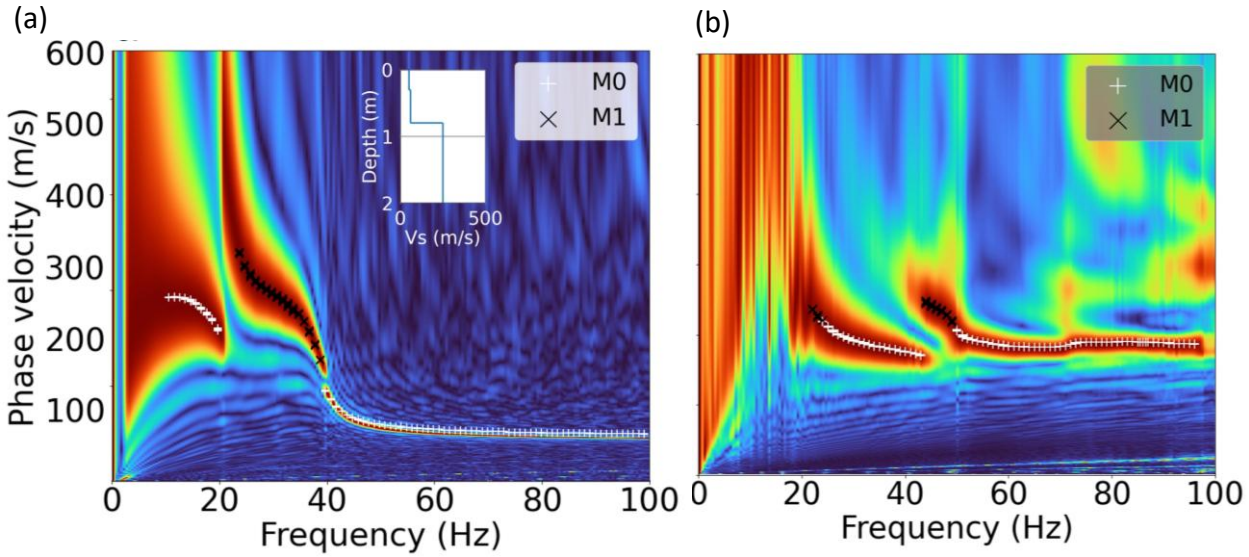

Figure 32: (a) U2-pick results on synthetic data. (b) U2-pick results on real data acquired along the French North HSL.

Towards a decision-support tool: probabilistic inversion

Accurate interpretation of seismic data is essential for the reliable characterization of RE. While surface-wave analysis provides valuable information about VS profiles, it is equally important to assess the confidence level associated with the inferred models. In this context, the inversion process is not only a tool for estimating physical parameters such as VS and layer thickness but also a critical means of quantifying the uncertainties associated with these estimations.
To address this dual objective, a probabilistic inversion approach grounded in Bayesian formalism has been implemented. The foundation of this method lies in Bayes' theorem, which provides a rigorous framework to update the probability of a model given observed data and prior knowledge. Mathematically, Bayes' theorem expresses the posterior probability of a model M, given data D, as:

$$P(M|D)=\frac{P(D|M)\cdot P(M)}{P(D)}$$

Here, P(M) represents the prior information about the model, for instance, expected values or ranges for VS or layer thickness based on construction standards, while P(D|M) is the likelihood, i.e., how well a model explains the observed data. The result, P(M|D), is the posterior probability distribution, which integrates both data and prior knowledge to provide a full probabilistic description of model parameters.

This Bayesian inversion framework offers several advantages over classical deterministic methods. First, it allows the incorporation of a priori knowledge about the expected structure of sub-ballast layers and subsoil, which is particularly valuable in highly standardized environments such as HLS, where the geometry and stratigraphy follow rigorous construction norms. Second, instead of yielding a single "best-fit" model, Bayesian inversion produces full a posteriori probability distribution for each parameter, allowing for a more transparent and comprehensive assessment of model uncertainty.

Initial tests of this methodology were conducted using a seismic dataset acquired along the North-European HSL. The probability density functions (PDFs) derived from the Bayesian inversion provide a detailed assessment of the resolution of each inverted parameter, along with their associated confidence intervals (*Figure **33**: (a) corner plot of a posteriori probability density function for each parameter of the mode. (b) a posteriori probability density function of the shear modulus (G) along the line.*). Each PDF not only indicates the most probable value of a given parameter but also quantifies the uncertainty surrounding that estimate, thereby enhancing the reliability and transparency of the interpretation.

*Figure **33**: (a) corner plot of a posteriori probability density function for each parameter of the mode. (b) a posteriori probability density function of the shear modulus (G) along the line.* focuses specifically on one key mechanical parameter: the shear modulus G, defined as:

$$G=\rho V_S^2$$

where ρ is the density. This parameter, which directly reflects the dynamic stiffness of the ground, is visualized along the study area based on the integration of seven seismic profiles performed along the investigation line. The spatial representation of G highlights variations in mechanical properties across the study site. In particular, the southern section of the profile exhibits PDFs indicating intermediate values of the shear modulus G. These variations are interpreted as the result of lateral changes in subsurface conditions, such as differences in compaction quality or material stiffness. These findings demonstrate the added value of the Bayesian framework, not only in estimating key parameters but also in identifying and localizing zones of lower model reliability.

While these results are encouraging and clearly demonstrate the added value of the probabilistic approach, the inversion codes remain in a prototype phase. Future work will focus on improving computational efficiency and ensuring seamless integration with the broader seismic processing workflow to facilitate routine application in operational contexts.

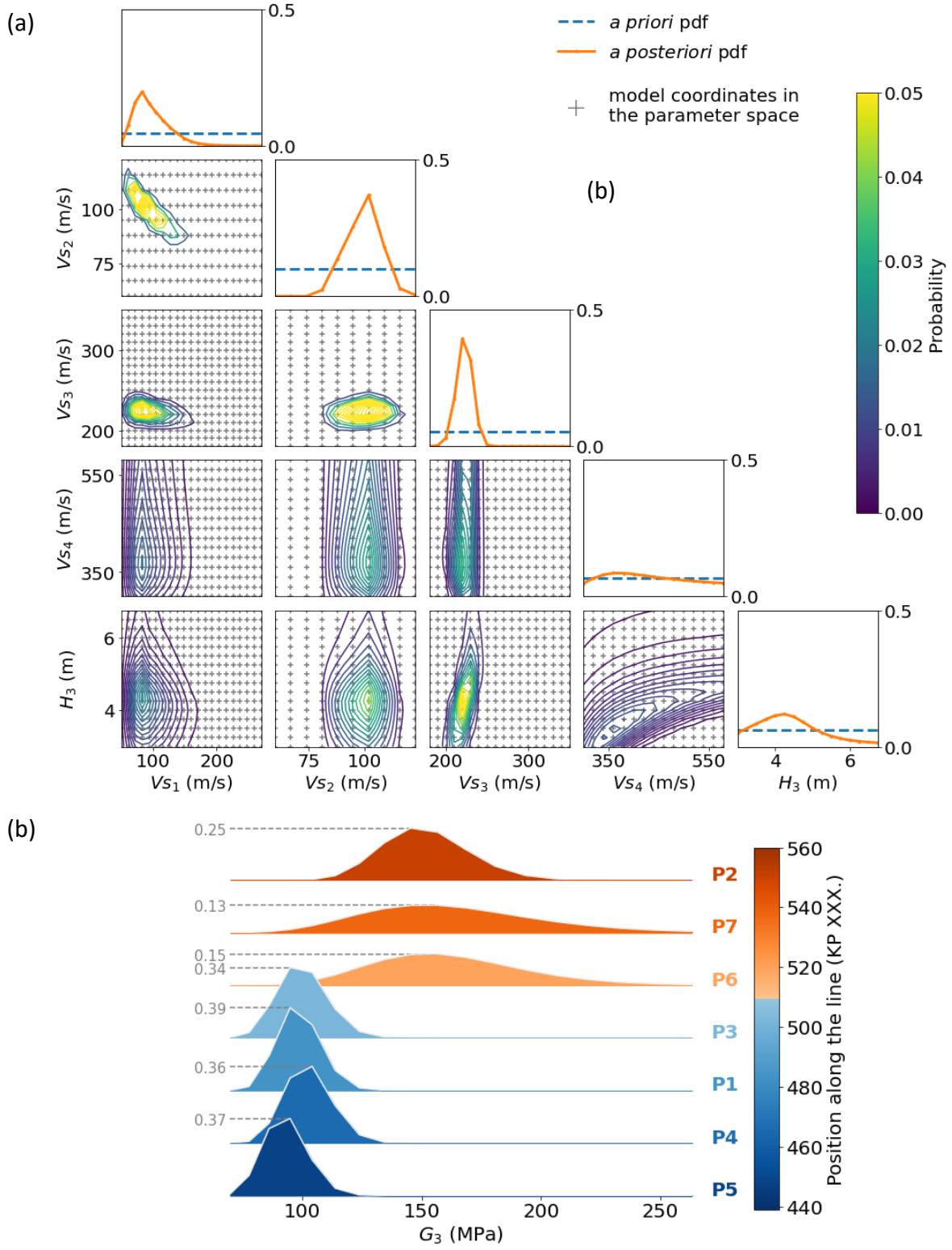

Figure 33: (a) corner plot of a posteriori probability density function for each parameter of the mode. (b) a posteriori probability density function of the shear modulus (G) along the line.

5.3.2. From seismic data to relevant parameters

5.3.2.1. Hydrological phenomena

A physics-guided deep learning model, combining 2D passive-MASW with an artificial neural network, has been developed to estimate daily 2D Groundwater table maps from a single piezometer. This hybrid approach offers an effective means of monitoring Groundwater tables with both spatial and temporal precision. The method extrapolates Groundwater table maps beyond the training piezometric dataset (Figure 34). Analysis of Groundwater table maps reveals spatial and temporal variations, offering a nuanced understanding of Groundwater table geometry and dynamics, and revealing valuable hydrogeological insights.

In parallel, ongoing analyses are focused on understanding the influence of hydrological phenomena (especially the water table variations) on the seismic signal, with the aim of enhancing the interpretation of geophysical data under varying moisture and saturation conditions.

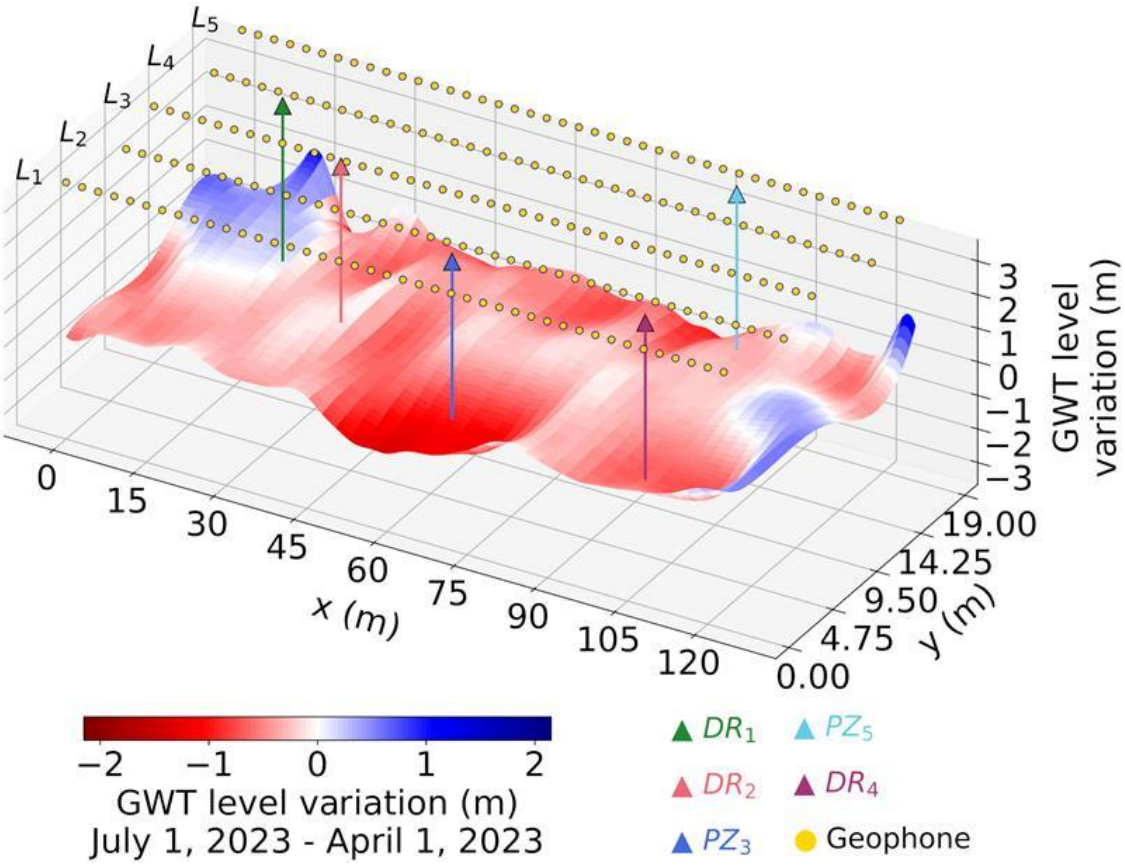

Figure 34: Groundwater table level variation map after training with both piezometers

5.3.2.2. Correlation between Vs and cone resistance

The objective of this section is to assess the correlation between Vs (obtained from surface-wave analysis) and mechanical parameters traditionally used in geotechnical engineering, such as cone penetration resistance (q_d) obtained from Dynamic Cone Penetrometer (DCP) tests. A correlation model between these two parameters, previously established in the literature, was selected and tested on a dedicated test site.

- Correlation of Kang et al. (2023) for the ballast layer: $Vs = 25,474 q_d^{0,7911}$
- Correlation for de Mayne (2007) according to mixed soils: $Vs = 78,15 q_d^{0,39}$

The pilot site, located in Ile de France, has undergone track renewal work. The renewed structure consists of a ballast layer, a subgrade, and the supporting soil (Figure 35 a).

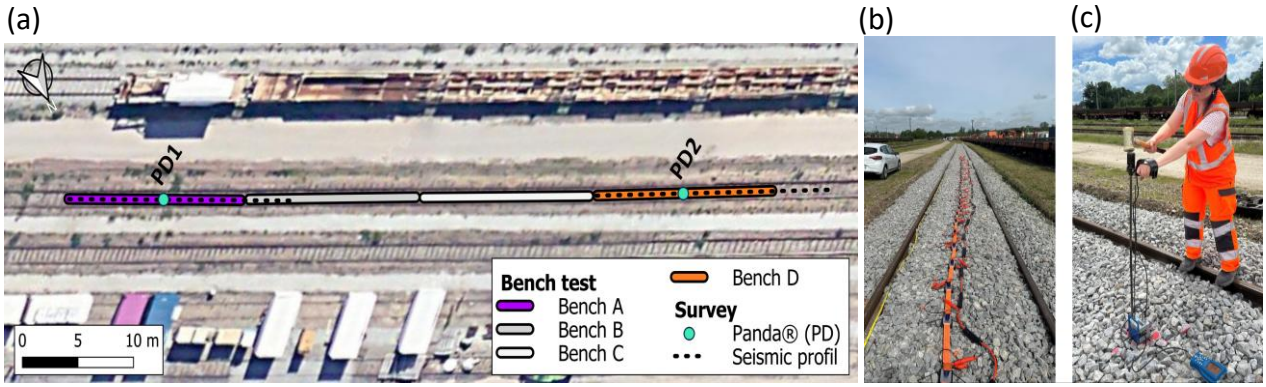

Figure 35: (a) Schematic representation of the study site. (b) Deployment of the seismic acquisition setup on the ballast. (c) DCP tests.

The aim of this renewal was to test the impact on subgrade bearing capacity of a thinner material (type 0/20) than the standard (type 0/31.5). To carry out this comparison, different structures and material thicknesses were defined to evaluate the optimum structure. A total of four benches, each 18 m long, with the following configurations:

- Bench A: 0.15 m of sub-ballast, giving a total thickness of 0.15 m ;
- Bench B: 0.20 m of sub-ballast and 0.15 m of capping layer, giving a total thickness of 0.35 m ;
- Bench C: 0.30 m of sub-ballast and 0.15 m of capping layer, giving a total thickness of 0.45 m ;
- Bench D: 0.20 m of sub-ballast and 0.25 m of capping layer, giving a total thickness of 0.45 m.

A Landstreamer-type seismic setup (as described in section 5.3.1) was deployed on site, and DCP tests (Panda®type) were carried out strictly at the same location (see Figure 35 b and c, respectively).

The results presented here are those for Bench D, showing the strongest contrast in thickness. The VS profile with depth from seismic is shown in orange, and that from correlation with q_d in blue in Figure 35. The results confirmed the relevance of the study correlation, showing good agreement between inverse seismic data and measured mechanical properties with DCP.

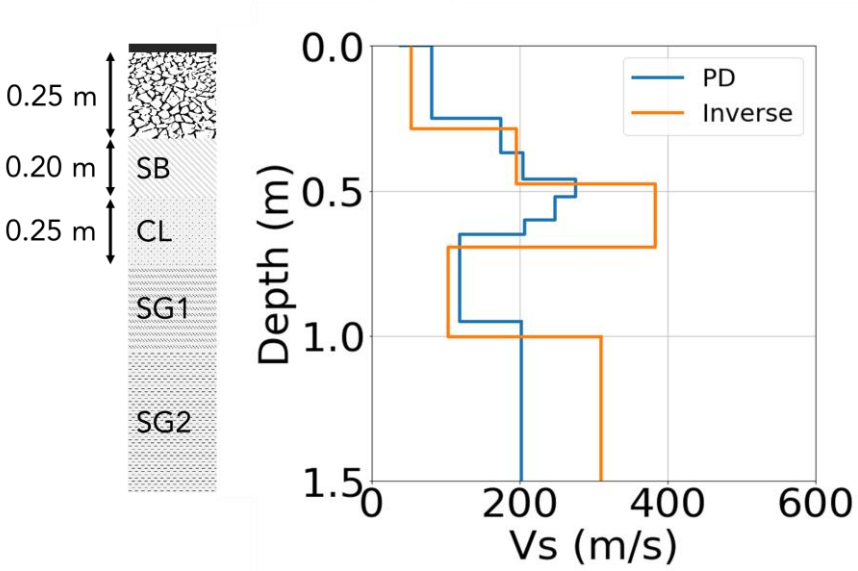

Figure 36: Shear wave velocity profile from inversion and correlation with cone resistance (PD: DCP test/(Panda®type) and Inverse: inverse seismic data)

6. Data Analysis for Condition Monitoring (Use Case 13.4, The Netherlands and Norway)

6.1. Introduction

This section describes the activities of Use Case 4, which investigates practical methods for condition monitoring of railway infrastructure, focusing on embankments and bridges. The Dutch and Norwegian demonstrators each address distinct structural challenges relevant to their national contexts yet contribute to a shared objective of developing monitoring strategies that are adaptable to other infrastructure systems and operating environments across Europe.

The Dutch contribution focuses on the stability of railway embankments in locations where excessive track deformation has occurred, using onboard sensing technology, specifically Axle Box Acceleration (ABA), to capture the dynamic train–track interaction from trains in normal operation. The ABA data is combined with track geometry data, which is the current standard method for assessing track support condition. The goal is to enhance the monitoring and evaluation of track support performance along selected corridors and to explore the added value of dynamic indicators derived from ABA signals.

The Norwegian contribution addresses the challenge of upgrading and extending the service life of existing railway bridges to meet growing demands for freight capacity. Many of these structures lack embedded monitoring and rely on conservative design assumptions that do not reflect actual in-service conditions. To support more accurate assessments, a predictive tool is being developed that combines advanced structural modelling with data from a multi-sensor monitoring system. This system will be demonstrated on a prestressed concrete bridge, located on the Ofoten Line, which carries high-frequency, heavy axle-load iron ore traffic.

Although the two national focuses differ in scope and methodology, both partners contribute to a common aim: enhancing infrastructure resilience through scalable, technology-driven monitoring. The approaches developed aim to inform transferable frameworks for condition-based maintenance that can be applied in other countries and infrastructure settings.

In alignment with the goals of WP13, this use case contributes to Technical Enabler 2 by building on high-TRL and industrially adopted measurement systems, such as onboard accelerometers, track geometry systems, and stationary bridge-mounted sensors. Rather than developing new sensor technologies, the focus lies on combining outputs from these systems and analyzing them within a unified framework to deliver more comprehensive and accurate insights into infrastructure condition. In the Dutch case, this is achieved through signal fusion from ABA and TG data for embankment assessment, while in the Norwegian case, a multi-sensor bridge monitoring setup is integrated with advanced numerical models to enhance diagnostic capability. Across both cases, the methodologies aim to reach TRL 5–6, supporting the implementation of scalable, data-driven monitoring strategies in real operational environments.

The following sections detail the monitoring strategies, analysis methods, and use-case findings from each partner.

6.2. Analysis of structural condition monitoring techniques (civil structures and works)

6.2.1. Pre-calculations and models of concrete bridge and transition zones. Methodology for evaluating increased axle load.

The use case includes two adjacent post-tensioned concrete railway bridges of twin-girder design and similar age (see *Figure **37***). The first bridge, named *"Søsterbekk bridge 1"*, is a 50-meter simply supported span located on a straight track section. The second bridge, named *"Søsterbekk bridge 2"*, is two spans (44 + 41 m) integrated with its central pier and situated on a curved alignment (R = 350 m). The curved bridge is subjected to bending and shear in two directions as well as load in torsion.

The bridges were originally designed for a 25-ton axle load for the iron ore trains. They were later assessed for a 30-ton axle load with new trains featuring longer wagons, which did not increase the load per meter on the bridges. The bridges are now being evaluated for an increase to 32.5 tons, which results in a slight increase in the load per meter.

The plan is to develop predictive models that simulate both static and dynamic responses, supported by sensor systems installed on the bridges and at the transition zones. The calibration and validation of the numerical models will be based on data from original bridge documentations, historical measurements, and data collected from new sensor systems installed on the bridge.

Figure 37: Use case bridges: Søsterbekk bridge 1 with straight track section (left side) and Søsterbekk bridge 2 situated on a curved alignment (right side).

To guide and inform the instrumentation plan of new sensor systems (see Section 6.2.1.1), SINTEF has conducted a preliminary study using both analytical (based on standard calculation) and numerical (based on Finite Element Analysis) methods, obtaining initial estimates for the bridges. The first step was to collect data from the original bridge documentation, including the original drawings and design reports. These data were evaluated and reassessed in accordance with the current Eurocode standard (EC2). Then, a static FE analysis was conducted to determine the maximum deflections of the two bridges, and the results were used in the planning process for sensor placement. The main global aspects of Bridge 1 were also evaluated analytically, using EC2 procedures. Due to its complex curved shape, the bridge Søsterbekk 2 was evaluated numerically by FE analysis.

The dynamic properties of both bridges were evaluated using modal FEA, to estimate their eigenfrequencies and mode shapes. Mode shapes from nodes corresponding to the proposed sensor placements were extracted from the FE models, and post-processing using the Modal Assurance Criterion (MAC) was conducted. The MAC analysis was used to verify the quality of the sensor placements for the two bridges. In Figure 38, the proposed sensor placements for bridge 2 are marked with red dots and were evaluated using a MAC-matrix, shown to the left on Figure 38 and Figure 39. The first six modes of bridge 2 are shown in Figure 39 for illustration.

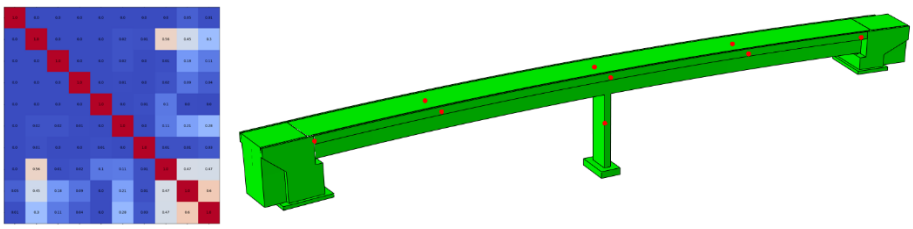

Figure 38: Nodes corresponding to sensor-placements for bridge 2, with MAC-matrix on the left.

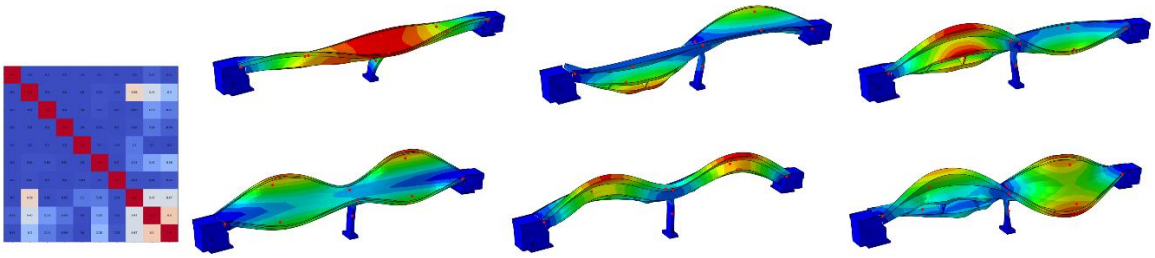

Figure 39: Mode shapes for the first six eigenmodes for bridge 2, with a MAC-matrix at the left.

The MAC-matrix shows mode shape correlations, where 1.0 (red) is a perfect correlation and 0.0 (blue) is zero correlation. A mode will correlate perfectly with itself at the diagonal, and ideally, should have a near-zero correlation with other modes (outside the diagonal), making it easily identifiable. The MAC-matrix was sampled using nodes based on the sensors setup proposed in Section 6.2.1.1 and results show this setup can distinguish between the first 7 modes. A similar analysis was conducted on the setup for bridge 1 and showed that the first 5 modes can be identified for this bridge.

In addition, accelerometers were placed before and after the second bridge to capture the abrupt change in track stiffness due to ballast settlement. The length of the affected area was estimated based on relevant railway standards, and the accelerometers were placed on sleepers in this region.

In WP13, measurement data obtained from the instrumentation of new sensor systems will be used to calibrate and then validate the FE models of the bridges. Once the FE models can digitally replicate the response of real bridges with acceptable accuracy, they can be used to explore variations in axle load and evaluate the effects of potential defects by a parametric study applied to the models. Using this approach, the influence of increased axle load can be evaluated through modelling.

Fault diagnostics for bridge tendons based on the Multiple Model-AutoRegressive (MM-AR) method

The Ofoten Line is used by passenger and freight trains [5], with the freight trains applying the most intense excitation on the railway line's bridges due to their weight. The freight company LKAB Malmtrafik operates the heaviest trains, with each train consisting of 68 wagons [5], weighing 8,600 tons [5], carrying 6,800 tons of ore [6] and operating at 60 km/h [5,7]. Apart from the excitation due to a train's passing, the bridge's structural state in a cold environment such as the subarctic climate of Northern Norway is also affected by repeated freeze-thaw cycles [8].

During freeze-thaw cycles, the water infiltrating the concrete can freeze and expand, exerting internal pressures that may exceed the material's tensile strength, leading to cracking and long-term degradation in concrete [9,10]. The frequency and severity of the freeze-thaw cycles are influenced by the variation in temperature and humidity [8,11], with the latter accelerating the corrosion of steel reinforcements within concrete [12]. Thus, these two environmental conditions via freeze-thaw cycles have a higher impact on the structural state of bridges than the wind [13].

Due to the concrete cracking and degradation caused by freeze-thaw cycles [9,10], moisture can penetrate more easily [14]. Consequently, the pre-tensioned tendons of concrete bridges, which are usually embedded in the concrete and protected by the surrounding material, become exposed. Thus, moisture can lead to the corrosion of these tendons, which are under high tensile stress, and eventually result in structural failure [15, 16]. The freeze-thaw cycles can also affect the ballast support of concrete bridges. The water can infiltrate between ballast particles, and this water expands when the temperature drops below freezing. Ultimately, the repeated freeze-thaw cycles can displace the ballast particles or lead to gradual breakdown (micro-fracturing of stones), thereby reducing the ballast size and strength, and ultimately compromising the ballast's ability to maintain proper track geometry [17,18,19]. Additionally, ice formation can block drainage paths, leading to water pooling on the bridge deck [19].

The examined Norwegian railway bridge in this project is located between the Sosterbekk and Katterat train stations, where the Ofoten Line traverses mountainous terrain, reaching elevations of between 373 meters (Katterat) [20] and 456 meters (Sosterbekk) [21] above sea level. According to the 2024 climate data provided for these two train stations, the air temperature, which affects the bridge temperature, can range from -31.6 °C in winter (Sosterbekk) [22] to 28.1 °C in summer (Katterat) [23]. Regarding humidity, the 2024 climate data shows that the humidity typically ranges between 31 % (Katterat) [24] and 100 % (Sosterbekk) [25].

The Multiple Model-AutoRegressive (MM-AR) based method will be used to remotely monitor the structural state of the examined railway bridge and detect damaged tendons and ballast. The MM-AR-based method is an automated machine learning approach equipped with multiple statistical models. Each model describes the bridge's dynamics under specific values of environmental conditions such as bridge temperature (°C) and humidity (%). A numerical model of the bridge will be used to generate acceleration signals for both healthy and damaged cases under various combinations of bridge temperature and humidity. The signals will be based on multiple spatial measurement points on the bridge. Some of the healthy signals will be used for training the method, whereas the remaining healthy signals and the signals from the damaged cases will be used for method validation. Additionally, the method will also be validated with acceleration signals measured via accelerometers from the actual bridge.

6.2.1.1. Bridge monitoring via the MM-AR-based method

The MM-AR-based method is equipped with multiple vector AutoRegressive (VAR) models. Each model is trained with multiple acceleration signals per pair of environmental conditions (bridge temperature and humidity) from n_y spatial measurement points on the healthy bridge (same number of signals per point). The VAR models' parameters represent the healthy bridge's dynamics in a proper subspace under varying environmental conditions, and damage is detected when the bridge's dynamics under the current unknown structural state do not belong to the subspace, see Figure 40. Data from the healthy state of the bridge are used in the training phase of the MM-AR-based method, whereas data from the current unknown bridge's state are used in the inspection phase.

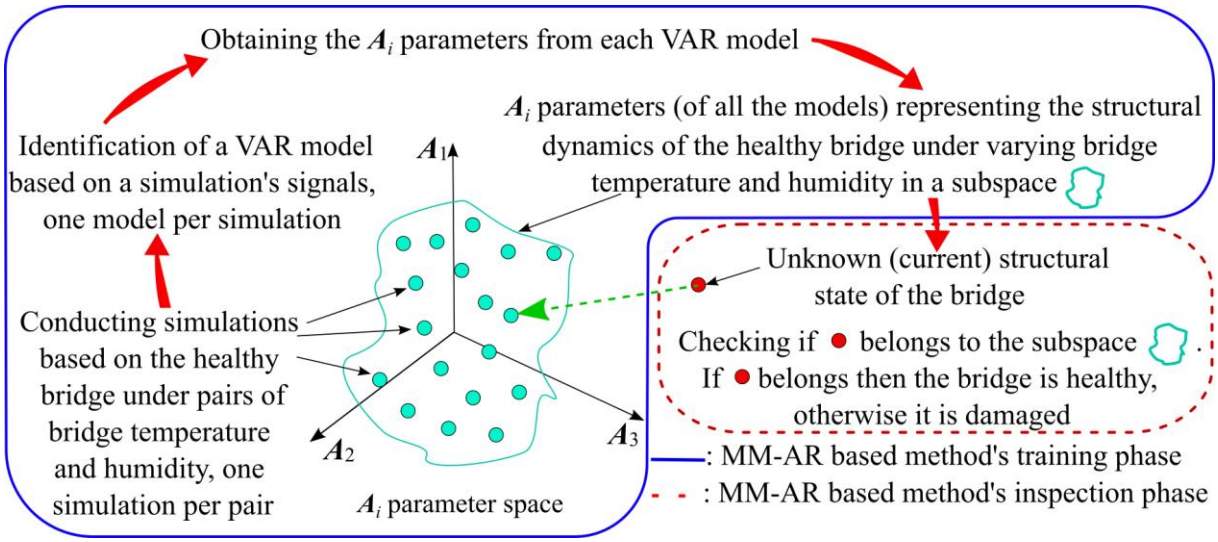

Figure 40: Damage detection concept based on the MM-AR based method equipped with VAR models [27].

6.2.1.2. The training phase

M simulations are conducted based on the healthy bridge and under a sample of Q pairs of bridge temperature and humidity. Each simulation is characterized by a specific bridge temperature T_s and humidity H_c in the form of a vector $\boldsymbol{k}_j = [T_s \;\; H_c]^T$, $j = 1, \dots, M$. The ranges $[T_{min}, T_{max}]$ and $[H_{min}, H_{max}]$ are covered by the discrete values $T_s \in [T_1, \dots, T_{Q_1}]$ and $H_C \in [H_1, \dots, H_{Q_2}]$ of the sample, respectively. n_y response signals

$$\boldsymbol{y}_{o,\boldsymbol{k}_j}[t] = \left[y^1_{o,\boldsymbol{k}_j}[t], \dots, y^{n_y}_{o,\boldsymbol{k}_j}[t] \right]^T_{[n_y \times 1]},$$

where $t = 1, \dots, N$, subscript o stating the bridge's healthy state, are generated based on n_y spatial measurement points in each simulation, and the signals $\boldsymbol{y}_{o,\boldsymbol{k}_j}[t]$ are used for a VAR model's identification (one VAR model per simulation). The M identified VAR models represent the dynamics of the healthy bridge under varying environmental conditions, with the AR parameters and the parameters' covariance matrix being obtained from each VAR model. A VAR model's equation is [26,27]

$$\boldsymbol{y}_{o,\boldsymbol{k}_j}[t] + \sum_{i=1}^{n_a} \boldsymbol{A}_i \cdot \boldsymbol{y}_{o,\boldsymbol{k}_j}[t-i] = \boldsymbol{e}_{o,\boldsymbol{k}_j}[t], \qquad (1)$$

with the AR order designated by n_a, the zero-mean, white (serially uncorrelated), normally distributed residual signals by

$$\$\boldsymbol{e}_{o,\boldsymbol{k}_j}[t] = \left[e^o_{1,\boldsymbol{k}_j}[t], \dots, e^o_{n_y,\boldsymbol{k}_j}[t] \right]^T_{[n_y \times 1]},$$

and the residual signals' $[n_y \times n_y]$ covariance matrix by $\boldsymbol{\Sigma}_{\boldsymbol{e}_{o,\boldsymbol{k}_j}}$. The AR matrix parameters $\boldsymbol{A}_i$ with dimensions $[n_y \times n_y]$ are formed in a parameter vector $\boldsymbol{\theta}_{o,\boldsymbol{k}_j}$ with dimensions $[n_y^2 \cdot n_a \times 1]$, they have a covariance matrix $\boldsymbol{\Sigma}_{\boldsymbol{\theta}_{o,\boldsymbol{k}_j}}$ with dimensions $[n_a \times n_a]$ and they are estimated via the Ordinary Least Squares (OLS) [26,27].

The identification of a conventional VAR model includes the selection of the optimum model order n_a and the validation of the model based on the selected order. The optimum order is selected by observing the Bayesian Information Criterion (BIC) for successive orders, and the convergence of the VAR-based Power Spectral Density (PSD) estimates to their Welch-based counterparts. The optimum order corresponds to the minimum BIC value. The validity of the model is confirmed by verifying the uncorrelatedness (whiteness) of the model's residual signals $\boldsymbol{e}_{o,\boldsymbol{k}_j}[t]$. White residual signals behave like white noise signals, which are sequences of uncorrelated random variables (no correlation between the signal values at different time points). If $100 \cdot (1-\alpha)$ % of the normalized AutoCorrelation Function (ACF) values $\rho^{o}_{e\,1,\boldsymbol{k}_j}[\tau], \ldots, \rho^{o}_{e\,n_y,\boldsymbol{k}_j}[\tau]$ ($\tau = 1, \ldots, h$ designates lags) based on $\boldsymbol{e}_{o,\boldsymbol{k}_j}[t]$ lie within a $100 \cdot (1-\alpha)$ % confidence interval at an α risk level, then the residual signals are white, and the VAR model can describe the bridge's dynamics and the majority of the correlation in the residual signals. The limits of the confidence interval are defined as $\pm \frac{z_p}{\sqrt{N}}$, with z_p as the inverse of the standard normal cumulative distribution function at the probability $p = 100 \cdot (1-\alpha)$ % [26,27].

For defining the limit d_{lim} in the MM-AR based method for damage detection, K additional simulations based on the healthy bridge are conducted. These simulations can be under all or some of the Q pairs of bridge temperature and humidity and if some of the Q pairs are considered, then these pairs should cover the minimum and maximum values of the bridge temperature and humidity. Based on the n_y response signals

$$y_{o,\boldsymbol{k}_l}[t] = \left[y^{1}_{o,\boldsymbol{k}_l}[t], \ldots, y^{n_y}_{o,\boldsymbol{k}_l}[t]\right]^{T}_{[n_y \times 1]},$$

from each of the K simulations ($l = 1, \ldots, K$), the parameters $\boldsymbol{\theta}'_{o,\boldsymbol{k}_l}$ of a VAR(n_a) model are estimated. Then, the MM-AR based method's detection metric D_l is obtained for each model's parameters $\boldsymbol{\theta}'_{o,\boldsymbol{k}_l}$ and it expresses the minimum Mahalanobis distance between $\boldsymbol{\theta}'_{o,\boldsymbol{k}_l}$ and the parameters $\boldsymbol{\theta}_{o,\boldsymbol{k}_j}$ of the M VAR models,

$$D_l = \min_{j=1,\ldots,M} f\left(\boldsymbol{\theta}_{o,\boldsymbol{k}_j}, \boldsymbol{\theta}'_{o,\boldsymbol{k}_l}\right) = \sqrt{\left(\boldsymbol{\theta}_{o,\boldsymbol{k}_j} - \boldsymbol{\theta}'_{o,\boldsymbol{k}_l}\right)^{T} \cdot \boldsymbol{\Sigma}^{-1}_{\boldsymbol{\theta}_{o,\boldsymbol{k}_j}} \cdot \left(\boldsymbol{\theta}_{o,\boldsymbol{k}_j} - \boldsymbol{\theta}'_{o,\boldsymbol{k}_l}\right)}\,.$$

The limit d_{lim} is set several standard deviations above the mean of the K D_l values. The number of standard deviations can be selected; thus, the limit is above the maximum of the K D_l values [27].

6.2.1.3. The inspection phase

Based on a new simulation or experiment under the bridge's current (unknown) state, response signals

$$\boldsymbol{y}_u[t] = \left[y^{1}_{u}[t], \ldots, y^{n_y}_{u}[t]\right]^{T}_{[n_y \times 1]}$$

are obtained and used for estimating the parameters $\boldsymbol{\theta}_u$ of a new VAR(n_a). Subsequently, damage detection is achieved by comparing the training-phase limit d_{lim} to the metric distance D which is the minimum Mahalanobis distance between the parameters $\boldsymbol{\theta}_u$ and the parameters $\boldsymbol{\theta}_{o,\boldsymbol{k}_j}$ of the M VAR models from the training phase (see Subsection 6.2.1.2), with

$$D = \min_{j=1,\dots,M} f\left(\boldsymbol{\theta}_{o,\boldsymbol{k}_j}, \boldsymbol{\theta}_u\right) = \sqrt{\left(\boldsymbol{\theta}_{o,k_j} - \boldsymbol{\theta}_u\right)^T \cdot \Sigma^{-1}_{\boldsymbol{\theta}_{o,\boldsymbol{k}_j}} \cdot \left(\boldsymbol{\theta}_{o,\boldsymbol{k}_j} - \boldsymbol{\theta}_u\right)}.$$

It is hypothesized that the bridge is in a healthy state and thus, $\Sigma_{\boldsymbol{\theta}_{o,\boldsymbol{k}_j}}$ is used in the Mahalanobis distance. If $D \leq d_{lim}$ then the bridge's structural state is healthy, and the training VAR models can represent the dynamics corresponding to the bridge's current state. Otherwise, the bridge is damaged [26,27].

6.2.1.4. Remarks on the method

The level of the representation of the healthy bridge's dynamics under varying environmental conditions by the statistical VAR models in the training phase depends on the discrete values of bridge temperature T_s and humidity H_c and the number of the combinations $\boldsymbol{k}_j = [T_s \ H_c]^T$ between these values (see Subsection 6.2.1.2). Defining the representation level requires the execution of the training phase with the following actions: (i) selection of several discrete values for T_s, H_c thus covering their ranges, (ii) conducting M number of simulations based on all the possible combinations between the T_s and H_c values along with K simulations, (iii) identification of the necessary VAR models, and (iv) selection of the detection limit (see Subsection 6.4). If the performance of the detection method is accompanied by a high percentage of missed damages or false alarms, then a higher number of discrete values for T_s, H_c should be selected, and the training phase with the four actions should be executed again.

However, the increased number of combinations between T_s and H_c values lead to a higher number of M simulations and M VAR models in the training phase. Subsequently, the multiple M models lead to multiple comparisons of model parameters for damage detection in the inspection phase. As a result of the increased number of combinations, the computation time is increased in both phases.

6.3. Assessing embankment stability using train-borne measurements

This section presents the contribution of the Netherlands site's role in Use Case 4, focusing on evaluating embankment stability related to its ability to support track superstructure components, known as track support conditions, by using Axle Box Acceleration (ABA) signals. The goal is to explore how dynamic responses recorded by instrumented trains can complement conventional monitoring approaches and provide deeper insights into substructure performance, in which embankment is included. Field campaigns on selected corridors in the Netherlands are used to demonstrate the capabilities of this approach, supported by comparative analyses, physical interpretation, and indicator development. The following subsections describe the methodology, findings, and implications for condition-based maintenance.

6.3.1. Evidence of ABA Capabilities for Track Support Condition Assessment Under Operational Conditions: The Netherlands, Sweden, and Norway

This subsection presents key findings from field campaigns carried out in the Netherlands, Sweden, and Norway, which collectively demonstrate the capability of Axle Box Acceleration (ABA) measurements to capture variations in track support conditions. Results in this subsection were presented in the 10th Transport Research Arena Conference (L. Wang, S. Unsiwilai, Y. Zeng, C. Shen, J. Hendriks, J Moraal, A. Zoeteman, A. Núñez, R. Dollevoet, and Z. Li, Condition monitoring of railway transition zones using acceleration measurements on multiple axle boxes: Case studies in the Netherlands, Sweden, and Norway, in TRA2024, 15-18 April 2024, Dublin, Ireland). The subsection forms the foundational evidence for interpreting and integrating ABA into more advanced condition monitoring frameworks, as discussed in the following sections.

The results consistently show that dynamic train-track interaction, measured via ABA, reflects localized differences in the support condition of the track, in which substructure and embankment play a key role. The spatial consistency and repeatability of the observations under varying operational and environmental conditions validate ABA as a promising tool for monitoring track support conditions. This approach can provide deeper insights to aid track maintenance decision-making, alongside conventional methods such as track geometry (TG), which are limited in sensitivity.

Figure 41: ABA measurement system on the CTO, TU Delft measurement wagon [1].

The Netherlands

In the Netherlands, ABA measurements were conducted over a series of bridge transition zones located along the double-track line between Dordrecht and Lage Zwaluwe. Multiple measurement runs were carried out in both directions, with train speeds ranging from approximately 15 to 34 m/s. Despite differences in train direction and speed, the ABA signals exhibited consistent dominant spatial frequency bands, particularly within the 3–25 m wavelength range. This wavelength band corresponds to the D1 wavelength according to EN standards and is typically associated with substructure irregularities.

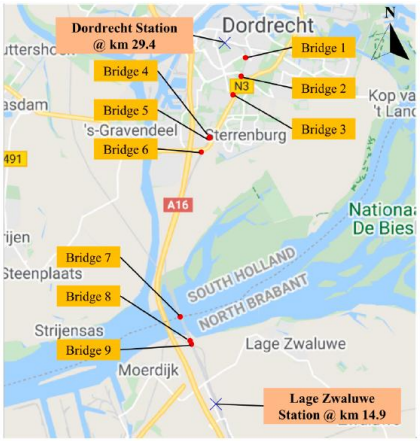

Figure 42: Location of case study railway bridge transition zones between Dordrecht and Lage Zwaluwe [2].

Detailed wavelet analyses revealed that intense ABA energy consistently appeared at similar locations across multiple runs, and that ABA signal amplitudes increased with speed, while the frequency content remained relatively stable. This indicates that the response patterns are repeatable and physically linked to the track structure, rather than being artifacts of operational variability. Moreover, energy asymmetries between entrance and exit transition zones, or between left and right rails, could be clearly identified and quantified, demonstrating the spatial resolution of ABA signals for track support diagnostics.

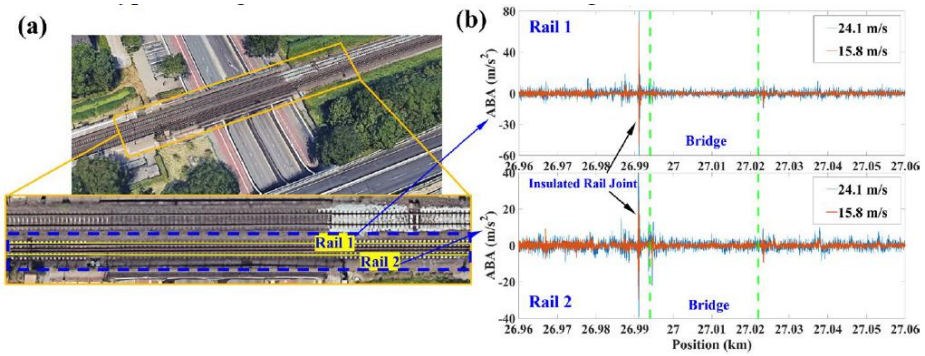

Figure 43: (a) Aerial photos of the transition zones at Bridge 3; (b) ABA signals in the time domain [1].

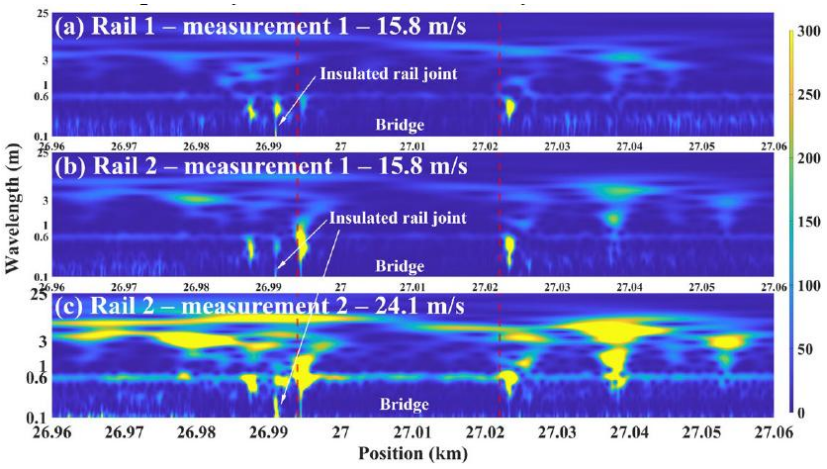

Figure 44: Wavelet Power Spectrum of ABA signals measured with different speeds and locations at Bridge 3; (a) Rail 1, 15.8 m/s; (b) Rail 2, 15.8 m/s; (c) Rail 2, 24.1 m/s [1].

Sweden

In Sweden, ABA measurements were carried out over a short-span bridge located on the freight-dominated, Iron Ore line, between Boden and Murjek, where prior inspection had revealed deterioration and visible cracking at the bridge's abutments. The structure, composed of a 4.2-meter concrete deck and two approach slabs, was reinforced with steel beams due to earlier concerns over stability, due to a degraded bridge structure. The ABA data showed particularly strong energy concentrations in the wavelength range of approximately 3–10 meters when the train passed over the bridge.

These results demonstrate that ABA is capable of detecting site-specific structural behaviour, particularly in locations where the track support condition changes between adjacent areas (such as a concrete deck and an embankment). In this case, the degraded condition of the bridge appeared to amplify the vertical interaction between train and track, resulting in strong localized ABA energy. The use of multi-axle measurements enabled signal averaging across wheelsets, further reducing noise and enhancing signal consistency.

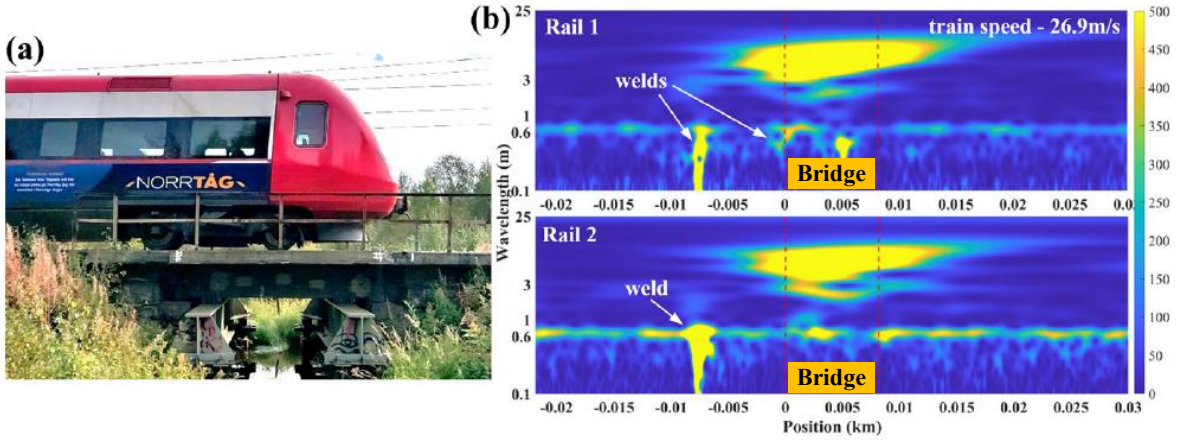

Figure 45: (a) Swedish case study location; (b) Wavelet Power Spectrum of ABA signals [1].

Norway

The measurement in Norway focused on a concrete bridge on the Ofoten Line, located between Sosterbekk and Katterat, which serves high-axle-load iron ore trains operating at speeds of 60–70 km/h. The ABA signals collected in this context showed intense energy at the bridge transition zones, particularly in the 1–10 m wavelength range. This range is also associated with substructure deformation and variations in local track support conditions. Compared to adjacent conventional track segments, the transition zones exhibited stronger responses in both the time and wavelet domains.

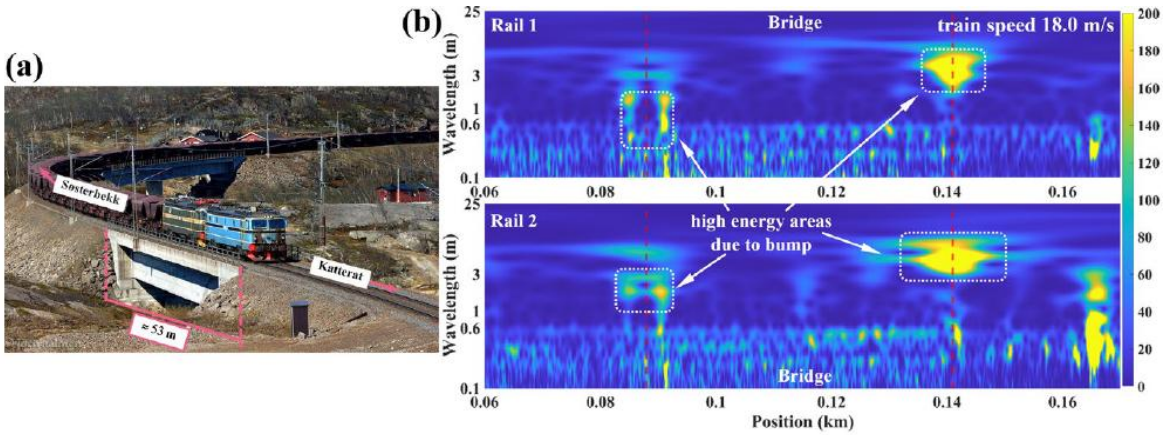

Figure 46: (a) Norwegian case study location; (b) Wavelet Power Spectrum of ABA signals [1].

In all three case studies, ABA measurements showed sensitivity to the structural features associated with the condition of track substructure, including the embankment. The key characteristics that support this conclusion are:

- Repeatability: Identifiable frequency bands and energy peaks consistently emerged across multiple runs, directions, and speeds.

- Location specificity: High-energy ABA responses aligned with anticipated physical changes in track support conditions (e.g., transition areas between a bridge track and a regular track).
- Operational robustness: Changes in train speed influenced the signal's amplitude but did not alter the dominant spatial frequency content, demonstrating the reliability of spatial analysis methods like the wavelet power spectrum.

The findings suggest that the identified ABA signal characteristics are not random nor site-specific but rather reflect underlying structural behaviour that can serve as a reliable indicator of substructure performance. This supports the broader hypothesis that ABA measurements can complement and potentially enhance conventional track monitoring approaches. Previous work in the IN2Track3 project established ABA's Technology Readiness Level (TRL) at 7 for detecting rolling contact fatigue, and current results from FP3-IAM4RAIL show consistent behaviour across different countries, infrastructure types, and operational settings. This reinforces the applicability of ABA for assessing the condition of substructures, including embankments. However, to move toward higher TRL levels for substructure diagnostics, further testing under typical passenger train operations and additional validation using trackside measurements will be necessary.

6.3.2. Sensitivity Comparison Between ABA and Track Geometry

To assess the relative sensitivity of Axle Box Acceleration (ABA) compared to traditional Track Geometry (TG) measurements, a performance indicator referred to as KPI1 was proposed in D12.1 and applied to a case study on the Dutch railway line between Dordrecht and Lage Zwaluwe. While TG remains the standard method for assessing vertical track quality, it primarily reflects geometric deviations. In contrast, ABA captures dynamic train-track interaction during train passage, which can reflect variations in vertical track support conditions.

A 200-meter track segment was selected as a case study, with both TG and ABA data reported at a spatial resolution of 0.25 meters. KPI1 quantifies the relative difference in the number of detected defects between the two measured signals. In this analysis, a defect is defined as a location where the measured signal exceeds a pre-defined threshold. For TG, the alert limit (AL) of longitudinal level in the D1 wavelength range (3-25 meters) was selected as the threshold, in accordance with EN 13848-5 standard. For ABA, the threshold was defined using the Scale Average Wavelet Power (SAWP) value within the same wavelength range at the location where TG exceeded the AL. The indicator is calculated using the following formula:

$$\mathrm{KPI1} = \frac{(\mathrm{defect}_{\mathrm{ABA}} - \mathrm{defect}_{\mathrm{TG}})}{\mathrm{defect}_{\mathrm{TG}}} \times 100$$

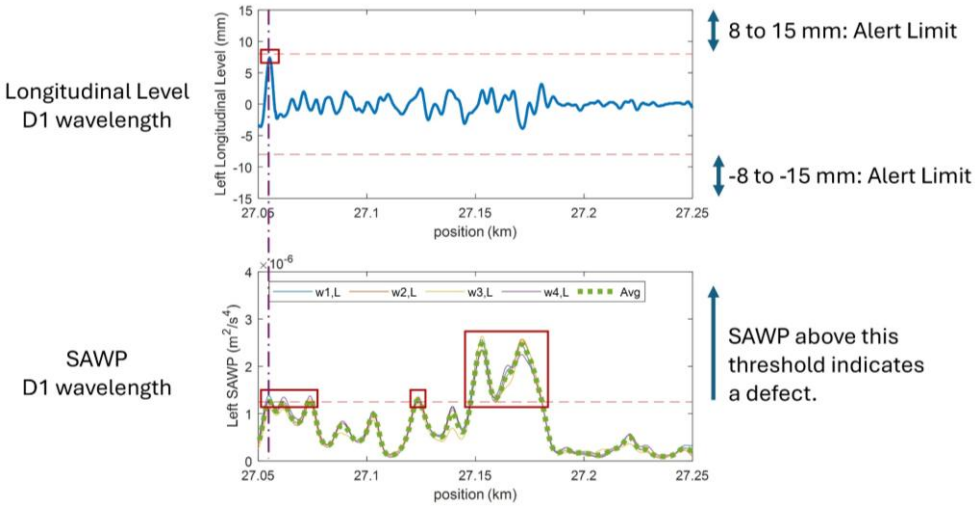

Figure 47: (a) Comparison of defect detection between two measured signals, longitudinal level from TG and SAWP from ABA, on a case study track segment.

The plot illustrates the comparison between TG-based and ABA-based defect detection on the selected segment. TG identified a single defect location where the longitudinal level exceeded the AL. In contrast, ABA detected three distinct locations of interest using the same energy level as the TG exceedance point as the reference threshold. The resulting KPI1 value of 200% suggests that ABA offers greater sensitivity to subtle or early-stage support degradation, which may not yet be reflected as geometric irregularities. While TG flagged one exceedance, ABA captured multiple positions with significant dynamic response energy.

These findings support the hypothesis that ABA serves as a valuable complementary monitoring source, capable of detecting deterioration that TG alone might miss. KPI1 thus provides a simple yet effective way to quantify the added value of ABA and also sets the stage for more advanced feature-level integration, such as the fused condition indicator introduced in Section 6.3.4.

6.3.3. Physical Interpretation of ABA Signals Using Impact Modal Testing

This subsection summarizes findings from field measurements conducted at a bridge transition zone on the Iron Ore Line in northern Sweden. The results were originally presented in the Journal of Civil Structural Health Monitoring, Springer Nature (S. Unsiwilai, C. Shen, Y. Zeng, L. Wang, A. Núñez, Z. Li, Vertical dynamic measurements of a railway transition zone: a case study in Sweden, J Civ Struct Heal Monit 14 (2024) 979-996). The objective of this study was to enhance the interpretability of ABA signals by associating their features with structural dynamics measured through impact modal testing. Two types of impact tests were conducted: hammer impact tests to identify resonance behaviour and falling weight device (FWD) impact tests to assess track deflection characteristics. Both were compared against spatial frequency characteristics extracted from ABA signals recorded at the same site.

The study site comprises a single-span bridge structure with a total length of 8.15 m. The bridge includes a 4.2 m reinforced concrete bridge deck (Zone B), a 1.9 m north approach slab (Zone A), and a 2.05 m south approach slab (Zone C). Cracking had previously been observed in the bridge abutments, prompting the installation of two steel beams spaced 2.6 m apart to reinforce the structure. The bridge is part of a ballasted single-track railway that serves both passenger and freight traffic, including iron ore trains with axle loads exceeding 30 tons.

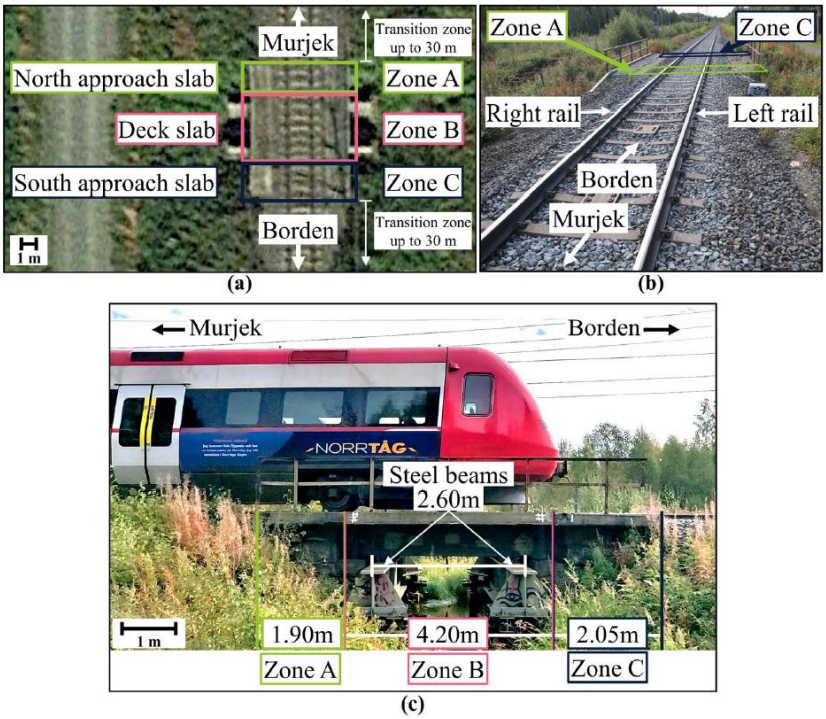

Figure 48: Case study bridge (a) a satellite photo (source: Google Maps); (b) ground photo; (c) side view photo [3].

Hammer impact tests were conducted at ten sleepers (sp_1 to sp_{10}) covering Zones A and B. A 5.5 kg PCB 086D50 modal hammer with a 76 mm plastic tip was used to apply vertical impacts to the rail head above each sleeper. The resulting vertical track responses were measured using a Brüel & Kjær 4514-004 uniaxial accelerometer mounted on the rail near the impact location. Five repeated impacts were conducted at each location, with both impact force and acceleration recorded at 25.6 kHz and averaged to ensure reliable spectral estimation. The resulting Frequency Response Functions (FRFs) were calculated as the ratio of acceleration over input force in the frequency domain. Each FRF was validated with coherence values above 0.9 in the 30–500 Hz range.

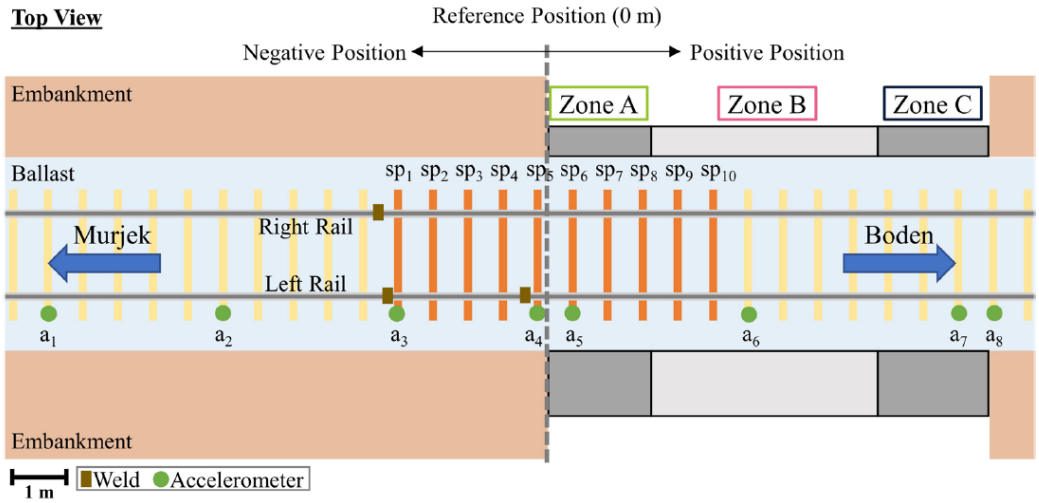

Figure 49: Sensor layout at the case study bridge [3].

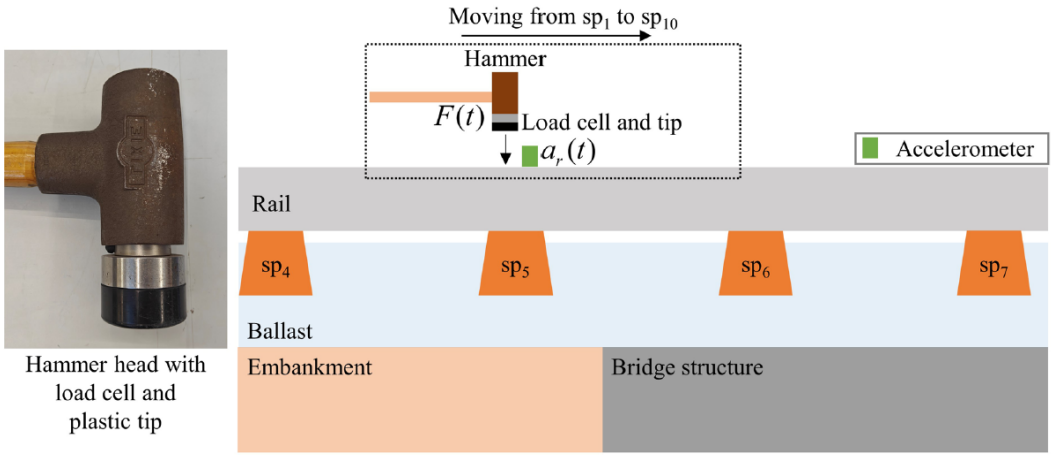

Figure 50: Hammer impact device and test diagram [3].

Falling weight tests were performed using a custom-built device designed to deliver controlled vertical impacts ranging from 60 to 100 kg. Impacts were applied to the rail head located between sleepers sp_5 and sp_6. The track vertical responses were recorded using eight accelerometers, the same model used in hammer tests, mounted at locations a_1 to a_8 on the sleepers. The impact force and acceleration from the eight sensors were recorded at a sampling rate of 25.6 kHz. The Operational Deflection Shapes (ODS) were derived from the imaginary part of the receptance, evaluated across selected frequency bands. The reliable frequency range for ODS analysis was identified as 10 to 100 Hz.

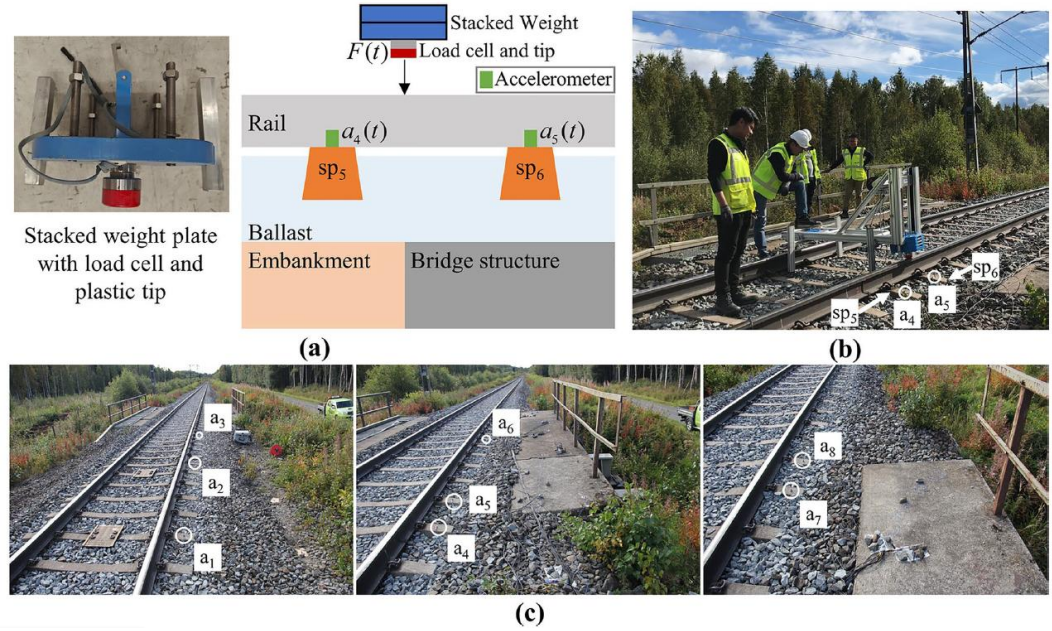

Figure 51: (a) Falling weight device (FWD) and test diagram; (b) FWD in operation; (c) Accelerometers at eight considered locations [3].

An example of FRFs at Sleeper Sp_5 in terms of mobility, calculated from track responses to both hammer and FWD impact tests, is shown below. Three distinct track resonance modes can be observed from the tests.

- TR-1 (Track Resonance 1), located around 300 Hz, reflects localized vibration of the rail relative to the sleeper, primarily involving components above the ballast layer. This resonance is clearly observed in the hammer impact test results.
- FT (Full Track) resonance, found at around 50 Hz, corresponds to the coupled vibration of the rail–sleeper–ballast system. FT characteristics are primarily determined by the properties of the ballast layer. This resonance is identifiable in both hammer and FWD impact tests.
- Below the FT resonance. The FWD impact tests, which excite the track with a broader and lower frequency input, revealed an additional resonance peak around 15 Hz. This low-frequency resonance was not observed in the hammer impact tests and is assumed to reflect deeper substructure-related vibration.

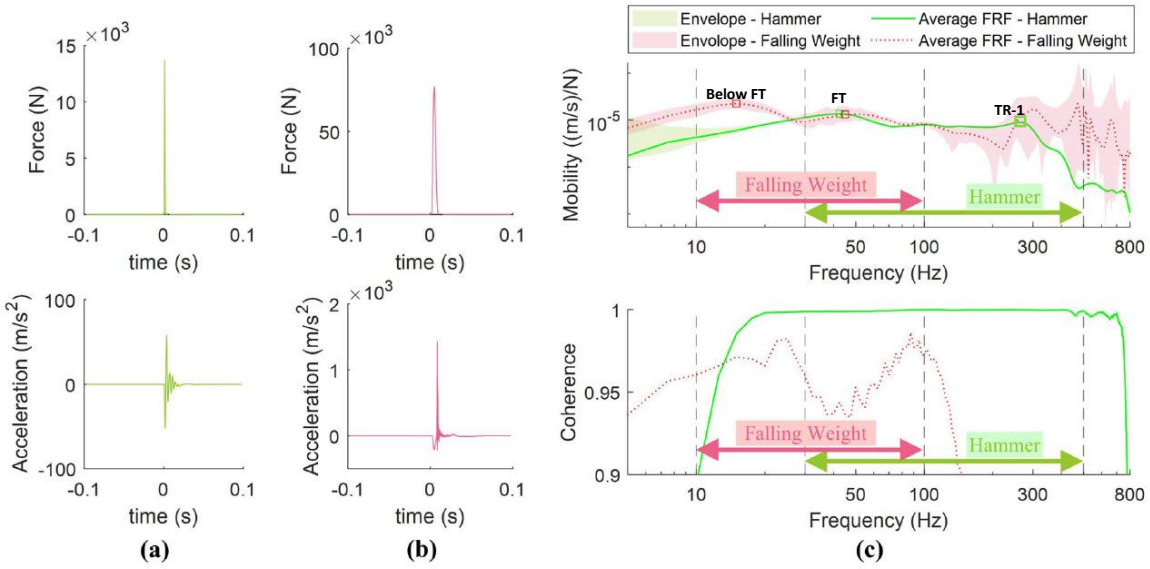

Figure 52: Figure NL-12: (a) an example of the impact force and the acceleration due to a hammer impact; (b) an example of the impact force and the acceleration from a 100 kg weight dropped from 47 cm above the rail head; (c) mobility and coherence of the track system from hammer and FWD impact tests, □ indicates resonance frequencies [3].

To understand how the dynamic response varies along the transition zone, the FRFs at sleepers sp_1 to sp_{10} were analyzed. The FT resonance, observed within a frequency range of approximately 30–60 Hz, and the TR-1 resonance, located between 270–320 Hz, appeared consistently along the track segment but exhibited spatial variation in their modal characteristics. On the embankment side (sp_1–sp_5), the FT resonance frequencies were slightly higher at sp_1 to sp_3 compared to sp_4 and sp_5. However, the mobility magnitudes at sp_1–sp_3 were 40–55% lower, and the damping ratios were 60–87% higher. These trends indicate more rapid energy dissipation at those locations and may suggest differences in local structural properties, such as changes in ballast condition or support behavior. For TR-1, sp_1 exhibited a higher resonance frequency than the other locations, but with approximately 30% lower mobility and 50% higher damping ratio compared to sp_2 to sp_5. These variations are likely related to local structural conditions. Across the bridge deck (sp_6–sp_{10}), both FT and TR-1 modes remained relatively consistent in frequency, amplitude, and damping. The reduced variation in modal properties indicates a more uniform mechanical behavior throughout the bridge structure. These results demonstrate that measurable shifts in modal behavior occur across the transition zone and that impact testing can reveal evolving dynamic characteristics across different support conditions.

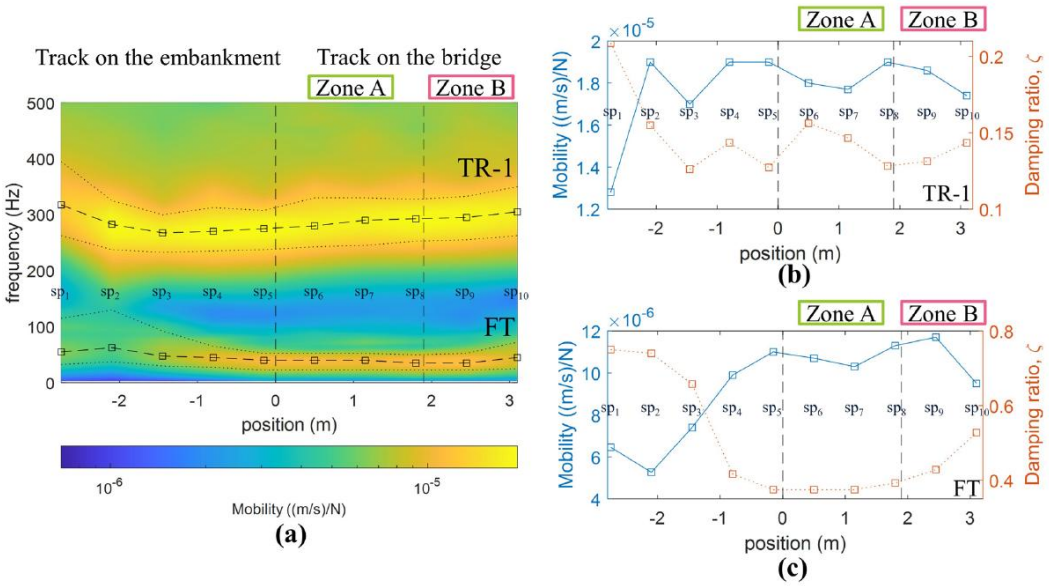

Figure 53: Variation in FT and TR-1: (a) a surface plot of the FRFs, including the dropped 3 dB band; (b) mobility magnitude and damping ratio of TR-1; (c) mobility magnitude and damping ratio of FT. □ indicates the positions of sleepers sp1-sp10, from left to right [3].

The deflection characteristics of the transition zone were evaluated by examining ODSs across three frequency bands: 10–30 Hz, 30–60 Hz, and 60–100 Hz. In the 10–30 Hz band, below the FT resonance, an additional resonance feature was observed, particularly in the response of sensor a_4 located at −0.15 m, which recorded the largest deflection due to its proximity to the impact location. Compared to the bridge section, the embankment side exhibited less overall deflection in this range, which may indicate a greater ability to transmit or dissipate energy. This low-frequency behaviour is presumed to be influenced by components beneath the ballast layer, which are more strongly excited by the broader impact energy of the falling weight compared to hammer excitation. In the 30–60 Hz range, associated with the FT resonance, the maximum downward deflection was observed at a_6, located at 3.75 m. In the 60–100 Hz range, a_6 again exhibited the largest response, but in the upward direction. As this location lies near the midspan of the bridge deck slab (Zone B), it appears more responsive across frequency ranges than Zones A and C, which are positioned closer to the abutments. These patterns confirm spatial variation in vertical compliance across the transition zone, which is captured by deflection-based features derived from impact excitation.

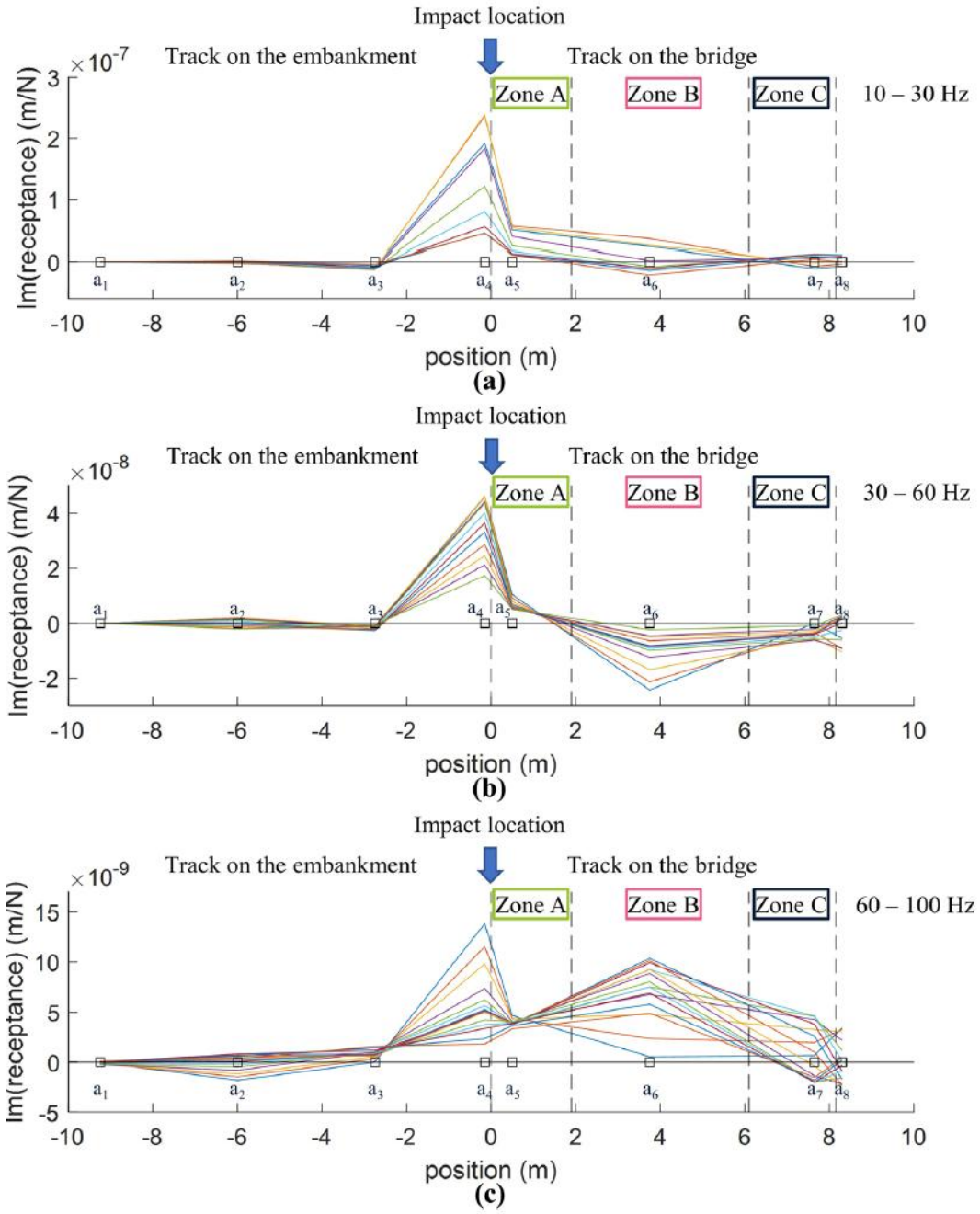

Figure 54: Operational deflection shapes of the track at different corresponding frequencies: a 10–30 Hz; b 30–60 Hz; c 60–100 Hz. □ from left to right, indicate the positions of accelerometer a1 to a8, respectively, and the arrows represent the impact location at 0 m [3].

To complement the findings from impact excitation tests, train-borne ABA measurements were also analyzed to assess whether features extracted under operational loading reflect similar structural behaviours. The objective was to determine whether dominant spatial components in ABA signals align with the dynamic characteristics observed in the hammer and FWD tests across the transition zone.

Vertical ABA data were recorded during four train passes, with speeds ranging from 30 to 34 m/s. Signals were collected using the mounted accelerometers at the axle boxes and analyzed using the wavelet power spectrum to identify dominant spatial frequency content. While minor variations were observed between wheelsets, the spatial locations of dominant energy peaks remained consistent across runs. Averaging across multiple axles reduced random effects and enhanced the clarity of spatial trends.

Two key spatial frequency bands were investigated. The first band, 1.05–2.86 m^{-1}, corresponds approximately to the sleeper spacing of 0.65 m ± uncertainty. Features extracted in this band, specifically the dominant frequency and the Scale Average Wavelet Power (SAWP), showed variation across the transition zone that aligned well with the FT resonance behaviour identified in the hammer test results. Since FT resonance is primarily influenced by ballast layer properties, it is likely that derived ABA features in this range reflect ballast-related structural behaviour.

The second band, 0.04–0.33 m^{-1}, corresponds to the D1 wavelength range (3-25 m). Prior studies have suggested that longitudinal track irregularities within the D1 wavelength are related to substructure conditions. In this study, high ABA energy within this range was observed, which coincides with areas of higher vertical deflection observed in the ODS analysis. This suggests that ABA features in this longer-wavelength band may be sensitive to deeper structural components, such as substructure components.

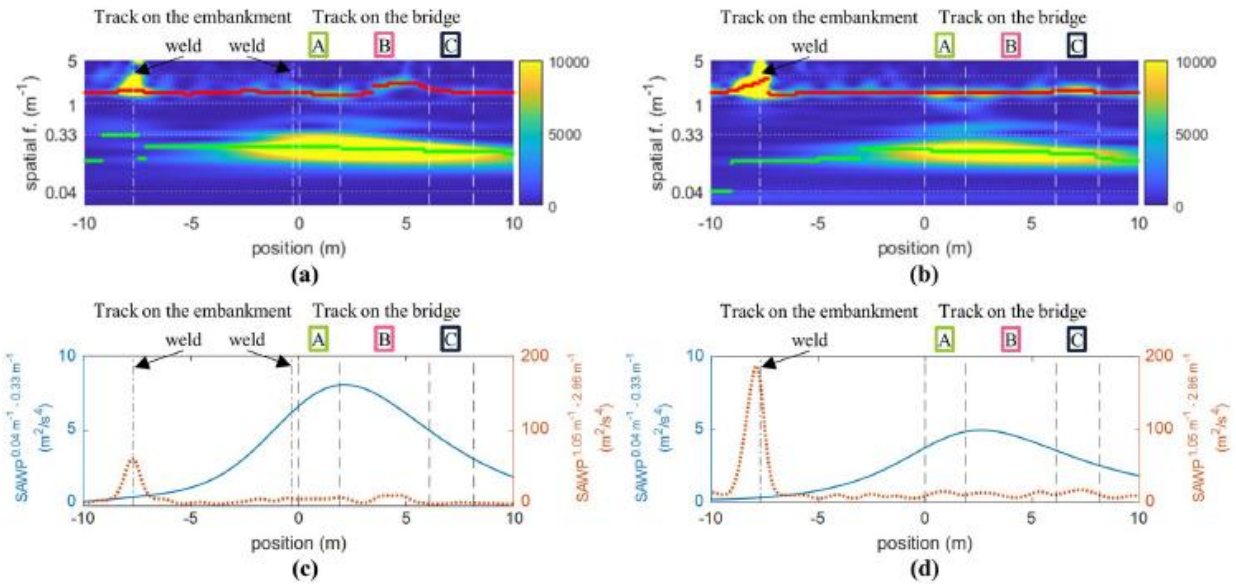

Figure 55: Variation in the ABA features at the considered track segment: (a), (b) dominant spatial frequencies on the left and right rails, • corresponds to the range of 0.04 m−1 to 0.33 m−1, • corresponds to the range of 1.05 m−1 to 2.86 m−1; (c), (d) SAWP of 2 considered bands on the left and right rails [3].

The ABA data also showed minor variation between wheelsets, but the location of dominant energy peaks remained stable. Averaging across multiple axles reduced random effects and enhanced spatial clarity of the signal.

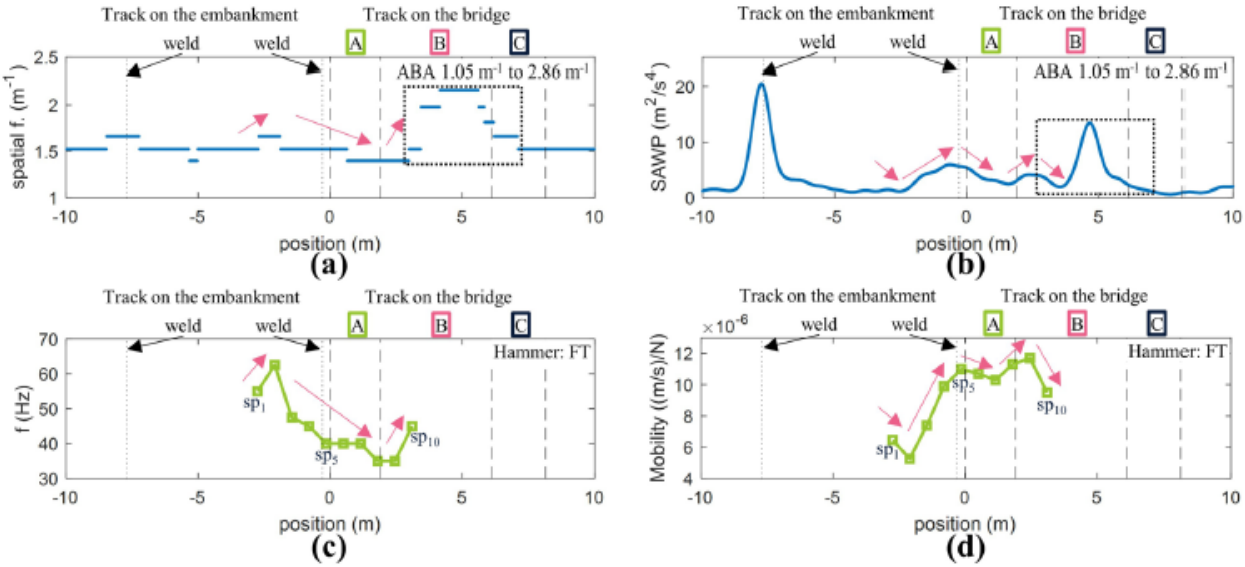

Figure 56: The features from the hammer tests and ABA measurements: (a), (b) the dominant frequency and SAWP in the range of 1.05–2.86 m−1; (c), (d) the FT resonance and its mobility magnitude; □ indicates the positions of sleepers sp1–sp10, from left to right, respectively [3].

In conclusion, the results from hammer and falling weight tests confirmed measurable variation in modal response and deformation behaviour across the bridge transition zone. FT and TR-1 resonances were observed at all sleeper locations, with spatial differences in mobility and damping that reflect local structural variation between the track segments on the embankment and the bridge. The falling weight tests further revealed a distinct low-frequency resonance around 15 Hz, not captured by hammer tests, and higher vertical deflection over the bridge deck, as shown by the ODSs. Train-borne ABA measurements, processed using wavelet analysis, identified dominant spatial frequency components associated with ballast and substructure-related behaviour. These results support the conclusion that ABA signals contain physically meaningful information that reflects track support conditions. Furthermore, the consistency of ABA features across different operational runs highlights their potential reliability for monitoring transition zones under in-service conditions.

6.3.4. Enhanced Vertical Track Quality Index (EnVTQI)

This subsection presents a summary of the development and evaluation of the Enhanced Vertical Track Quality Index (EnVTQI), an indicator designed to improve the assessment of vertical track support conditions by combining features from the vertical ABA signals with longitudinal level, one of the conventional track geometry parameters that reflect vertical track irregularities. The results presented here are based on the study published in Heliyon, Cell Press (S. Unsiwilai, W. Phusakulkajorn, C. Shen, A. Zoeteman, R. Dollevoet, A. Núñez, Z. Li, Enhanced vertical railway track quality index with dynamic responses from moving trains, Heliyon (2024)).

The EnVTQI is a segment-level track quality indicator that integrates multi-source, interpretable features to enable a more comprehensive representation of track support performance. The primary focus is to enhance sensitivity to structural variability, especially in the ballast and substructure layers, by fusing information from multiple monitoring systems. The evaluation was conducted on a Dutch railway line, utilizing two adjacent straight tracks labelled as Track I and Track II. Each track was divided into 24 segments, each 200 meters in length, following the EN 13848-6 standard. This resulted in a total of 48 segments, named I-1 through I-24 and II-1 through II-24. The selected segments excluded turnouts, joints, and civil structures to reduce variability caused by local discontinuities.

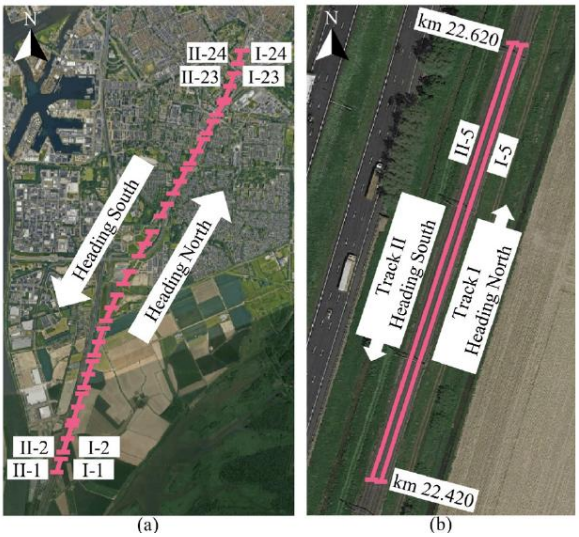

Figure 57: Case study track segments: (a) location of 48 segments; (b) zoom-in detail of track segments I-5 and II-5 (source of satellite photos: Google Maps) [4].

The longitudinal level data were obtained from the BBMS system and processed using a spatial bandpass filter to retain wavelengths between 3 and 25 meters, reported at a spatial resolution of 0.25 meters, as defined in EN 13848-1. The standard deviation of longitudinal level (SD_{LL}) was computed separately for each 200 m segment of the left and right rails, and their average was used as the geometry-based input feature, denoted as avg(SDLL).

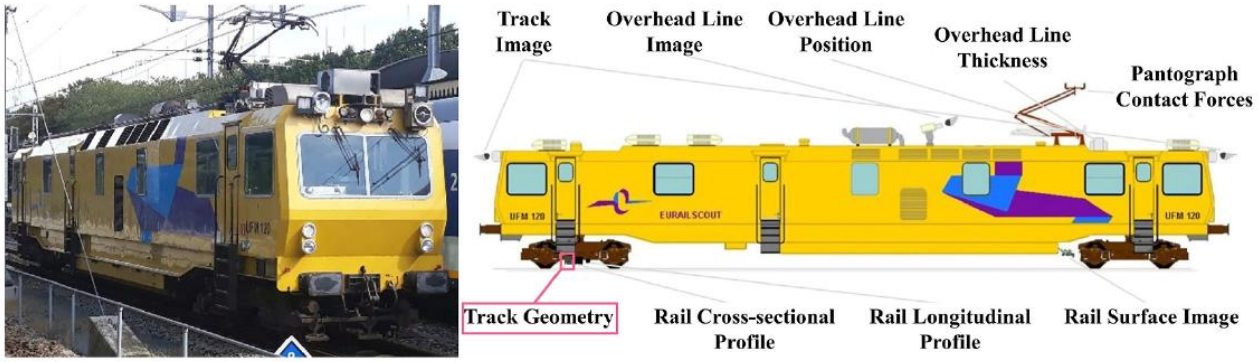

Figure 58: The universal track recording vehicle, in which the measured datasets can be retrieved from the BBMS, the Dutch central database system [4].

ABA measurements were conducted using the CTO, TU Delft's instrumented wagon. The ABA data were recorded at 25.6 kHz and then downsampled to 256 Hz following a low-pass filter with a cutoff frequency of 100 Hz. Each signal was converted from time to space domain using the local train speed and resampled at 0.25-meter intervals to match the geometry resolution. To reduce speed-dependent variations in acceleration amplitude, the ABA signals were normalized by dividing each trace by the square of the train's average segment speed. This ensured consistency in extracted features across runs with slightly different speeds.

ABA Feature extraction was based on the Continuous Wavelet Transform (CWT) using a Morlet wavelet. Two spatial frequency bands were defined to capture dynamic responses from different structural depths:

- $SAWP_S$, the Scale Average Wavelet Power in the range 0.04–0.33 m^{-1}, corresponding to the D1 wavelength (3-25 m). This feature is associated with substructure-related behaviour, as discussed in 6.3.3.
- $SAWP_B$, the Scale Average Wavelet Power in the range 1.25–2.5 m^{-1}, which corresponds approximately to the sleeper interval (0.6 m ± uncertainty). This feature is associated with ballast-related behaviour, as discussed in 6.3.3.

From each band, two statistical features were extracted: the standard deviation (SD_S for $SAWP_S$ and SD_B for $SAWP_B$) and the area under the curve (AUC_S and AUC_B for $SAWP_S$ and $SAWP_B$, respectively). These, together with avg(SD_{LL}), gave five features per segment. The values were averaged over four wheelsets and normalized using min–max scaling across all 48 segments.

The EnVTQI was then formulated as a weighted sum of the five features, as shown below.

$$\mathrm{EnVTQI}^j = \alpha_1 \overline{\mathrm{SD}}_{\mathrm{LL}}{}^j + \alpha_2 \overline{\mathrm{SD}}_{\mathrm{S}}{}^j + \alpha_3 \overline{\mathrm{AUC}}_{\mathrm{S}}{}^j + \alpha_4 \overline{\mathrm{SD}}_{\mathrm{B}}{}^j + \alpha_5 \overline{\mathrm{AUC}}_{\mathrm{B}}{}^j$$

where EnVTQI^j is the indicator of segment j, $\overline{\mathrm{SD}}_{\mathrm{LL}}{}^j$ is the rescaled avg(SD_{LL}) of segment j, $\overline{\mathrm{SD}}_{\mathrm{S}}{}^j$ is the rescaled SD_S of segment j, $\overline{\mathrm{AUC}}_{\mathrm{S}}{}^j$ is the rescaled AUC_S of segment j, $\overline{\mathrm{SD}}_{\mathrm{B}}{}^j$ is the rescaled SD_B of

segment j, $\overline{\mathrm{AUC}_{\mathrm{B}}}^{\mathrm{j}}$ is the rescaled $\mathrm{AUC_B}$ of segment j, α is the weight factor of each parameter while $\sum_{i=1}^{i=5} \alpha_i$ = 1.00.

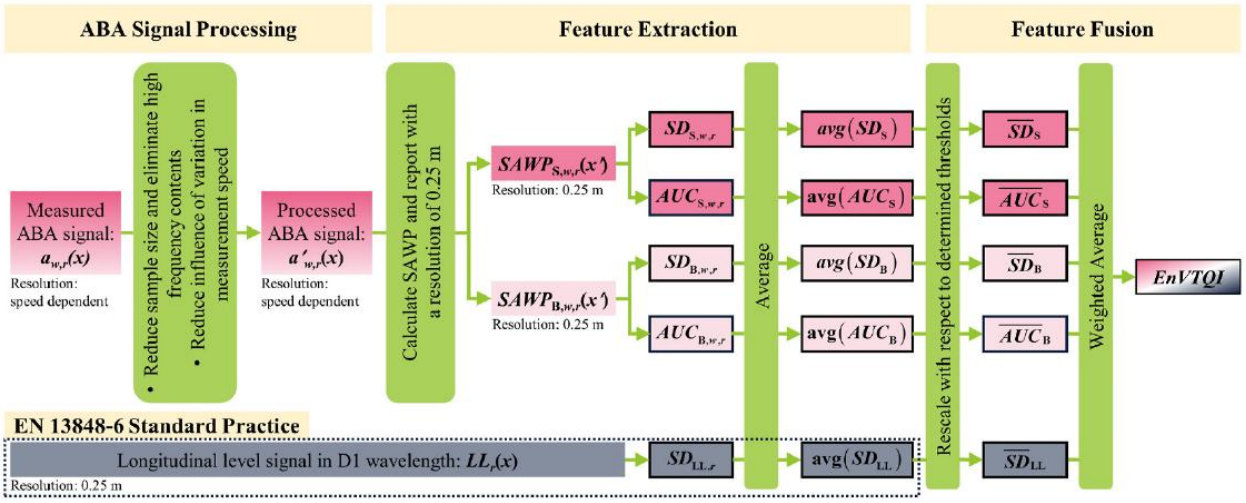

Figure 59: The framework for designing EnVTQI [4].

The EnVTQI scores were computed for all 48 segments and ranked in descending order. For each configuration, the top 10% (5 segments) were labeled as poor condition. For example, in the equal-weighting configuration, segments II-23, II-22, I-18, I-10, and I-23 ranked as the highest-scoring segments. Among those poor segments, I-18 was not detected by avg(SD_{LL}), the current industry practice. Additionally. the weighting setup enables users to customize the EnVTQI according to their specific application. For example, users can increase the weights assigned to ballast-related parameters to better support maintenance decisions regarding activities like ballast tamping.

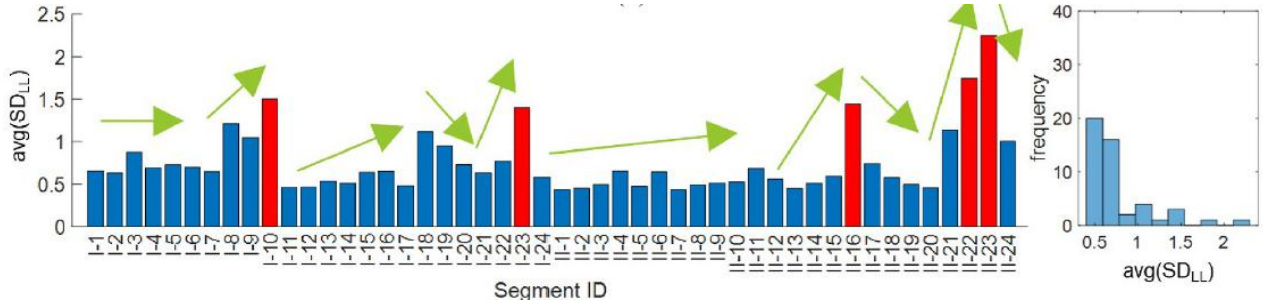

Figure 60: Track quality with respect to avg(SDLL), the industry practice indicator [4].

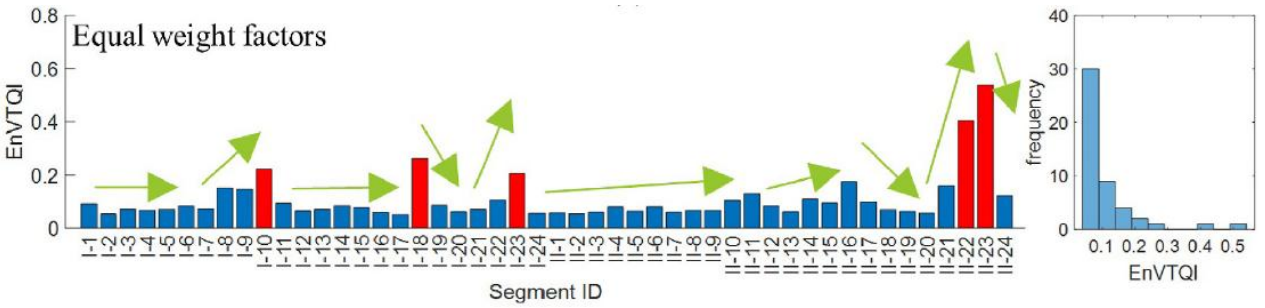

Figure 61: Track quality with respect to the proposed EnVTQI with equal weight configuration [4].

A segment-wise analysis revealed meaningful variation between geometry-only and fused configurations. For instance, I-11 and I-12 had similar avg(SD_{LL}) values, but I-11 had much higher $SAWP_S$ variability, leading to a higher EnVTQI score.

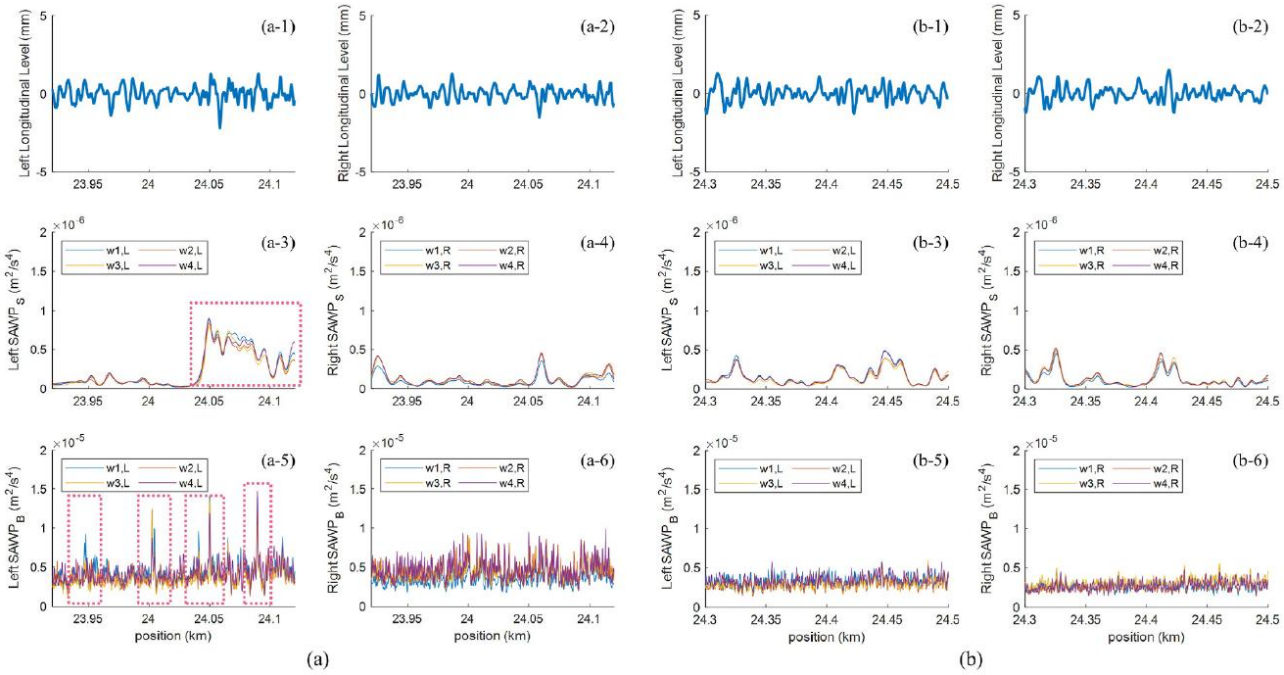

Figure 62: Signals corresponding to the track segment: (a) track segment I-11; (b) track segment I-12. Subfigures 1 and 2 are longitudinal levels at the left and right rails, subfigures 3 and 4 are SAWPS at the left and right rails, and subfigures 5 and 6 are SAWPB at the left and right rails [4].

To evaluate repeatability, the EnVTQI was computed from two ABA runs performed at different speeds. Without speed correction, the segment-wise difference was an average of 45.8%. After speed normalization, the difference was reduced to 6.6%, confirming the consistency of the ABA-based features when corrected. This highlights the robustness of EnVTQI under varying operating conditions.

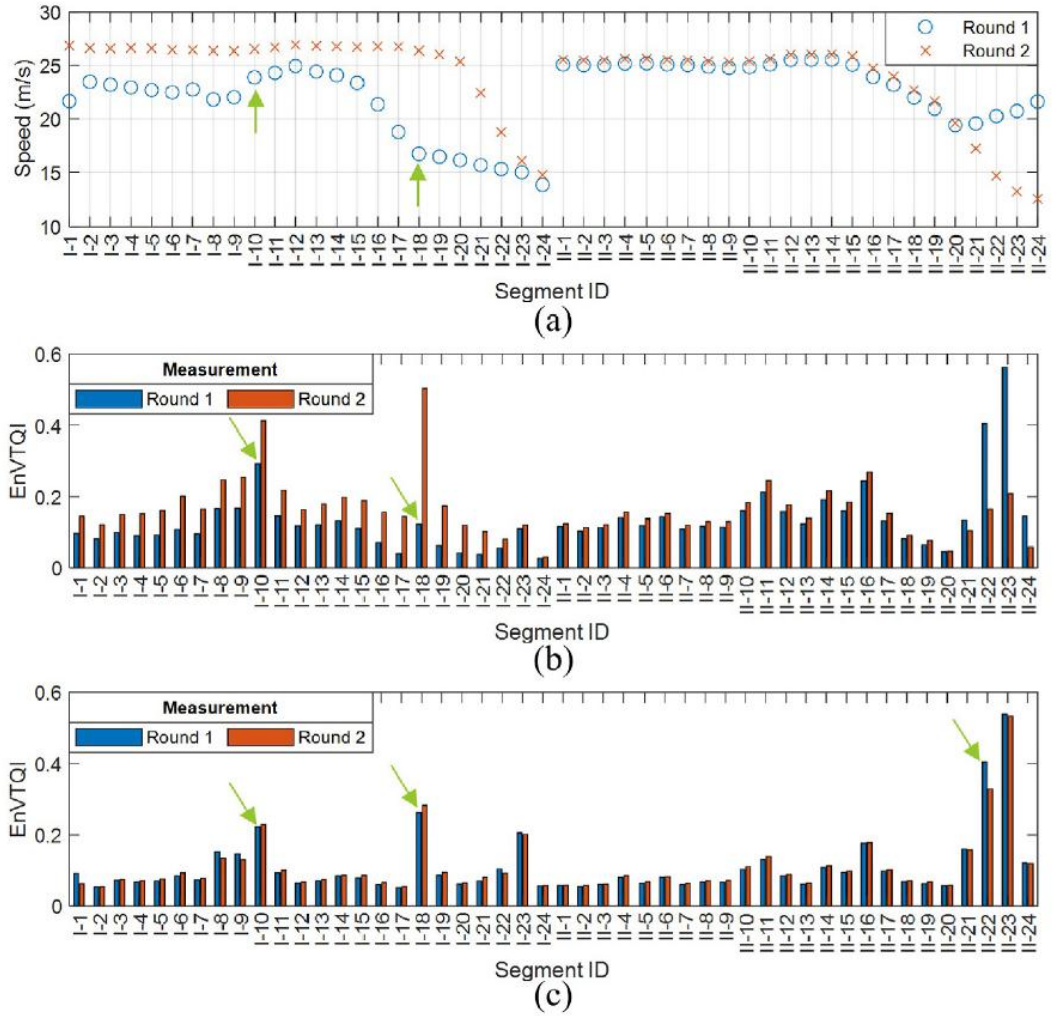

Figure 63: Comparison of EnVTQI between 2 rounds of ABA measurement: (a) measurement speeds from 2 rounds at a particular segment; (b) EnVTQI from ABA signals without reducing the influence of speed variation; (c) EnVTQI from ABA signals with reducing the influence of speed variation [4].

The evolution over time of EnVTQI was evaluated using historical measurements on the same track segment across multiple years. According to BBMS geometry data, the avg(SD_{LL}) increased steadily from 1.423 in 2018 to 2.742 in 2020, indicating progressive degradation, and then dropped significantly to 1.168 in 2021, reflecting improved condition after maintenance. The EnVTQI, computed with equal weight factors, followed a similar pattern, rising by 67.4% from 2018 to 2019 and then decreasing by 57.4% in 2021, consistent with the improvement in track condition. ABA-derived features, including $SAWP_S$ and $SAWP_B$, exhibited similar changes, with higher values near the bridge in 2019 and a marked decrease in 2021. These results indicate that EnVTQI effectively captures condition changes over time, responding to both geometry and ABA signals. Further supporting evidence was found in historical satellite imagery, which showed noticeable changes in ballast appearance near the bridge between 2019 and 2021, suggesting renewed ballast placement consistent with the improved track condition.

Figure 64: Historical satellite photos of an example segment for temporal consistency analysis. Changes can be seen as evidence of track maintenance activities in ballast appearance [4].

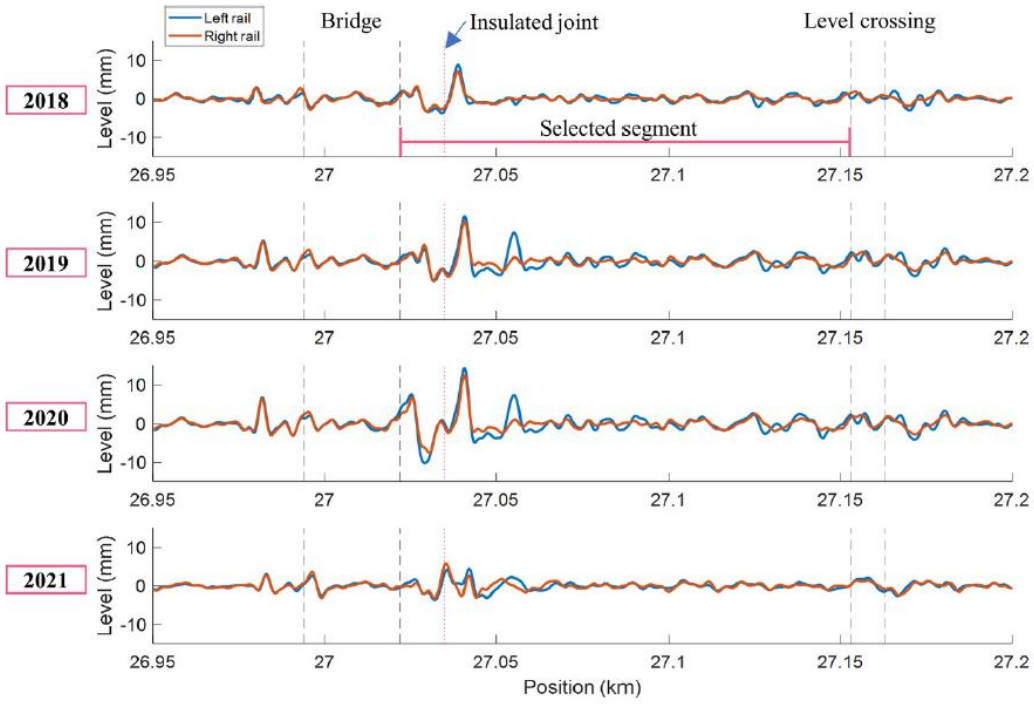

Figure 65: Evolution of longitudinal level from 2018 to 2021. The reduction in magnitude between 2020 and 2021 indicates a result of track maintenance efforts [4].

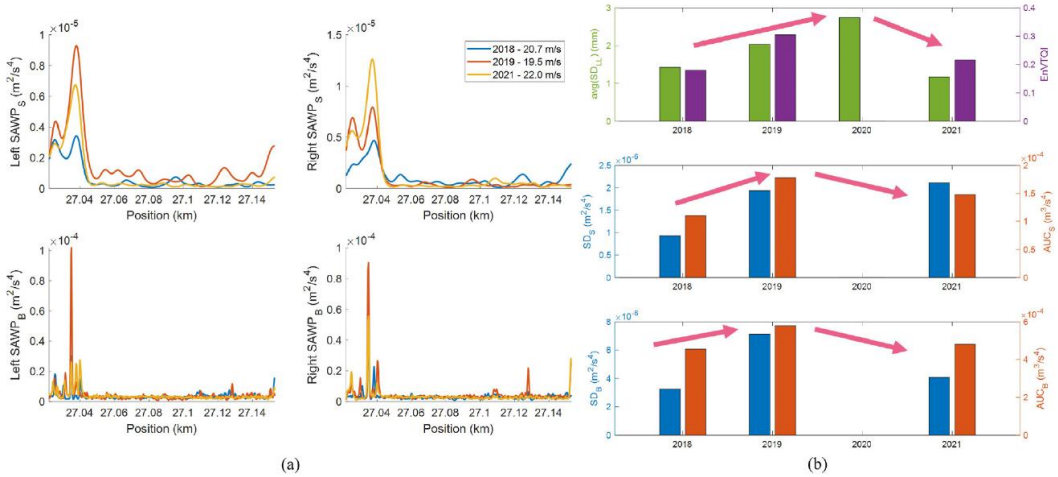

Figure 66: (a) SAWPS and SAWPB at the left and right rails from 3 different measurement years, (b) the evolution of EnVTQI and the corresponding features over time [4].

The analysis demonstrated that all five input features contributed meaningfully to the EnVTQI values. While avg(SD_{LL}) remained relatively stable across most segments, the ABA-derived features, SD_S, AUC_S, SD_B, and AUC_B, varied more significantly and captured differences in train–track dynamic interaction between segments. Among them, AUC_S and AUC_B were particularly sensitive to absolute energy levels, while SD_S and SD_B reflected variation within individual track segments. The fusion of these features within EnVTQI enabled a more comprehensive and layered representation of track condition than avg(SD_{LL}) alone.

EnVTQI was applied to a Dutch railway line, and its performance was shown to be consistent under varying train speeds and across historical measurement campaigns that included known maintenance interventions. These findings support the use of EnVTQI as a fusion-based condition indicator suitable for deployment in realistic field conditions. Moreover, the results highlight the potential of EnVTQI to identify segments with poor support conditions, particularly in areas where embankment or substructure issues, such as excessive deformation, contribute to track degradation.

6.4. Alignment of key findings with technical enablers

The findings and methods presented in this report contribute directly to Technical Enabler 2: Unmanned and non-invasive monitoring and inspections, as defined in the IAM4RAIL framework. Two specific sub-items within this enabler are particularly relevant to the Dutch and Norwegian demonstrators:

- Improvement in terms of cost reduction and/or better accuracy and implementation of inspection systems, such as onboard accelerometers and other non-contact sensors, enabling asset diagnostics.
- Data fusion algorithms to combine information from different inspection techniques, enhancing the ability to determine the health status of railway infrastructure.

In alignment with the objectives of WP13, this use case builds on high-TRL and industrially adopted monitoring systems, such as onboard accelerometers (ABA), track geometry (TG), and stationary bridge-mounted sensors. Rather than developing new sensing technologies, the work focuses on analyzing and integrating the outputs from these systems within a unified framework to provide more comprehensive and interpretable assessments of track and bridge condition.

In the Dutch case, this is achieved through the fusion of ABA and TG features to monitor track support conditions, especially in embankment areas prone to excessive deformation. The developed Enhanced Vertical Track Quality Index (EnVTQI) combines five interpretable features, derived from both geometry and ABA measurements, into a segment-level condition indicator. The results show that EnVTQI captures ballast and substructure-related behaviours that may not be reflected in geometry data alone. Findings also demonstrate consistency across different train runs, speeds, and even multiple years, including both pre- and post-maintenance conditions. These outcomes support the potential of ABA to complement and enhance conventional monitoring, aligning with a work towards a Technology Readiness Level (TRL) of 5–6 for substructure condition assessment. While ABA reached TRL 7 for detecting rolling contact fatigue under the IN2Track3 project, further validation under passenger train operations and with additional validations with trackside measurements is required to raise the TRL in this new application domain.

In the Norwegian case, a multi-sensor system has been deployed on an operational railway bridge. This system integrates different types of sensors under live traffic and is complemented by structural modelling to enhance the accuracy of diagnostics. While complete analysis is ongoing, the setup demonstrates practical implementation of non-invasive inspection to reach TRL 6.

Together, the Dutch and Norwegian contributions demonstrate how established monitoring technologies can be extended through advanced feature extraction, physical interpretation, and multi-source data fusion. These approaches support a transition from traditional inspection toward predictive, scalable monitoring in line with the goals of Technical Enabler 2.

7. Demonstration and evaluation plan

The first part of the chapter affirms the assets for KPIs evaluation in the deliverable D13.2. In the second part, the performance indicators of the demonstration are discussed in detail.
To start with, we report a table highlighting the influence of UC13.3 (Franch and Spain Use case) and UC13.4 (Netherlands and Norway Use case) to the MAWP KPIs

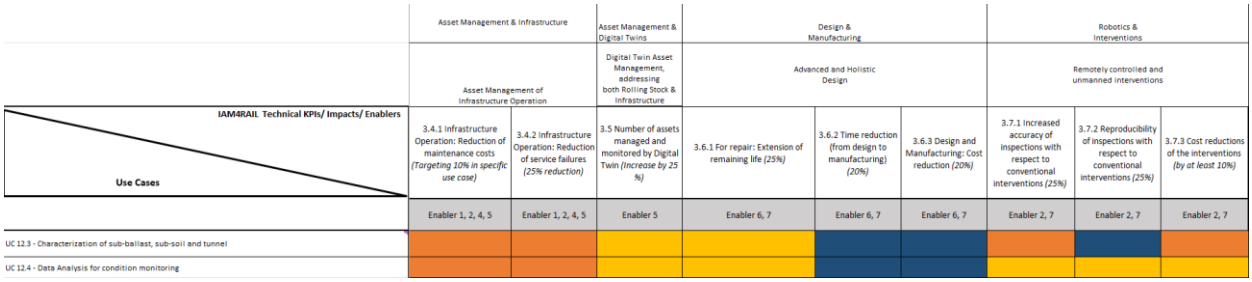

Figure 67: Use Case MAWP-KPI

Furthermore, in the next table, the Use Case KPIs are explicitly related to the various prototypes set as benchmarks for the demonstration.

Table 3: UC12.3 and UC12.4 KPIs

UC		Description
UC12.3	KPI1	Reduction of maintenance time
	KPI2	Reduction of maintenance cost
UC 12.4	KPI1	Track condition monitoring
	KPI2	Detectability of incipient known failures

Table 4: Prototype-MAW-KPI

PROTYPE ID	PROTOTYPE NAME	TARGETED MAWP KPI	USE CASE KPI (s)	Baseline
12.3.1	Monitoring of sub-ballast layers & subsoil	3.4.1	KPI1+KPI2	Survey in the field
12.3.2	Tunnel inspection	3.4.1	KPI1+KPI2	Survey in the field
12.3.3	Prediction of tunnel degradation via A	3.4.1	KPI1+KPI2	Survey in the field
12.3.4	Magnetic microwires	3.4.1	KPI2	Survey in the field
12.4.1	Data analysis for condition monitoring – embankment and transition zones	3.4.1 + 3.4.2	KPI 1	Measurement of track geometry
12.4.2	Data analysis for condition monitoring – bridges and transition zones	3.4.1 + 3.4.2	KPI 2	Manual inspection of the bridge

7.1. Monitoring of tunnel, sub-ballast layers, subsoil, and predictive maintenance for tunnels

7.1.1. Description of the demonstrators

7.1.1.1. Tunnel monitoring and predictive maintenance

7.1.1.1.1. Tunnel predictive maintenance

The prediction tool integrates data from digital defect surveys conducted as part of the detailed inspections carried out every six years, for all SNCF Réseau tunnels (approximately 1,400 in total). The ADN OST application, developed as part of this project, enables the simulation of defect evolution over different years.

This tool also allows users to view all characteristics of the defects and perform analyses at the scale of one or several structures, a railway line, a region, or the entire network.

The precise and comprehensive data provided by the application cannot be disclosed for confidentiality reasons related to the condition of the SNCF Réseau infrastructure. However, a few examples are presented below.

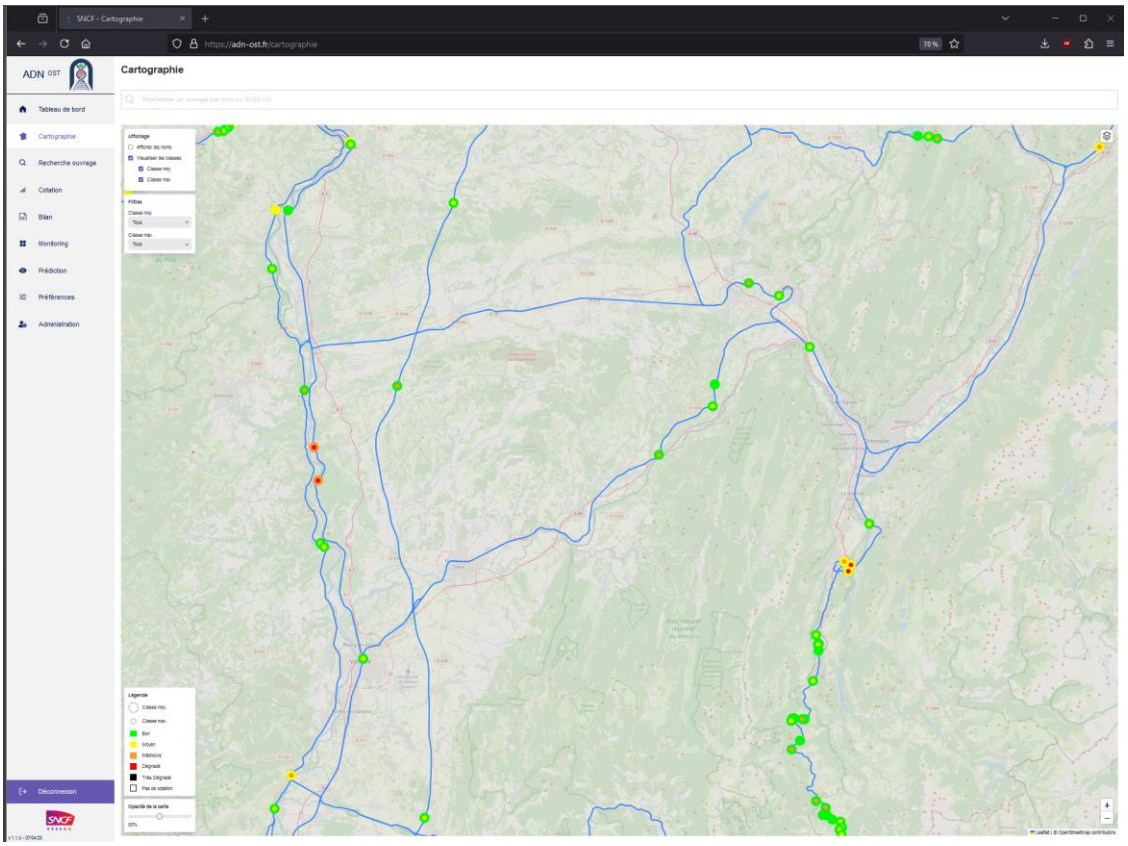

Figure 68: Mapping interface

Figure 69: Status Data Viewing Interface for a tunnel

Figure 70: Predictive Degradation Modeling Interface for a Tunnel (2030 & 2041)

7.1.1.1.2. High efficiency tunnel inspection technologies

Demonstrations were conducted in operational and abandoned railway tunnels to simulate disorders:

- Operational tunnels :
  - COLROY-LUBINE tunnel ;
  - BRECHE tunnel ;
  - COL DE TENDE tunnel.
- Abandoned tunnels :
  - POMMERAIE tunnel ;
  - MARNAY SUR MARNE tunnel.

These tunnels were selected due to their structure composed of different types of masonry representative of the majority of tunnels in the SNCF Réseau heritage.

The inspection systems used are as follows:

- TS4 from the German company SPACETEC;
- ELISE co-developed by SNCF Réseau and the Swiss company Amberg;
- SCANTUBES developed by the French company SITES.

The demonstration and evaluation phase of the project aims to validate monitoring methodologies and processing tools under representative field conditions. Demonstrators have been selected to reflect a variety of geotechnical and operational contexts. The tools developed as part of monitoring of tunnel, sub-ballast layers, subsoil and predictive maintenance are being evaluated in terms of the accuracy and reliability of seismic measurements, the feasibility of deploying acquisition setup (landstreamer) in operational contexts, and the added value for decision-making.

The HSL context was selected as a priority due to the availability of more input data and prior knowledge about the structure compared to conventional lines (CL). Two HSL study sites were selected for their distinct characteristics, namely the North European French HSL and the South-East French HSL. These two sites exhibited trackbed disorder, including track geometry irregularities and mud-pumping phenomena. These conditions were deemed conducive to the experimental evaluation of the active seismic approach. In contrast, the site chosen for groundwater monitoring (named Sarrebourg) is in an area affected by sinkhole risk associated with the presence of gypsum in the subsoil, offering a representative case for assessing hydrogeological influences on infrastructure stability.

All aspects of seismic data processing (both for active and passive seismic methods) have been thoroughly addressed with the objective of developing tools for each step of the seismic workflow. The optimization of data acquisition and the automation of processing steps lead to a significant reduction in overall execution time. These efforts have led to the development of individual python libraries or modules capable of handling various types of seismic data.

The next key step is to integrate these developments into a unified and user-friendly tool. Such a tool would enable full autonomy in seismic data processing, from quality control to final interpretation. It would serve as a robust decision-support system for infrastructure characterization and monitoring across different use cases.

7.1.1.1.3. Passive contactless magnetic microwire

The goal of this demonstrator is to evaluate the use of **passive, contactless magnetic microwire sensor arrays** for **high-definition tunnel convergence monitoring**. This technology is proposed as an innovative alternative to traditional methods such as convergence tapes and topographic measurements.
The data obtained through these sensors will allow us to:

- **Detect and quantify deformations** in the tunnel structure over time with high spatial and temporal resolution.
- **Identify deviations from the intended alignment**, offering early warnings of structural changes.
- **Compare real ground behavior** with theoretical or empirical models used in tunnel design, especially in areas with significant geotechnical uncertainty.
- **Assess the homogeneity of the excavated environment**, identifying sections with greater instability or movement.
- **Estimate the technical and economic feasibility** of using this system in real tunnel environments, including measurement times and associated costs.

To achieve these objectives, the demonstrator includes laboratory testing to:

- Determine the **optimal orientation of the microwires** for maximum sensitivity to deformation.
- Define the **most effective setup and installation method** for the sensor arrays.
- Perform **stress-strain measurements on laboratory-scale tunnel models**, validating the system's ability to detect realistic deformations.

7.1.1.2. Sub-ballast layers and subsoil monitoring

Figure 71 represents the context diagram, highlighting the principal function of the processes, and which is "to manage risks and incidents" and illustrating the various major actions involved in the processes. It represents a diagram illustrating the typical response process following an incident occurring on or near railway tracks. The first step involves analysing the broader context of the event, which generally requires an on-site visit for visual inspection. Once the initial observations are completed, the process continues with the collection and review of existing site data—such as historical records, geological characteristics, and other relevant information. Based on this assessment, an action plan is then drafted. It includes considerations such as the required budget, available human resources, and possible service disruptions. The result is a set of recommendations outlining the necessary investigations and interventions, along with their proposed schedule and prioritization.

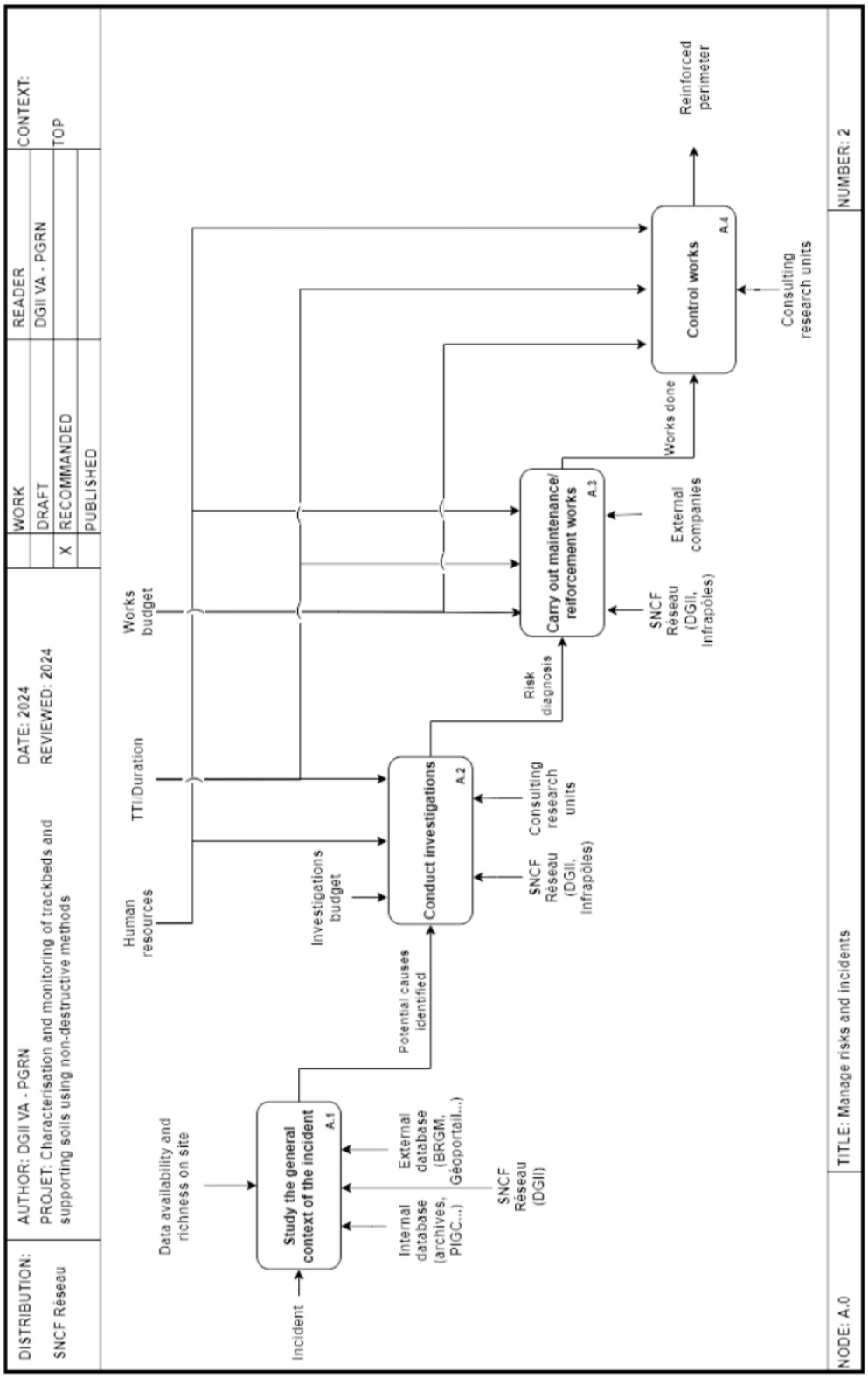

Figure 71: Detailed Context Diagram

7.1.2. Evaluation: Key Performance Indicators

7.1.2.1. Tunnel predictive maintenance

It is important to emphasize that predictive models cannot substitute for the technical diagnosis and risk assessment performed by engineers, which are essential for precisely defining the required interventions (including the specific locations, types of treatment, and associated technical timelines).

Nevertheless, in an asset management context, predictive models allow for decision-making aimed at optimizing the financial and capacity impact of tunnel reinforcement work.

Even though it is not possible to define KPIs that are suitable for all tunnels (since each case is different), the following example is presented to illustrate the potential benefits.

According to SNCF Réseau's tunnel regeneration policy, reinforcement work must be considered within 6 years for tunnel zones with a rating above 60.

In the example below, based on the rating curve from the last inspection conducted on 11/05/2020, a zone of approximately 25 meters has a rating above 60 and therefore requires the scheduling of a regeneration operation in 2026.

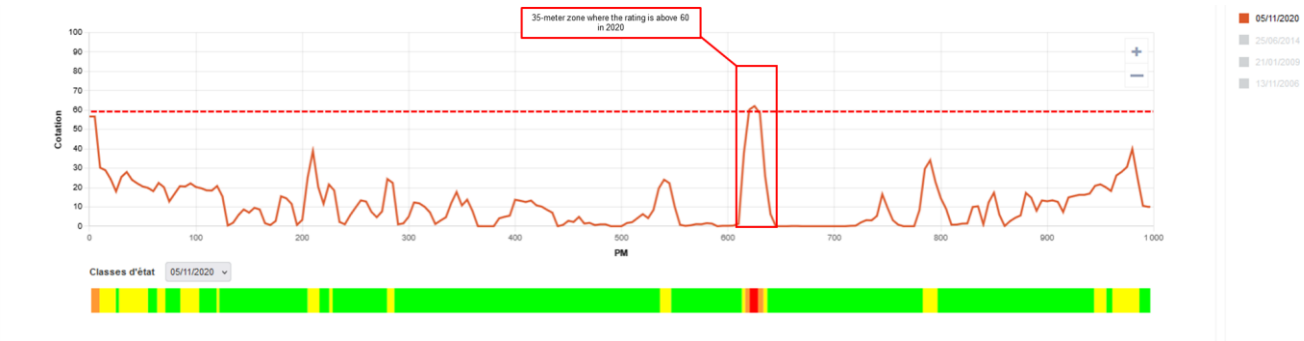

Figure 72: Tunnel rating curve

However, the simulation of the structure's deterioration by 2026 shows that another 10-meter-long zone is likely (based on geological and geomorphological configuration, structural characteristics, type and evolution of defects, etc.) to reach a rating level of 60 by 2026, thus potentially requiring another intervention around 2032.

By incorporating these predictions, it becomes possible to anticipate these maintenance needs and plan a single work phase to address all 60 meters, rather than two separate phases.

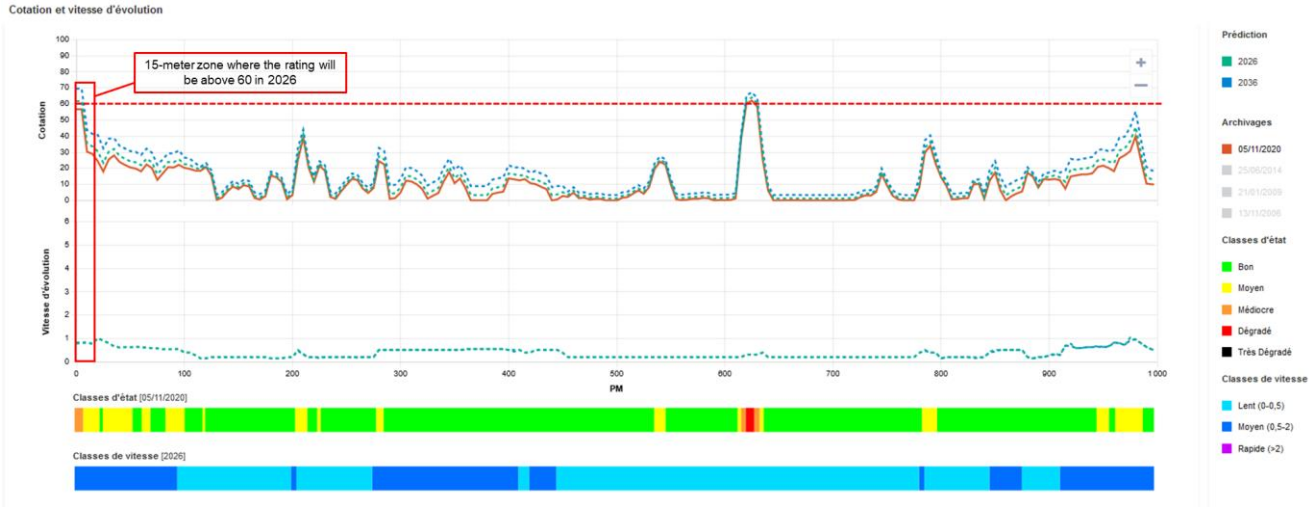

Figure 73: Simulation of the tunnel rating in 2026 and 2036

Provided as references, the following presents an evaluation of the key performance indicators (KPIs) for this example. Combining the work requirements leads to time and cost savings, particularly through optimized setup and logistics using work trains.

$$KP1\ (\%\ time\ savings) = \frac{Time_{tradicional\_method} - Estimated\ time_{new\_method}}{Time_{tradicional\_method}} \times 100 = 27\%$$

Where:

- $Time_{tradicional_{method}}$= Time of the works considering two phases (≈ 11 weeks)
- $Estimated\ time_{new\_method}$ = Time of the works considering a single phase using predictive models (≈ 8 weeks).

$$KP2\ \%\ (cost\ savings) = \frac{Equ.\ cost_{t.m.} - Equ.\ Esti_{n.m.}}{Equ\ cost_{t.m.}} \times 100 = 7\%$$

Where:

- $Equ.\ cost_{t.m.}$ = Cost of the works considering two phases (≈ 0.625 M€)
- $Equ.\ Esti_{n.m.}$= *Cost of the works considering a single phase using predictive models (≈ 0.580 M€).*

7.1.2.2. High efficiency tunnel inspection technologies

These new technologies do not cover all the points that need to be noted during a traditional tunnel inspection and therefore must be used at this stage as a complement to the traditional method.

However, they provide valuable assistance for the identification and characterization of failures and offer an improvement in the accuracy of failure records and therefore in the evaluation of the degradation of structures (gain in terms of quality).

Even if they generate an additional cost, they help optimize the duration of inspections in the structures. The visualization of outputs before the visit, with possibly digital assistance to automatically detect changes compared to the previous measurement, indeed facilitates the prior detection of sensitive areas.

Comparisons of actual inspections will need to be carried out to estimate the following KPI:

$$KP1\ (\%\ time\ savings) = \frac{Time_{tradicional\_method} - Estimated\ time_{new\_method}}{Time_{tradicional\_method}} \times 100$$

Where:

- $Time_{tradicional_{method}}$= Time of a traditional inspection method
- $Estimated\ time_{new\_method}$ = Time of a traditional inspection method with new technologies assists Passive contactless magnetic microwire

7.1.2.3. Passive contactless magnetic microwire

The main objective of this KPI is to check whether the time needed to perform a measurement is able to control the convergence of the tunnels can be reduced. For this purpose, sensors ("micro-wires") capable of providing accurate information on the convergence of the tunnels will be used. This factor is directly related to correct preventive maintenance, by knowing in real time what data is being generated, this allows infrastructure managers to detect any changes in convergence early and take corrective action if necessary.

As it has a low technological maturity level (TRL4), it will not be tested in a relevant environment, but will be tested in laboratories, **we can obtain estimates of the time it may take to perform the inspection** and compare it with traditional methods to establish the time saving ratio that could be achieved with the application of this technology.
To evaluate this KPI we can use the following formula.

$$KPI\_1_{(\%\ time\ saving)} = \frac{Time_{traditional\_method} - Estimated\ time_{new\_method}}{Time_{traditional\_method}} \times 100$$

- *Traditional Method Time* is the time required to perform an inspection using the traditional method.
- *Estimated time New Method* is the time required to perform an inspection using the new method.

If KPI_1 is positive, the new method takes less time than the traditional one (time saving). If it's negative, the new method takes more time.

Similarly, to estimate cost savings, the following KPI will be used:

$$KPI\_2_{(\%\ cost\ savings)} = \frac{(Equ.cost_{t.m.} + Wf.cost_{t.m.}) - (Equ.Esti_{n.m.} + Wf.Esti_{n.m.})}{Equ\ cost_{t.m.} + Equ\ cost_{t.m.}} \times 100$$

Where:

- *Equipment costs of the traditional method of an inspection* ($Eq.cost_{t.m.}$): refers to the costs associated with the purchase, maintenance and calibration of the equipment necessary to carry out the inspection.
- *Workforce cost of the traditional method of an inspection* ($Wf.cost_{t.m.}$). This is the expenditure related to the time and human effort required to perform the inspection.
- *Estimated equipment cost of new method of an inspection* ($Eq.Esti_{n.m.}$): refers to the estimated costs associated with the acquisition, maintenance and calibration of the equipment necessary to carry out the inspection.
- *Estimated workforce cost of a new method of inspection* $Wf.Esti_{n.m.}$). This is the expenditure related to the time and human effort required to perform the inspection.

If the KPI_2 is positive, the new method costs less than the old one (cost saving). If it's negative, the new method is more expensive (increased costs).

7.1.2.4. Sub-ballast layers and subsoil monitoring

The developments and the proposed methodology significantly improve the efficiency of sub-ballast layers, subsoil characterization by combining optimized seismic acquisition and automated data processing.

The proposed KPI 1 is about the reduction of seismic acquisition time with the following relation:

$$KP1\ (\%\ time\ savings) = \frac{Time_{tradicional\_method} - Estimated\ time_{new\_method}}{Time_{tradicional\ method}} \times 100$$

Where:

- Traditional Method Time is the time required to maintenance and works including investigation by the traditional method.
- Estimated time new method is the time required to maintenance and works including investigation by the new method.

KPI 1 is calculated for a 150 m section on the pilot site where the landstreamer was tested. The seismic acquisition time is evaluated for the traditional setup and for the new technique (i.e. landstreamer):

- The time required to survey 150 m with the conventional setup is 9h ;
- The time required to survey 150 m with the landstreamer setup is 5h ;

$$KPI\ 1(\%\ time\ saving) = \frac{9h(for\ 150m) - 5h\ (for\ 150m)}{9h(for\ 150m)} \times 100 = 44\%$$

The KPI 1 can reach more than 44% regarding the time saving of maintenance and work for sub-ballast and sub-soil and concerning tunnel inspections and the planning of repairs operations. Furthermore, the integration of our automated processing tool reduces interpretation time by half, while minimizing the need for manual user intervention. Overall, the acquisition time is reduced by approximately 44%, and the full workflow (from field data to interpreted results) is considerably accelerated.

7.2. Data Analysis for condition monitoring

7.2.1. Assessing embankment stability using train-borne measurements

This section outlines the ongoing and planned demonstration activities for Use Case 4 (UC4) in the Netherlands. Within Deliverable D13.2, demonstration efforts have been successfully completed on the Dordrecht – Lage Zwaluwe in the Netherlands, as well as in Sweden and Norway. These demonstrators have validated the use of ABA measurements, impact test interpretation, and data fusion techniques as described in Section 6.3.

In line with the Grant Agreement, a follow-up demonstration is planned on the Delft–Schiedam line, one of the oldest operational corridors in the Dutch railway network. The goal is to apply the validated approaches, including multi-ABA response [2], ABA interpretation through impact modal testing [3], and fusion-based track condition indicator [4], to evaluate their transferability to a corridor with different infrastructure and operational conditions. While relevant datasets have already been collected, further analysis is ongoing and will be reported in Deliverable D13.3. The demonstration will focus on evaluating the reliability and consistency of results from this corridor and exploring the feasibility of using fused data for condition monitoring.

7.2.1.1. Description of the demonstrators

The demonstration will take place on the Delft–Schiedam line, which has already been monitored using TU Delft's instrumented wagon, providing ABA measurements from four wheelsets, alongside track geometry (TG) data retrieved from the BBMS system.

The goal is to apply the previously developed and validated methods, including wavelet-based ABA feature extraction, segment-based indicator calculation, and cross-comparison with TG data, using a consistent analysis framework. The work will include:

- Processing ABA signals to extract Scale Average Wavelet Power (SAWP) features in ballast- and substructure-related frequency bands.
- Comparing ABA response characteristics with longitudinal level measurements.

- Applying segment-level indicators across standardized lengths (e.g., 200 m).

Although data collection has been completed, the analysis is still ongoing. The Delft–Schiedam demonstration will focus on validating the method's applicability to this specific corridor and will serve as an important case study for the upcoming Deliverable D13.3.

7.2.1.2. Evaluation: Key Performance Indicators

Two key indicators will be used in the evaluation:

- KPI1 – ABA vs. TG sensitivity:

This index compares the number of defects detected in ABA signals relative to those in TG data. A defect is defined as a location where a given signal exceeds a defined threshold. KPI1 is calculated as:

$$\mathrm{KPI1} = \frac{(\mathrm{defect}_{\mathrm{ABA}} - \mathrm{defect}_{\mathrm{TG}})}{\mathrm{defect}_{\mathrm{TG}}} \times 100$$

KPI1 was previously validated on the Dordrecht–Lage Zwaluwe line and will now be applied to Delft–Schiedam to quantify the relative detection sensitivity of ABA.

- EnVTQI – Enhanced Vertical Track Quality Index:

This segment-based condition index fuses five normalized features: avg(SD_{LL}) from TG and four SAWP-derived features from ABA (SD_S, AUC_S, SD_B, AUC_B), as follows:

$$\mathrm{EnVTQI}^{j} = \alpha_1 \overline{\mathrm{SD}}_{\mathrm{LL}}{}^{j} + \alpha_2 \overline{\mathrm{SD}}_{\mathrm{S}}{}^{j} + \alpha_3 \overline{\mathrm{AUC}}_{\mathrm{S}}{}^{j} + \alpha_4 \overline{\mathrm{SD}}_{\mathrm{B}}{}^{j} + \alpha_5 \overline{\mathrm{AUC}}_{\mathrm{B}}{}^{j}$$

The EnVTQI will be computed using multiple weight configurations, including equal weighting and layer-sensitive configurations focusing on ballast or substructure response. Segments will be ranked based on EnVTQI values to identify segments with poor support conditions, which can potentially be supporting evidence for identifying excessive embankment deformation.

While the relevant data have already been acquired, further calculation and application of the indicators for the Delft–Schiedam line are ongoing. The demonstration will evaluate the consistency and reliability of the results and test the effectiveness of using fused data to inform infrastructure condition monitoring.

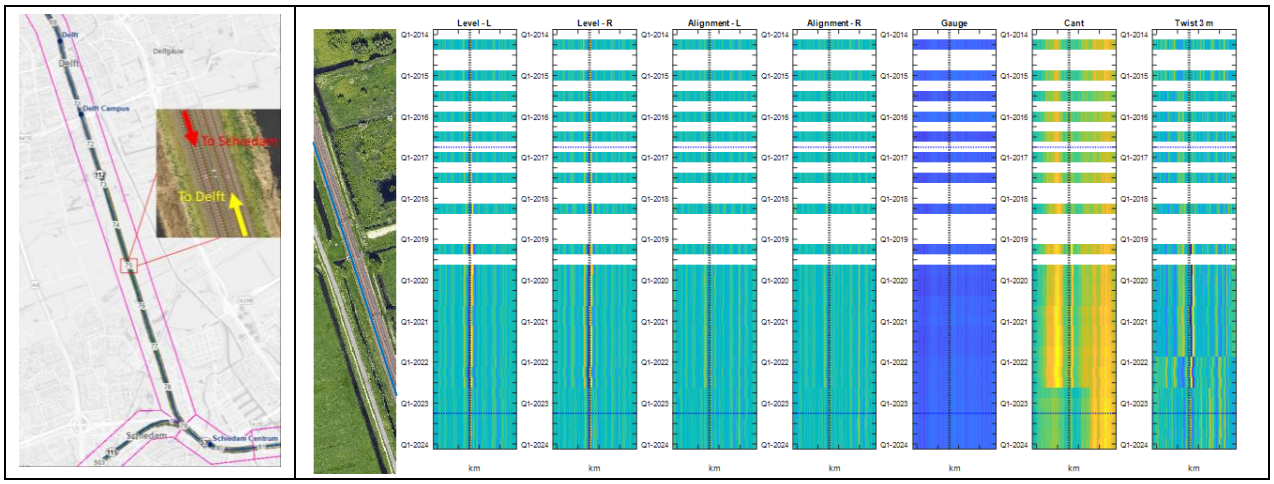

Figure 74: Overview of the Delft–Schiedam line and the evolution of track geometry in an example track segment.

Figure 75: ABA measurement with the CTO, TU Delft's measurement wagon. The photo was taken as the train passed Delft Campus station.

7.2.1.3. Exploratory Integration of InSAR, ABA, and TG for Higher-Frequency Monitoring

In addition to the Delft–Schiedam demonstration, an exploratory study is being developed to integrate InSAR (Interferometric Synthetic Aperture Radar) with ABA and TG data on the Dordrecht–Lage Zwaluwe line. This effort aims to address a key limitation of current monitoring practices—namely, the low measurement frequency of track geometry data (typically 3–4 times per year in the Netherlands). In contrast, InSAR data can be acquired every week, and in future applications, ABA monitoring could be implemented using daily passenger trains. Fusing these data sources enables higher-frequency, broader-coverage substructure monitoring, addressing the need for early detection of degradation in critical areas such as transition zones.

This approach will involve predicting the longitudinal level using a hybrid neural network model (CNN-LSTM/GRU), which combines interpolated InSAR and ABA signals. A new performance index based on predicted longitudinal level has been proposed to track condition evolution over time at

higher resolution. This method shows potential for supporting prescriptive maintenance planning through enhanced integration of sensing.

For this section, Deliverable D13.3 will focus on the methodology, model performance, and insights into the added value of multi-sensor fusion for infrastructure condition monitoring, exploring the potential benefits of increased measurement frequency, improved spatial coverage, and early degradation detection capabilities.

7.2.2. Analysis of structural condition monitoring techniques (civil structures and works)

As the installation of the monitoring system for the two Søsterbekk bridges is contracted for installation during the summer of 2025, no data has yet been recorded for testing the analysis techniques. Although a finite element model has been developed, it has not been calibrated yet due to the lack of measurement data, so it was evaluated that testing the developed analysis methods on the synthetic data would not yield any meaningful insight.

7.2.2.1. Description of the demonstrator

As part of WP12, Sub-task 12.3.4, a proposal has been developed to instrument Søsterbekk bridges and their transition zones for monitoring structural integrity during train operations. Alongside the monitoring plan, a detailed technical specification for the measurement systems has also been prepared. The use case includes two prestressed concrete bridges:

- *Søsterbekk bridge 1*, which is a single-span prestressed concrete bridge, approximately 50 meters long
- *Søsterbekk bridge 2*, which is a two-span prestressed concrete bridge, approximately 100 meters in length.

The Søsterbekk bridge 2 is situated within a track curve with a radius of 350 meters. Therefore, it was decided to increase the sensor systems installed on Søsterbekk bridge 2 while a simplified sensor system was considered for Søsterbekk bridge 1. For the same reason, the transition zones connected to Søsterbekk bridge 2 will be instrumented.

Procurement process: Bane NOR, as the national railway infrastructure manager, was appointed to lead the procurement process. Technical support throughout the process was provided by SINTEF and NORCE. Upon completion of the project, Bane NOR will retain ownership of the measurement system. The organization also has a vested interest in maintaining an operational monitoring system to ensure safe rail transport, especially given the increase in permitted axle load as described in Section 6.2.1, but also due to the increase in train frequency and annual gross tonnage.

The procurement was announced 11.02.2025 and published on Mercell Tendsign plattform, and Bane NOR received bids from two companies. Following a negotiation round and evaluation of both the commercial and technical aspects of the proposals, Bane NOR awarded the contract to NGI, as a main contractor with the subcontractors Dewesoft for accelerometers, Sisgeo SRL for inclinometers, Strainstall by SES Group for strain gauges on rails, Temposonics for extensiometers,

Apogee Electronics for relative humidity instruments and Høyden AS for technical access for installation (climbing).

Sensor Systems and Instrumentation plan: The scope of the new sensor systems covers structural integrity, including measurements of deformations, strains, and vibrations in bridge structures, as well as deformations, track condition, and vibrations in transition zones during train passages. It also covers environmental conditions, including air and rail temperature and relative humidity (RH). The instrumentation of Søsterbekk bridge 1 and Søsterbekk bridge 2 is illustrated in *Figure **76*** and *Figure **77***, respectively, with a detailed view of the instrumentation of the transition zones in *Figure **78***. The figures show the type of the sensors and their placement.

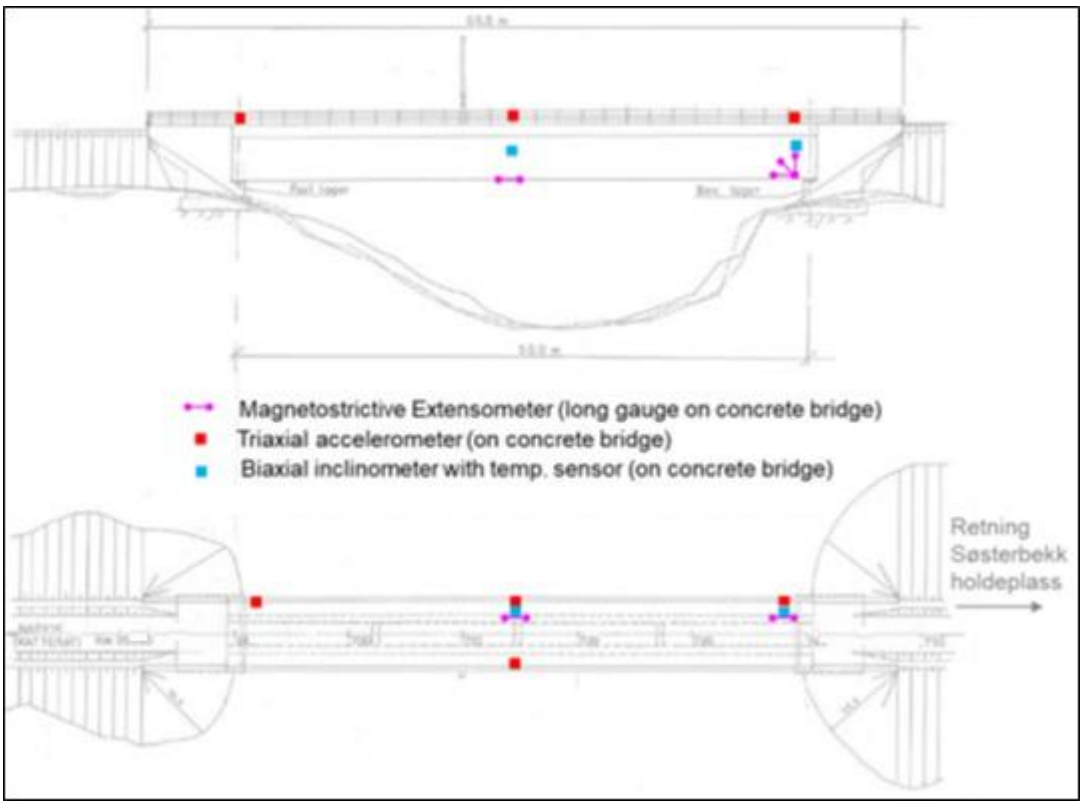

Figure 76: Instrumentation plan of sensor systems for Søsterbekk bridge 1 showing type and placement of sensors.

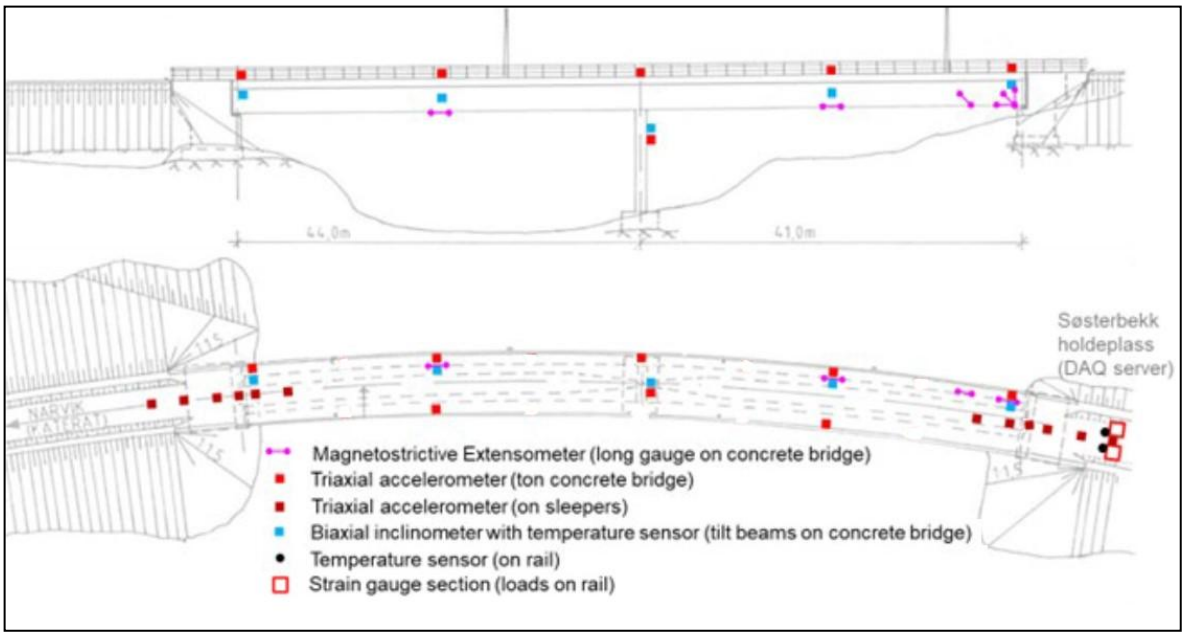

Figure 77: Instrumentation plan of sensor systems for Søsterbekk bridge 2, showing type and placement of sensors.

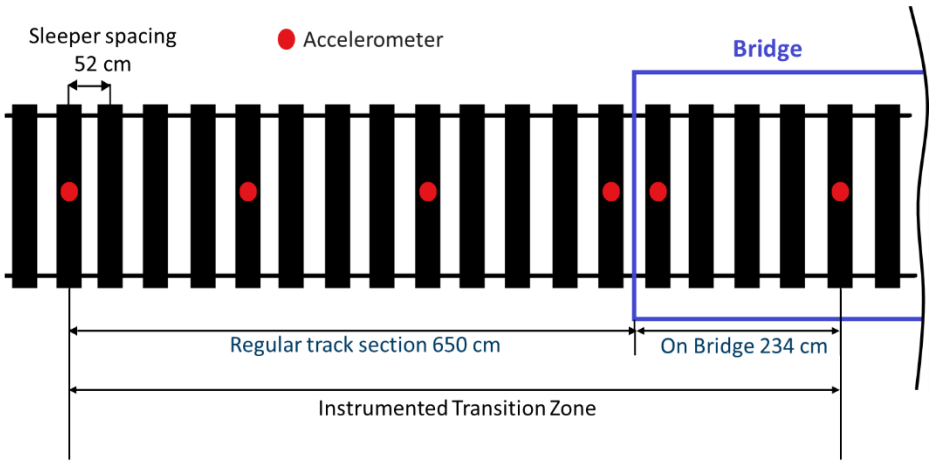

Figure 78: Placement of accelerometers in the transition zone of Søsterbekk bridge 2 on one side of the bridge. Similar installation is also used in the transition zone on the other side of the bridge.

The sensor systems of Søsterbekk bridge 1 involve four Magnetostrictive extensometers for shear measurement at the support point, four triaxial accelerometers on top of the bridge, and two biaxial inclinometers on tilt beams and midspan of the bridge beam. The sensor systems of Søsterbekk bridge 2 involve six magnetostrictive extensometers for shear measurement at support points, eight triaxial accelerometer on the top of the bridge and on the centre column, ten triaxial accelerometer on sleepers in the centre of rail, two inclinometers on tilt beam and midspan of the bridge beam, two temperature sensors on each rail, 2 times eight strain gauges on each rail for measuring vertical, lateral and axial rail loads during train passage.

The bridge instrumentation involves various sensors to enable comparative analysis. The

magnetostrictive extensometers combine the advantages of high resolution, adaptation for dynamic measurements, and flexibility for installation. However, displacement measurements by extensometers can be affected by temperature gradients, resulting in temperature-related fluctuations over an extended period. This can be compensated based on the temperature measurement by a thermal sensor. The inclinometers are designed to measure bridge deflection. Particular attention will be paid to the measurement frequency, as it has limitations for fast dynamic measurements. The inclination from the tiltmeter is a point measurement; therefore, its placement is crucial. The tiltmeter also has a built-in temperature sensor for compensating for temperature variations. For dynamic measurements, the accelerometers offer high precision with flexible connections for robust installation. The highest precision of the accelerometer is in the frequency range 10-250 Hz. For the dynamic measurement in the transition zones, the same type of accelerometers will be used to monitor the sleepers. For measuring the dynamic forces, the strain gauges on the track (right and left rails) will be considered. The weight-in-motion method may be considered for estimating the vertical load, while the lateral load may be estimated based on horizontal shear forces at the rail foot or on vertical loads at two levels on the rail neck.

For long service life, high capacity, and minimum maintenance, the instrumentation is based on power supply and signal transmission via cable. A distributed system with EtherCAT data bus has been chosen for minimal cable routing and maximum flexibility when it comes to sensor connection.

Both operating status per sensor, measurement series from train passages, and statistical data will be transferred to NGI's cloud solution *"NGI Live"*. The cloud-based solutions ensure data security, access control, and user authentication with notification by SMS or email on deviation.

When a train passage is detected, strain and deformation measurement at a specific frequency will be extracted from the ring buffer, from approx. 20 seconds before detection to time *t* corresponding to the train passage through. These data from the entire period will be both stored locally and immediately transmitted to NGI's cloud solution. In addition to high-frequency data from train passages, the system will continuously calculate statistical data for each sensor and continuously transmitted to NGI's cloud solution for visualization in web-based dashboards. Operating parameters and status for each sensor or interface unit will also be transmitted together with the statistical values.

Transfer of measurement data from Søsterbekk to NGI's cloud solution will be done via fibre optic technology. High-frequency measurement series from each train passage will automatically be transmitted continuously. Operating status per sensor and statistical data are transferred at configurable intervals. Local copies of measurement series logged when trains pass will be kept at least until the measurements have been transmitted.

Installation of the monitoring systems will be carried out in conjunction with the annual railway maintenance activities, scheduled to begin at the end of May and conclude in September 2025. According to the project timeline, the system is expected to be commissioned by late September or early October. Once operational, it will begin generating measurement data that will serve as a critical input for the research activities under WP13.

7.2.2.2. Platform for monitoring of new instrumented sensor systems

As mentioned above, the instrumentation of bridges and transition zones is led by Bane NOR as the employer with the main contractor and subcontractors[1] incorporates "*NGI Live*" platform, which is a remote monitoring platform running in NGI's cloud solutions. The sensors and settings are managed using a web portal supporting monitoring of sensors and measurements in real-time. The measurement frequency can be increased or decreased depending on the scope and the capacity of the measurement system.

NGI Live supports several protocols for data transfer, including the machine-to-machine (MQTT) protocol, the Constrained Application Protocol (CoAP), and the Short Message Service (SMS) protocol. Data can be retrieved from various data sources and data loggers (for example, via file upload, file transfer protocol, or third-party API).

Monitoring of sensors and visualization of data are performed using web-based dashboards that support various types of visualizations, including maps, graphs, and tables. An overview of metadata, statistics, and time series, along with the option to download data, can be managed. An overview of sensors and locations is obtained using an integrated map solution with zooming and navigation tools. *Figure **79*** shows an example of how to limit periods, filter on sensors and other metadata, and overview metadata, statistics, and time series, as well as the option to download data.

[1] Main contractor is NGI with subcontractors Dewesoft for accelerometers, Sisgeo SRL for inclinometers, Strainstall by SES Group for strain gauges on rails, Temposonics for extensometers, Apogee Electronics for relative humidity instruments and Høyden AS for access technique for installation (climbing).

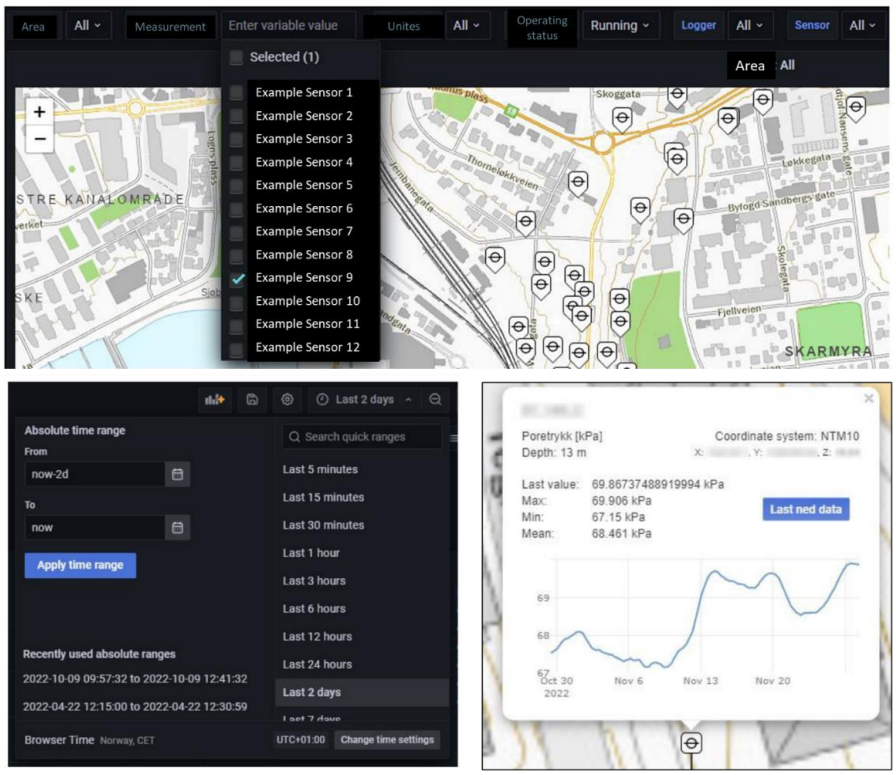

Figure 79: Web-based dashboards of NGI Live platform used for monitoring of new sensor systems and visualization of data.

In the dashboard, you can set up an alarm and notification for each individual sensor or group of sensors to indicate deviations. Notifications can be based on absolute values, average values, differences, or percentage deviations. The system can also notify when a sensor does not send data as expected.

Data from the instrumented sensors is securely transferred to the NGI cloud for further processing, quality assurance, and analysis. Automatic quality control of data is done by comparing received data to system alarm thresholds, which are set to identify unrealistic measurements that indicate errors in the sensor system. The management of access rights to data is handled through the dashboard solution.

7.2.2.3. Evaluation: Key Performance Indicators

Short description. At baseline, incipient faults are either detected through regular inspections (noticed, reported, and assessed by ad-hoc inspections) or, in the worst case, through failure if the fault is fully developed. Regular inspections may not capture all relevant faults at a sufficiently early stage, for example, due to accessibility issues or long periods between inspections. Early detection will increase safety and give time to plan and execute maintenance actions at a lower overall cost without compromising safety. If successful, the numerical model, coupled with data from continuous monitoring instrumentation, will enable the description of the properties and behaviour of the bridge and transition zones in much greater detail than can be provided by instrumentation. This will provide insight into the link between the measurements and

degradation mechanisms. Defects and damage may also be introduced to study their impact on the bridge response. This allows earlier prediction of failure. However, it is essential to note that predictions generated by a simulation must be understood within the context of model validity and underlying assumptions.

Evaluation of the KPI. As the data analysis has not yet been completed, the KPI cannot be evaluated at this time. The KPI will be computed based on a statistical comparison of performance in detecting known incipient faults with that of regular baseline inspection (manual inspection). The KPI will be computed by:

$$\text{KPI2} = \frac{n_{mon}}{n_{mon} + m_{ins}} \times 100\ (\%),$$

where n_{mon} is the number of faults detected by the monitoring system deployed in this project, while m_{ins} is the number of faults detected by inspection or other means without first being detected by the monitoring system. The main failure cases targeted will be:

1. Loss of prestress in tendons,
2. Loss of stiffness in transition zones.

The KPI will be calculated individually for the two failure cases.

8. Conclusions

The work carried out on tunnels aims to improve the maintenance of these structures by deploying:

1. Prediction models for structural degradation, to accurately plan necessary repair operations.

2. New inspection technologies to optimize the cost and duration of monitoring activities.

For the first point, the objective is to use all data collected during periodic inspections to predict the degradation of tunnels. After significant effort to structure and improve the quality of the database, several prediction models were evaluated. The selected model is a gradient boosting model, which proved to be the most suitable for the data and delivered the best predictive performance, estimated at 70%.

This performance level was assessed through a retrospective analysis, where the model was asked to predict the current state of the structures based on past data. The model's limitations were also identified. Notably, it is not suitable for anticipating sudden degradation resulting from exceptional events (such as drought, flooding, earthquakes, etc.).

Once the model was selected, a tool called ADN OST was developed to allow civil engineers responsible for structural diagnostics to easily perform simulations. This tool facilitates decision-making regarding the scheduling and urgency of repair operations. It is especially valuable given that many SNCF Réseau tunnels are numerous and belong to the same generation.

However, the tool is still in a testing phase, during which critical feedback is being collected from engineers. Once fully validated, the next step will be to develop a module that cross-references prediction data with repair costs, to establish long-term investment planning strategies for structure regeneration.

For the second point, new inspection technologies were tested to assess their potential for reducing the costs and durations of monitoring operations. These technologies are based on photography, LiDAR, and infrared thermography.

Test results showed that, while these technologies improve the quality and accuracy of defect detection, they cannot yet replace traditional inspections. In particular, hammer sounding has no economically viable alternative, yet it remains essential for older structures with masonry linings.

For long tunnels or those with very short traffic interruption windows, these technologies can nonetheless optimize inspection durations by pre-identifying sensitive areas, especially since algorithms can detect visual or geometric changes between two surveys.

Further work is needed to define the appropriate use cases for these technologies from a technical, efficiency, and financial perspective. These efforts will also help define the minimum technical specifications required to meet tunnel inspection needs and support the prototyping of a specialized inspection vehicle.

This document demonstrates the relevance and operational feasibility of surface-wave methods, particularly MASW, for diagnosing shallow RE. Through the comparison of two acquisition systems (conventional and a landstreamer) we show that the landstreamer setup offers a significant reduction in acquisition time (up to 40%). It makes it highly suitable for rapid diagnostics in railway environments where track availability is limited.

To further support the large-scale deployment of these methods, we developed an automated processing tool for surface-wave dispersion extraction, based on a deep learning architecture. Trained on synthetic data and tested on real data, this tool has proven its ability to identify dispersion curves efficiently. However, its performance on noisy or complex datasets also underlined the necessity to enrich the training set with more representative field cases, thus improving its robustness and generalisation capability.

Seismic data also provide valuable insights into the hydrogeological context of a specific area. When combined with local geological and geotechnical knowledge, low-velocity zones can help delineate the position of the water table and infer piezometric heights. This indirect estimation of groundwater levels is especially relevant in areas where hydrogeological processes (e.g., seasonal rise of the water table, poor drainage) may affect the long-term stability of the railway structure. The ability to infer hydrogeological conditions non-invasively opens new perspectives for coupling structural monitoring with environmental monitoring and guiding preventive maintenance.

Looking forward, the next step is the development of a modular and open surface-wave processing toolbox. This toolbox will integrate data processing, dispersion curve extraction (semi-automatic and automatic with U2-pick), and inversion modules. In particular, the inversion process will be designed to provide outputs in the probabilistic framework, allowing the quantification of uncertainties and enabling its use as a decision-support tool. The aim of this toolbox is to provide practitioners with a flexible, scalable, and partially automated tool for analysing surface-wave data.

The work carried out has shown that the results obtained with the use of magnetic microwires meet the expectations for this deliverable, confirming their potential as a monitoring technology for tunnels.

The tests conducted have provided a solid foundation to continue advancing in this line of research. The next step will be to conduct trials in more representative environments, such as those planned at CEDEX, with the aim of moving the technology closer to a relevant environment or even testing it in a real tunnel.

The deliverable also reports the results of the obtained relationship between dynamic train loading (via ABA) and the rate of change in track geometry (via standard TG measurements). By analyzing axle box acceleration and track geometry measurements, a methodology to assess the condition of the track support is proposed, from which the stability of embankments can be explicitly analyzed concerning excessive deformation in TG. In the first contributions, we focused on transition zones, which are locations with a sharp discontinuity of the embankment. We demonstrated the effectiveness of multi-ABA measurements in monitoring health conditions

across various transition zones in Europe, including the Netherlands, Sweden, and Norway. The research revealed that different bridges and transition zones exhibit unique characteristics, including dominant wavelengths and energy distributions. Notably, higher train speeds accentuated these characteristics. The study suggests that understanding these unique features enables the evaluation of the geometry and support conditions of transition zones. Then, we investigated the vertical dynamic behaviour of railway bridge transition zones through experimental assessments using impact tests and onboard measurements, to obtain physical interpretability of ABA signals. The results indicated that variations in track resonance frequencies, observed through hammer and falling weight tests, reflected differences in track vertical dynamics at different locations within the transition zone. Furthermore, the analysis of Operational Deflection Shapes (ODSs) from falling weight tests showed distinct deflection patterns between embankment sections and bridge sections of the track. ABA signals also revealed that variations in train-track interactions are closely linked to the health conditions of the tracks. These findings highlighted the potential of combining different measurement techniques, such as ABA and falling weight tests, to provide a comprehensive understanding of transition zone health and improve health monitoring at the network level. Finally, with the experimental validation of ABA in different countries and the field tests that enabled the interpretability of ABA at lower frequencies, we introduced an innovative framework that combines longitudinal levels and ABA signals to assess track conditions, particularly focusing on track support (substructure and ballast layers). This new framework, termed EnVTQI, accounts for the influence of varying measurement train speeds and is effective in detecting local track condition changes, including both dynamic responses and track geometry deviations. In comparison to traditional track quality indices (TQI), EnVTQI proved more sensitive to local track issues. Future work could consider a TQI that integrates vertical, lateral, and longitudinal interactions between trains and tracks, and could also focus on long-term trend analysis and standardization of this method, which could improve the way railway track quality is monitored, especially in varying operational conditions.

Finally, the deliverable also describes a measurement system for two concrete bridges located on the Norwegian Ofotbanen line. The line is known for high axle loads and thus rapid degradation processes, which yield an important test arena for studying infrastructure degradation phenomena. Tracking the loss of prestress in tendons and how it affects the bridge response, and the loss of stiffness in transition zones and how it will affect the dynamic loading in concrete bridges, are planned as part of the demonstrator. The applied methodology combines finite element modelling and analysis with static and dynamic measurements from the bridge and transition zones, obtained from multiple sensors, utilizing advanced digital signal processing and statistical-based methods for anomaly detection and severity tracking. The model will be finalized after the installation of the measurement system that is currently on-going, followed by demonstrating the effectiveness of the proposed methods for the two specified degradation modes according to the specified KPIs.

In the bigger picture of the work performed in this deliverable within WP12/13, the tools developed in the described use cases constitute complementary building blocks of what can constitute an integrated support system for both railway operation and maintenance of infrastructure. Integration enables a more efficient allocation of maintenance activities, particularly when coordination reduces resource utilization and minimizes service disruptions.

A key challenge all the presented use cases contribute to is how to obtain updated knowledge of the entire infrastructure through real-time monitoring. Each contribution targets specific parts of the infrastructure, such as tunnels, bridges, transition zones, sub-ballast layers, embankments, and substructure, as they are governed by very different dynamical processes, with varying mechanisms of degradation and strong dependencies on local conditions. Investigation techniques, monitoring methods and models effective in one site cannot simply be transferred elsewhere without careful adaptation and tuning to local characteristics. Still, the cases reported contribute to achieving possible generalization of methodologies by providing evidence-based examples that demonstrate how tailored, site-specific solutions can inform a broader framework for future railway infrastructure management.

Another common challenge faced by the use cases refers to the integration of multiple data sources. Data fusion in railways is particularly complex, as it requires combining heterogeneous signals that differ in scale, sensitivity, measurement conditions, and relevance, depending on the asset and local conditions. Nevertheless, the combined data from these monitoring systems were used in different analyses that produced results useful for building decision-making procedures. The combination of multiple data sources, as presented in this document, helps strengthen decision support algorithms, reduce uncertainty, and increase the reliability of these novel methods.

As part of the final remarks, the information extracted from the infrastructure monitoring itself can be used for both timely decisions and to assess the long-term future of the monitored system. The latter can also help in the design of new infrastructure and, possibly, be used to update the relevant standards. Note also that the civil structures and the railway track components monitored in this deliverable, when failing, can have significant financial and operational consequences. Finally, the use cases (prototypes) presented contribute to establishing a foundation for harmonized monitoring approaches across European railway infrastructures, while acknowledging the need for local adaptation.

9. References

[1] L. Wang, S. Unsiwilai, Y. Zeng, C. Shen, J. Hendriks, J Moraal, A. Zoeteman, A. Núñez, R. Dollevoet, and Z. Li, Condition monitoring of railway transition zones using acceleration measurements on multiple axle boxes: Case studies in the Netherlands, Sweden, and Norway, in: the 10th Transport Research Arena Conference (TRA2024), 15-18 April 2024, Dublin, Ireland.

[2] S. Unsiwilai, L. Wang, A. Núñez, Z. Li, Multiple-axle box acceleration measurements at railway transition zones, Measurement 213 (2023) 112688.

[3] S. Unsiwilai, C. Shen, Y. Zeng, L. Wang, A. Núñez, Z. Li, Vertical dynamic measurements of a railway transition zone: a case study in Sweden, J Civ Struct Heal Monit 14 (2024) 979-996.

[4] S. Unsiwilai, W. Phusakulkajorn, C. Shen, A. Zoeteman, R. Dollevoet, A. Núñez, Z. Li, Enhanced vertical railway track quality index with dynamic responses from moving trains, Heliyon (2024).

[5] *Ofoten Line (Ofotbanen)*. https://www.rail-pass.com

[6] *The Train Derailment in Narvik: Hopes to Resume Limited Ore Traffic Shortly*. High North News

[7] *Malmbanan – Sveriges vackraste järnvägssträcka*. Swedish Rail Administration.

[8] H. Cui, Y. Zhuo, D. Ke, Z. Li, S. Li. *Chloride ion erosion of pre-stressed concrete bridges in cold regions*, Journal of Infrastructure Preservation and Resilience, Vol. 4(12), 2023.

[9] S. Kaewunruen, L. Wu, K. Goto, Y.M. Najih. *Vulnerability of Structural Concrete to Extreme Climate Variances*, Climate. Vol. 6(2), 40, 2018.

[10] X. Qin, S. Meng, D. Cao, Y. Tu, N. Sabourova, N. Grip, U. Ohlsson, T. Blanksvärd, G. Sas, L. Elfgren. *Evaluation of freeze-thaw damage on concrete material and prestressed concrete specimens*, Construction and Building Materials, Vol. 125, pp. 892-904, 2016

[11] X. Ge, M. Ke, W. Liu, H. Wang, C. Lu, G. Mei, H. Yang. *Effect of the Internal Humidity of Concrete on Frost Resistance and Air Void Structure under Different Low Temperature Conditions*, Materials, Vol. 15 (15), 5225, 2022.

[12] V.M. Rădulescu, G.M.T. Rădulescu, S.M. Naș, A.T. Rădulescu, C.M. Rădulescu. *Structural Health Monitoring of Bridges under the Influence of Natural Environmental Factors and Geomatic Technologies: A Literature Review and Bibliometric Analysis*, Buildings, Vol. 14 (9), 2811, 2024.

[13] H. Li, Y. Zhang, H. Guo. *Numerical Simulation of the Effect of Freeze–Thaw Cycles on the Durability of Concrete in a Salt Frost Environment* , Coatings, Vol. 11(10), 1198, 2021.

[14] S. Zhang, B. Tian, B. Chen, X. Lu, B. Xiong, N. Shuang. *The Influence of Freeze–Thaw Cycles and Corrosion on Reinforced Concrete and the Relationship between the Evolutions of the Microstructure and Mechanical Properties*, Materials, Vol. 15(18), 6215, 2022.

[15] M. Carsanaa, F. Biondini, E. Redaellia. *Diagnostic procedure for corrosion assessment of existing concrete bridges: Experimental case study*, Structure and Infrastructure Engineering, pp. 1–17, 2025.

[16] K.A. Khan. *Detection, protection, repair and rehabilitation of corroded prestressed concrete structures*, Master Thesis, Ryerson University, Canada, 2005.

[17] H. Heydari, S. Nadermohammady. *Laboratory Study of Freezing-Thawing Impacts on Railway Ballast Aggregate*, International Journal of Railway Research, Vol. 11(2), pp. 39-47, 2024

[18] J. Latvala, P. Kolisoja, H. Luomala. *Water content variation of railway track sub-ballast layer*

in seasonal frost area: A case study from Finland, Transportation Geotechnics, Vol. 38, 100926, 2023
[19] A. Lotfi, M.S. Virk. *Railway operations in icing conditions: a review of issues and mitigation methods*, Public Transport, Vol. 15, pp. 747-765, 2023.
[20] *Katterat station* . Bane NOR.
[21] *Søsterbekk station* . Bane NOR.
[22] *Temperature observations from Bjørnfjell measuring station*. https://www.yr.no/en
[23] *Temperature observations from Katterat measuring station*. https://www.yr.no/en
[24] *Humidity observations from Katterat measuring station*. https://www.yr.no/en
[25] *Humidity observations from Bjørnfjell measuring station*. https://www.yr.no/en
[26] N.P. Anastasiadis, C.S. Sakaris, R. Schlanbusch, J.S. Sakellariou. *Vibration-based SHM in the synthetic mooring lines of the semisubmersible OO-Star wind floater under varying environmental and operational conditions*, Sensors, Vol. 24(2), 543, 2024.
[27] C.S. Sakaris, X. Wen, R. Schlanbusch, M.C. Ong. *Multi-spatial measurement points based structural health monitoring in the tendons of an offshore aquaculture farm's fish cage*, Proceedings of the 44th ASME International Conference on Ocean, Offshore and Arctic Engineering (OMAE), 2025, Vancouver, British Columbia, Canada.